ABSTRACT

Title of Thesis: LITHOSPHERIC EXTENSION ON VENUS: HOW TO FORM NARROW RIFTS

Alexis Ann Martone, Master of Science 2017

Thesis Directed By: Professor Laurent G. J. Montési, Department of Geology

The Venusian rifts of Devana and Ganis Chasmata have been noted for their similar morphology to some rifts on Earth (i.e., the East African rift system). These are narrow rifts that are associated with localized deformation. This thesis aims to explore the link between lithospheric structure and rift style using a force analysis model, following previous work by Buck (1991), in order to determine under what conditions narrow rifts are predicted for Venus conditions. Results for two cases, one using a constant lithospheric thermal conductivity and another using a depth dependent thermal conductivity, are initially determined; Devana and Ganis Chasmata are predicted to be wide rifts rather than narrow rifts. Lithospheric weakening mechanisms (rheological weakening and diking) are implemented to determine their effect on localizing deformation and, thus, forming narrow rifts. Diking did not produce any effect on forming narrow rifts. Rheological weakening, likely due to a combination of melt and a transition to grain size sensitive creep, appears necessary to produce narrow rifts.

LITHOSPHERIC EXTENSION ON VENUS: HOW TO FORM NARROW RIFTS

by

Alexis Ann Martone

Thesis submitted to the Faculty of the Graduate School of the
University of Maryland, College Park, in partial fulfillment
of the requirements for the degree of
Master of Science
2017

Advisory Committee:
Professor Laurent G. J. Montési, Chair
Professor Wenlu Zhu
Professor Nicholas Schmerr

Acknowledgements

I first want to thank my advisor, Professor Laurent Montési, for his invaluable guidance for the past 2.5 years. He has always been supportive and it was a pleasure to learn from him. I would also like to thank Wenlu Zhu and Nicholas Schmerr for agreeing to serve on my committee and for their time and feedback.

I always want to thank my fellow graduate students who have made my graduate school experience enjoyable.

My family, of course, has been a source of endless support and I am grateful for your constant reassurance. I am also very thankful that I had my boyfriend, Alex Sage, by my side through this whole experience.

Table of Contents

List of Tables

List of Figures

1. Motivation

Owing to their similar location in the solar system, Venus and Earth likely formed at similar times with similar materials (Svedhem et al., 2007). However, despite their similarities in bulk composition and size, Venus is currently a starkly different planet compared to Earth, with a high surface temperatures (450°C), a thick CO_2-dominated atmosphere, and a lack of water (Prinn and Fegley, 1987). Little is known about Venus' evolutionary history due to a resurfacing event about 500 Myr ago that erased geological indicators of past conditions. Venus is currently in a stagnant lid convection regime (Solomatov and Moresi, 1996; Reese et al., 1998), which means the forces behind the observed tectonics differ from those on Earth. The lack of information regarding the planet's history means we need to make inferences from current observations in order to better constrain its thermal and geophysical evolution, and to differentiate it from Earth's evolution.

The goal of this research is to use a one dimensional (1D) force analysis of lithospheric extension in order to predict what kind of rifts will form under Venusian conditions. The model used is based off the work in Buck (1991), who formulated a pure shear model of rifting. Using literature estimates of crustal thickness and surface heat flux I can assess whether the model matches geologic observations. I also determine the importance of other processes that influence the lithospheric structure, such as weakening mechanisms and diking, which may promote narrow rifts.

The research presented herein aims to provide more insight into these young (Basilevsky and Head, 1993; Basilevsky and Head, 2007) features on Venus, the rifts, which have been noted in various literatures for their similar morphology to

extensional features on Earth, notably the East African rift system) (Stofan et al., 1989; Foster and Nimmo, 1996; Kiefer and Swafford, 2006, Montési, 2013). Doing so allows for more constraints on the thermal and mechanical structure of the Venusian lithosphere, which will contribute to unraveling the enigmatic history of Venus.

1.1 Geology of Venus

While Earth-like plate tectonics are not currently active on Venus, it has been speculated that plate tectonics may have been active in the past (Arkani-Hamed, 1994; Herrick, 1994; Phillips and Hansen, 1998). Crater counting indicates a surface age of ~500 Ma (Phillips et al., 1992; McKinnon et al., 1997), although some studies (Bottke et al., 2016) propose it could be as young as ~200 Ma. It is thought that a resurfacing event erased most of the surface features, although the exact nature of the event is debated (Basilevsky et al., 1997; Turcotte et al., 1999; Romeo and Turcotte, 2010; Ivanov and Head, 2015). Since the resurfacing event, numerous tectonic episodes generated distinctly different terrain (Solomon et al., 1992). Tessera regions constitute ~10 % of the planet's surface and are defined by a high standing, densely fractured terrain (Hansen et al., 1997); these are on average the oldest terrain and some have speculated that tessera are remnants of the surface before the resurfacing event (Basilevsky and Head, 2000). Volcanic plains, which include smooth plains and plains with wrinkle ridges, sit at ~1.5 km below the mean planetary radius and constitute ~80% of the planet's surface (Hansen et al., 1997). Volcanic rises are the youngest units and features rifts and volcanic edifices. They are likely related to mantle plumes (Kiefer and Hager, 1991). While Venus displays convergent,

divergent, and shear tectonics (Solomon et al., 1992; McKenzie et al., 1992), the deformation does not show the global connections seen on Earth. McKenzie et al., (1992) and Schubert and Sandwell (1995) have speculated that some features called coronae may be subduction related, although others have proposed models for forming these features without the involvement of subduction (Stofan and Smrekar, 2005; Hoogenboom and Houseman, 2006; Piskorz et al., 2014).

Without plate tectonics, Venus must lose its internal heat differently than Earth. On Earth, 65% of heat lost is related to plate tectonic processes, especially plate creation (Sclater et al., 1980). For Venus, heat loss is limited by conduction through a thick, stagnant lithosphere; conduction is estimated to be only 20% of the heat loss on Earth (Sclater et al., 1980). Thus, the lithosphere of Venus is expected to have more uniform interior temperature than the Earth, with a shallower thermal gradient (Kaula, 1999) averaging of ~ 10 °C km^{-1} (James et al., 2013). Although heat cannot escape as efficiently as on Earth, the deep interior of Venus may be hotter than on Earth and potentially heating up (Schubert et al., 1997; Nimmo and McKenzie, 1998).

1.2 Study Regions

The Beta-Atla-Themis (BAT) region of Venus (figure 1) contains the youngest geologic features on the planet and covers roughly one third of the surface area (Grosfils and Head, 1994a). The region contains various types of terrain: tessera, plains, volcanic rises, and chasmata (Basilevsky and Head, 2007). Chasma (plural chasmata), as defined by the USGS, is planetary nomenclature for a deep, elongated, steep-sided depression. On Venus some chasmata, which form from extensional

tectonics, have similar morphology to continental rifts on Earth. Many rifts on Venus are associated with coronae, which are quasi-circular volcano-tectonic features. Their origin is still debated, but mantle dynamics (upwellings and/or delamination) are thought to play a significant role (Stofan and Smrekar, 2005; Hoogenboom and Houseman, 2006; Piskorz et al., 2014). Potential Earth analogues to coronae have been noted in various literatures (Lopez et al., 1999; Buchan and Ernst, 2016; Bethell et al., 2016). The main focus of this study is on Ganis and Devana Chasmata, on Atla and Beta Regiones, respectively, with secondary attention paid also to Parga and Hecate Chasmata.

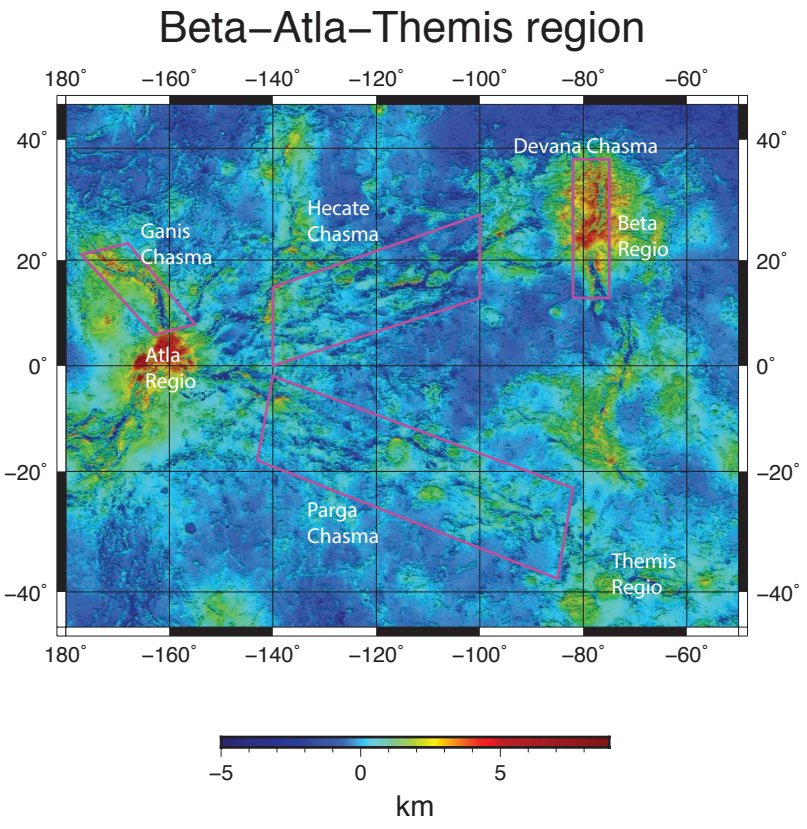

Figure 1: The Beta-Atla-Themis (BAT) region on Venus, which is the focus of this study. Young volcanic rises and rifts dominate the area. The four chasma studied in this work are outlined. Topographic data from Magellan, with original radar altimeter data from Ford and Pettengill, 1992.

The rifts of Devana and Ganis Chasmata have been compared to narrow terrestrial rifts, such as the East African rift system (Stofan et al., 1989; Foster and Nimmo, 1996; Kiefer and Swafford, 2006; Montési, 2013). These systems are all fault-bounded triple junctions marked by modest volcanism, potentially related to plume activity. Venusian rifts have larger maximum widths than seen in East Africa (Kiefer and Swafford, 2004); this difference is likely due to the rheological difference between a wet, silicic terrestrial crust and a dry diabase Venusian crust (Foster and Nimmo, 1996).

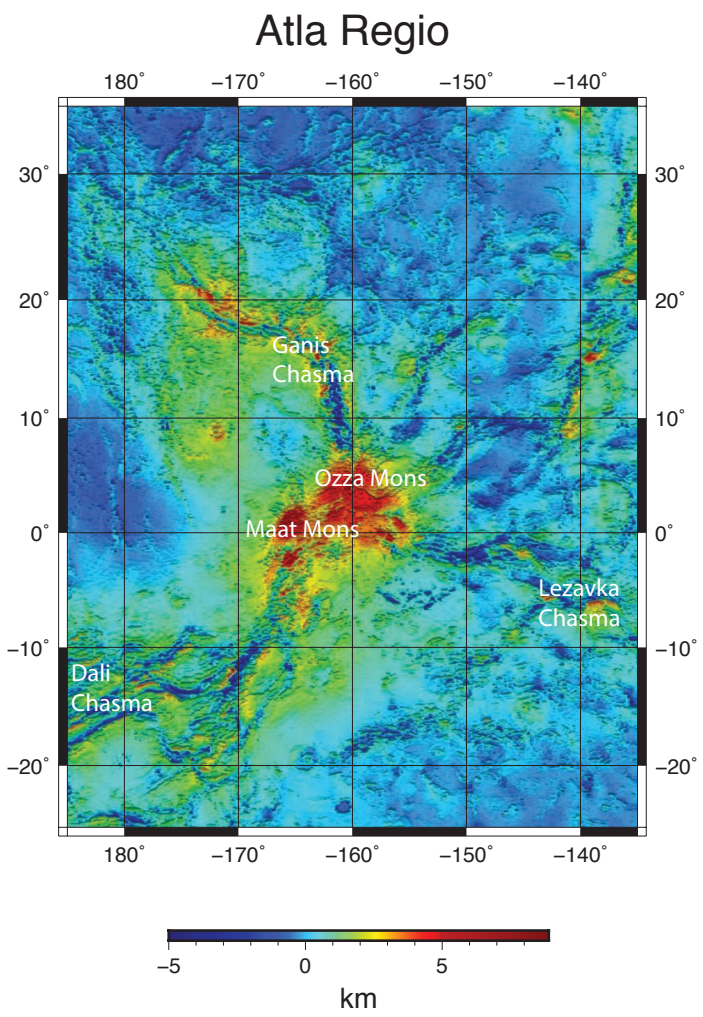

Figure 2: Atla Regio, a volcanic rise that contains the rift Ganis Chasma that extends northward from the volcanic center of Maat and Ozza Mons. Topographic data from Magellan, with original radar altimeter data from Ford and Pettengill, 1992.

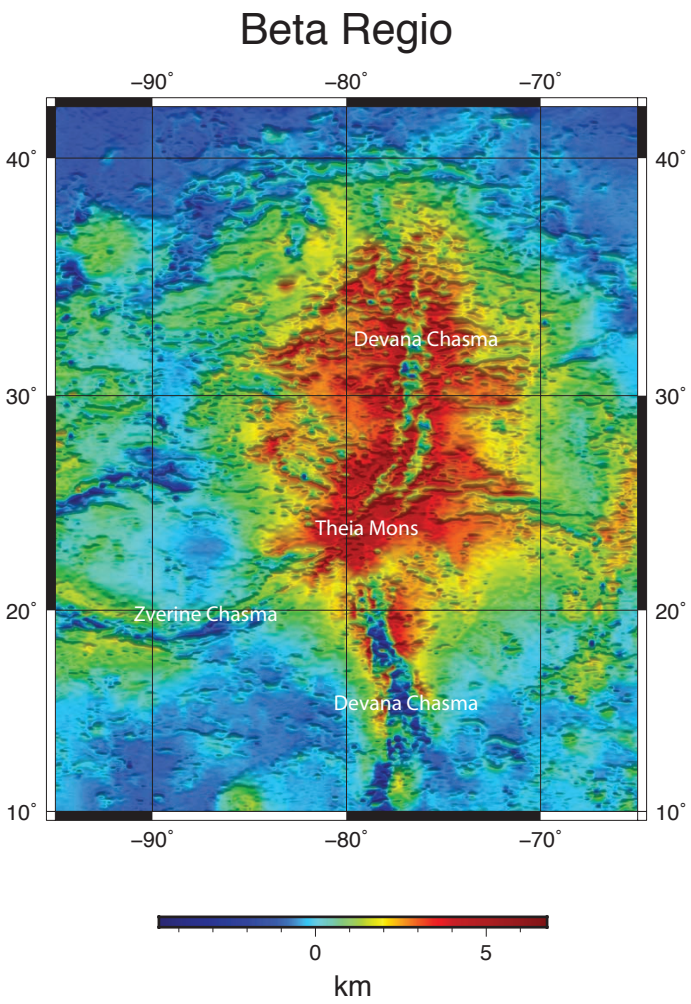

Figure 3: Beta Regio, a volcanic rise containing the rift Devana Chasma that extends northward and southward from the volcano Theia Mons. Topographic data from Magellan, with original radar altimeter data from Ford and Pettengill, 1992.

Atla Regio (figure 2) has two volcanic centers, Ozza and Maat Montes; Maat Mons is the tallest volcano on Venus at 5 km above the mean planetary radius (Smrekar et al., 1997). Beta Regio (figure 3) is volumetrically the largest volcanic rise on Venus and has one volcanic center, Theia Mons (Smrekar, et al., 1997). Devana and Ganis Chasmata both have limited volcanism and do not feature coronae, which means that convective mantle processes are not a significant factor in the extensional tectonics. Both rifts have experienced roughly 10 km of extension (Foster and

Nimmo, 1996; Nimmo and McKenzie, 1998; Rathburn et al., 1999). The elastic thickness for Beta and Atla Regiones were found to be 29 km and 32.5 km, respectively (Barnett et al., 2000). Devana and Ganis Chasmata are the main focus of this work as they are not associated with significant coronae activity, so I can focus on the tectonics of rifting without needing to include the extensive magmatism and plume activity that likely accompany coronae.

I also analyze the rifts Parga and Hecate Chasmata (figure 4). These rifts differ from Ganis and Devana Chasmata in that they are wider rifts with more diffuse deformation. They are not associated with volcanic rises and are instead corona-dominated rifts (Hansen et al., 1997). Investigating two rifts with different morphology is beneficial to the overall discussion of extensional deformation of Venus' lithosphere. However, the presence of coronae with the rift suggests that mantle dynamics are involved in rift development, which limits the applicability of my model to these rifts.

Parga Chasma is a 10,000 km long fracture with deformation that varies in width from 60 to 590 km. 131 coronae are associated with the rift (Martin et al., 2007). Hecate Chasma is 8,000 km in length and 100 to 200 km wide. Individual grabens are 2-50 km, with spacing between graben reaching 20 km (Hamilton and Stofan, 1996). Hecate Chasma has 50 coronae associated with the rift (Smrekar et al., 2010). The relationship between coronae and rifts is not entirely understood. Coronae are also accompanied by extensive volcanism (Stofan et al., 1997) and, thus, magmatic processes will have an impact on extensional tectonics. When evaluating

results I acknowledge that not all major geologic processes are taken into account for Parga and Hecate Chasmata.

Smrekar et al., (2010) conducted gravity analyses of Parga and Hecate chasmata in an attempt to understand the connection between coronae and rifts. In their work they determined Apparent Depth of Compensation (ADC), crust thickness, and elastic thickness values for both rifts. Whether crust thickness or elastic thickness was estimated depends on whether the gravity data was fit using a top loading (topographic features arise from a load at the surface, i.e., a volcano) or bottom loading (topographic features arise from an anomaly at depth, i.e., a plume). Both Parga and Hecate Chasmata have significantly lower ADC values than Beta and Atla Regiones, closer to 100 km rather than >300 km for the latter two regions (Schubert et. al., 1994; Smrekar et al., 2010). This gravity data indicates that these rifts are not driven by an underlying plume, which differentiates them again from the rifts on Beta and Atla Regiones. Smrekar et al., (2010) determined an average crust thickness at Hecate Chasma of 40 ± 5 km, and at Parga Chasma crust thickness was estimated as 47± 4 km. These values are used when evaluating the model results in section 5.2.

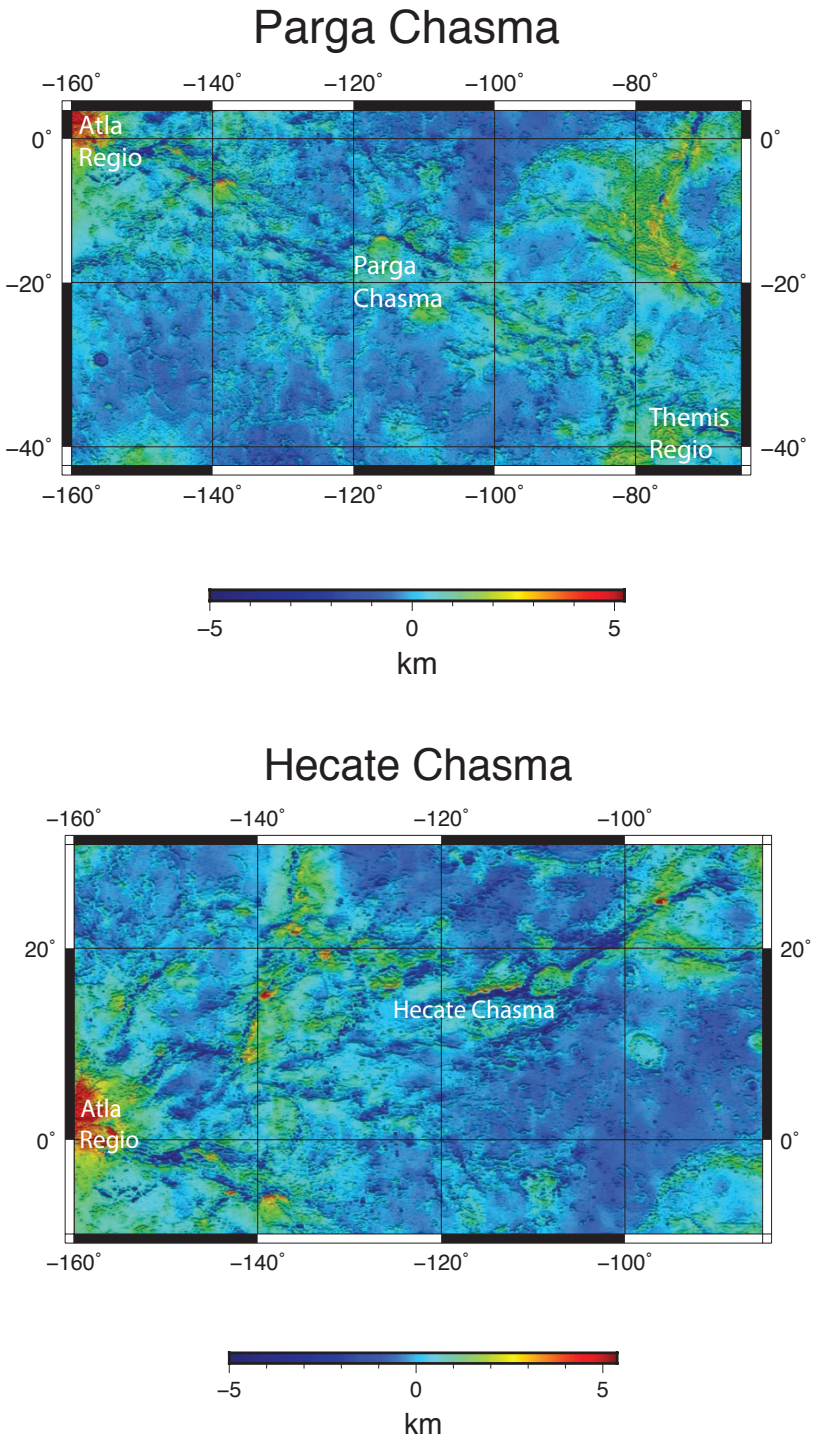

Figure 4: Parga (top) and Hecate (bottom) Chasmata. Both are wide rifts with more diffuse deformation that at Devana and Ganis Chasmata. Parga Chasma extends from southern Atla Regio to Themis Regio. Hecate Chasma extends from eastern Atla Regio to western Beta Regio. Topographic data from Magellan, with original radar altimeter data from Ford and Pettengill, 1992.

2. Lithospheric Extension

The structure, both thermal and mechanical, of the lithosphere is thought to play a key role in determining the evolution of extensional tectonics (Buck, 1991; Bassi, et al., 1993; Brun, 1999; Gueydan et al., 2008). The lithosphere at the time of rift initiation will largely decide what type of rift will develop. Rifting is categorized into two types, active and passive, depending upon whether rifting is driven by an active mantle upwelling or whether the upwelling is a passive response to lithospheric extension (Şengör and Burke, 1978). The Buck (1991) model only considers passive extension.

2.1 Styles of Rifting

Rifts on Earth are categorized into three types: wide rifts, narrow rifts, and core complexes. Narrow rifts have a width roughly equal to the lithospheric thickness (Buck, 1999). These types of rifts, such as the East African rift system and the Rio Grande rift, may lead to continental breakup and require a weakened lithosphere to localize deformation throughout the lithosphere. Localization in the brittle regime is achieved through faulting; the ductile regime requires more complicated physics to achieve localization (Montési, 2013). Ductile localization mechanisms are discussed in detail in section 5.4.2. The lithosphere as a whole can weaken either due to the mechanical effect mentioned here, or because its thermal structure or crustal thickness changes.

The Basin and Range and the Aegean are two terrestrial examples of wide rifts. Wide rifts accommodate extensional strains over broad regions up to 1000 km (Brun 1999). They are observed to form in regions with greater than average heat flux

and thickened crust (Buck et al., 1999). These types of settings allow for the delocalization of deformation necessary for wide rifts.

The third classification, core complexes, requires a hot weak, hot lower crust that can flow easily. Lower crustal flow removes horizontal crustal thickness variations that act to drive wide rifting (Buck, 1991). In this regime, as extension proceeds, middle to lower crustal rocks are exposed at the surface.

2.2 Competing Mechanisms

The style of rifting is defined by whether deformation is localized or delocalized. Our analysis assumes that extension is always concentrated in the weakest region of the lithosphere. Narrow rifts form when deformation continues in a localized region of decreased strength whereas wide rifts form when deformation migrates to a weaker region (Bassi et al., 1993), which in the context of my model, implies that the deforming region becomes stronger. Localized deformation is a response to mechanisms that act to decrease the force needed to continue deforming the lithosphere: 1) Strain weakening mechanisms (i.e., temperature or structural evolution), and 2) Thermal buoyancy. Delocalized deformation is favored by mechanisms that act to increase the force needed to continue deforming the lithosphere: 1) Strain hardening mechanisms (i.e., a thinned crust replaced by a stronger mantle), and 2) Crustal buoyancy. The balance of the integrated lithospheric strength, crustal buoyancy and thermal buoyancy controls the resulting rift style.

2.3 Thermal Structure

The strength on the lithosphere, a key parameter of my model, depends on temperature. Therefore, it is important to understand the initial temperature profile of

the lithosphere and the data that can be used to constrain it. In addition, the thermal structure of Venus is key in understanding the volcanic and tectonic evolution of the planet. Therefore, it is important to conclude from our modeling effort the possible thermal structures of regions that display clear evidence of rifting.

2.3.1 Steady State Temperature Profile

The steady state temperature profile describes the scenario when there is no change in temperature over time. In this case, the amount of heat leaving the lithosphere equals the amount entering from beneath plus the amount produced by heat production. The amount of heat leaving the lithosphere (surface heat flux) is related to temperature through Fourier's Law,

$$Q_s = \kappa_{tc} \left.\frac{\mathrm{d}T}{\mathrm{d}z}\right|_s \tag{1}$$

where Q_s is the surface heat flux, κ_{tc} is the thermal conductivity, and $\left.\frac{\mathrm{d}T}{\mathrm{d}z}\right|_s$ is the temperature gradient at the surface. I assume all heat production is contained in the crust. Using the heat equation,

$$\frac{\mathrm{d}Q}{\mathrm{d}z} = H \tag{2}$$

where H is the volumetric heat production, we can formulate an equation describing the steady state temperature,

$$T_{ss} = \begin{cases} -\dfrac{H * z^2}{2\kappa_{tc}} + \dfrac{Q_S * z}{\kappa_{tc}} + T_s & \text{for } z \le z_{moho} \quad (3) \\ T_{moho} + \dfrac{(Q_S - H * z_{moho})}{\kappa_{tc}}(z - z_{moho}) & \text{for } z > z_{moho} \quad (4) \end{cases}$$

where H_{crust} is the crustal heat production and T_s is the surface temperature and T_{moho} is the temperature at the base of the crust (Moho).

2.3.2 Crustal Heat Production

The Soviet Venera missions returned several measurements of the geochemical composition of the Venusian crust (Surkov et al., 1987). Venera 9 and 10 performed measurements near the edges of Beta Regio, which features several of the rifts studied here. The heat producing element (U, Th, and K) abundances of the crust in this region were similar to tholeiitic basalts but with a calc-alkaline trend (Schubert et al., 1997). Venera 9 determined a heat production value of 5×10^{-7} W m^{-3} and Venera 10 determined a value of 2.15×10^{-7} W m^{-3}. A uniform distribution throughout the crust of an average value of 3.5×10^{-7} W m^{-3} was used in my calculations. Three significant errors in these measurements are noted by Grimm and Hess (1997): 1) large analytical errors 2) samples were regolith and not bedrock 3) the atmosphere of Venus has likely altered the crustal material after it was emplaced (the crust is elevated in sulfur as seen in the high SO_3 content). Grimm and Hess (1997) note that elements such as Ca and the alkalis are mobilized during metamorphism, while elements such as Al are not affected (Beswick, 1982). Measurements from Venus indicate low CaO and low CaO/Al_2O_3 ratios when compared to terrestrial values, implying that metamorphic processes have mobilized CaO. This means that K (an alkali) could have also been affected. Despite these uncertainties, since these are the only estimates available they are used in this work for determining both the steady state and time-dependent temperature profiles.

2.3.3 Thermal Conductivity

The thermal conductivity of a material describes the ability of that material to conduct heat; a higher κ_{tc} indicates high rate of heat transfer, while low κ_{tc} indicates a poor ability to transfer heat. Thermal conductivity has a direct influence on the

thermal gradient and steady state temperature profile, as shown in equations 3 and 4. Figure 5 shows two steady state temperature profiles. Both scenarios have the same surface heat flux but differ in thermal conductivity values, thus the geothermal gradients differ.

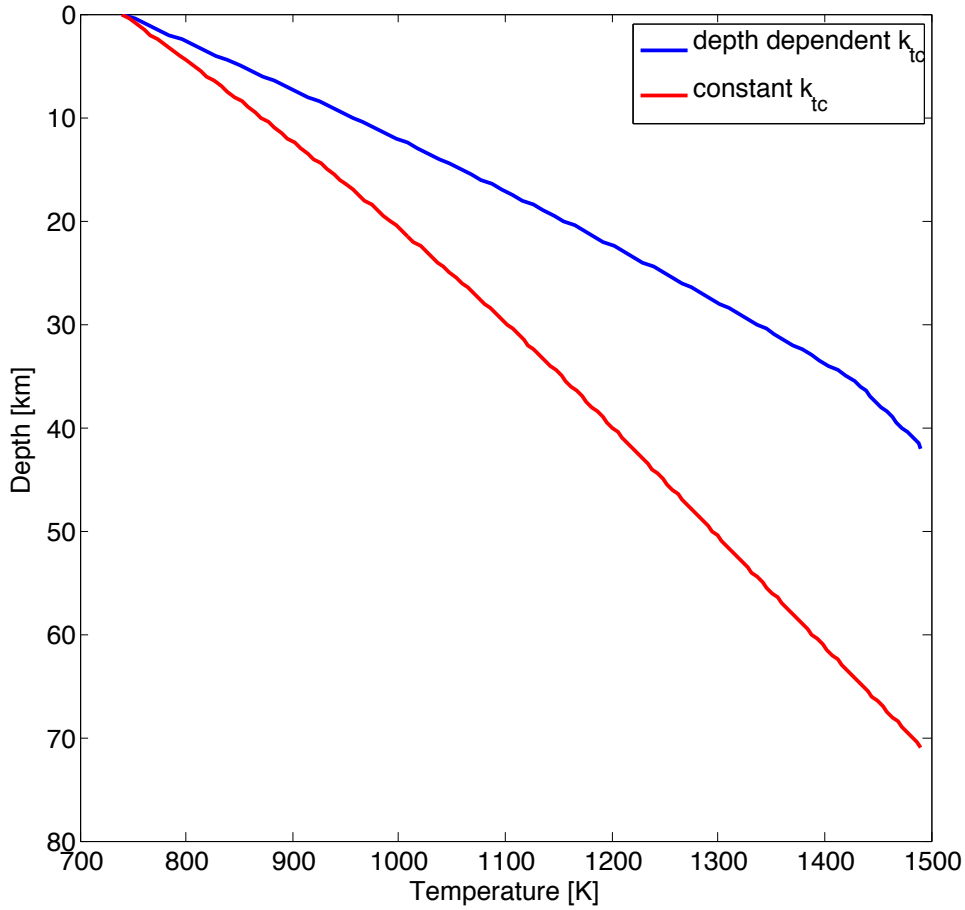

Figure 5: Temperature profiles through the Venusian lithosphere constructed using a constant thermal conductivity, 3.3 W m^{-1} K^{-1} (red) and a depth dependent thermal conductivity, 2 W m^{-1} K^{-1} in the crust and 3.3 W m^{-1} K^{-1} in the mantle (blue). In both cases, the surface heat flux is 45 mW m^{-2}, the heat production is $3.5*10^{-7}$ W m^{-3} in the crust, and the crustal thickness is 40 km.

The red profile describes a constant lithospheric thermal conductivity of 3.3 W m^{-1} K^{-1}. For the blue profile the thermal conductivity in the crust is reduced to 2 W m^{-1} K^{-1}, thus, changing the geothermal gradient in the crust. For both cases the crustal

heat production is $3.5*10^{-7}$ W m^{-3}, the surface heat flux is 45 mW m^{-2}, and the crust is 40 km, however, due to variations in the thermal conductivity, the temperature at the base of the crust differs by 200 K between these models. It is clear that the thermal conductivity has a substantial influence on the steady state temperature of the lithosphere.

3. Methods

The model used here follows the work of Buck (1991), who defined a pure shear extension model that relates force evolution to rift development. This model assumes edge-driven tectonics, which are appropriate for a plate tectonics setting where horizontal (ridge push-slab pull) motions drive tectonics, but admittedly may not be appropriate for a single plate planet such a Venus where tectonics are considered to originate from vertical rather than horizontal motion (Solomon and Head, 1982; Phillips et al., 1991). However, lateral gravitational potential energy gradients could be a driving force in rifting, as noted by Stamps et al., (2010) for the East African rift system, and would act similarly to the edge forces considered here. Therefore, horizontal motion induced by gravitational stresses is a possible mechanism for the extensional features on Beta and Atla Regiones.

The edges are pulled apart at a constant rifting velocity (u), where it is assumed that the necessary amount of force to initiate rifting is available. A diagram of the initial model setup is shown below.

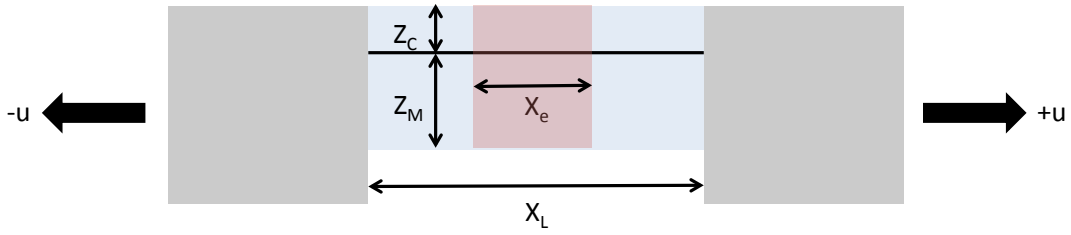

Figure 6: Schematic diagram modified from Buck (1991) showing the model setup. The gray blocks are undeforming lithosphere that enable extension and pull apart at speed *u*. Z_c is the crust thickness, Z_m is the mantle thickness, X_L is the width of the uniform lithosphere, and X_e is the region where extension is localized.

Determining the resulting rift style is reduced to a force balance problem. The model tracks the evolution of the integrated yield strength, crustal buoyancy, and thermal buoyancy. If the change in total force is positive then more force is necessary to continue rifting and a wide rift forms. If the total change in force is negative then less force is necessary to continue rifting and a narrow rift or core complex forms.

Table 2 lists the parameters and values used. The two main varying parameters are the initial crust thickness (Z_C) and the surface heat flux (Q_S). A strain rate of 10^{-16} s^{-1} is used for all Venus runs; such a low strain rate is appropriate for a planet without plate tectonics where surface deformation is driven solely by mantle dynamics (Nimmo and McKenzie, 1998).

Z_C	Initial crust thickness	10-70 km
Q_S	Surface heat flux	10-70 W m^{-2}
$\dot{\varepsilon}$	Strain rate	10^{-16} s^{-1}
H_{crust}	Crustal heat production	$3.5*10^{-7}$ W m^{-3}
k_{tc}	Thermal conductivity	2-4 W m^{-1} K^{-1}
k_{td}	Thermal diffusivity	10^{-6} m^2 s^{-1}
η	Viscosity at the base of the lithosphere	10^{21} Pa s
ε	Strain limit	0.25
X_e	Width of applied extension	317 km
u_x	Rifting velocity	0.1 cm yr^{-1}
ρ_c	Crustal density	2900 kg m^{-3}
ρ_m	Mantle density	3300 kg m^{-3}
gB	Proportionality constant used for the brittle yield strength	19.9 MPa km^{-1}
g	Gravity	8.87 m s^{-2}

Table 1: Description of parameters and value(s) used for Venus.

3.1 Model Setup

The extensional velocity is set to 0.1 cm yr^{-1}, following Smrekar et al., (2005). Rifting continues for 48 Myr, corresponding to a strain of 0.15.

The rheology of Venus' lithosphere is described by dry diabase in the crust (Mackwell et al., 1998) and dry peridotite in the mantle (Hirth and Kohlstedt, 2003). Buck (1991) follows the work in Brace and Kohstedt (1980), who, assuming Byerlee's law, define the brittle stress for extensional tectonics as:

$$\sigma_B = gB \cdot z \tag{5}$$

Where gB defines the amount the brittle yield strength linearly increases with depth, z. Brace and Kohlstedt (1980) estimate gB to be 22 MPa km^{-1} for zero pore pressure, which becomes 19.9 MPa km^{-1} after gravity, g, is adjusted for Venus.

The ductile strength is modeled with a dislocation creep flow law.

$$\sigma_D = (\dot{\varepsilon}/A)^{1/n} \exp(E/nRT) \tag{6}$$

Where $\dot{\varepsilon}$ is the strain rate, T is the temperature, R is the universal gas constant, and n, A, and E are experimental constants (Table 1). The ductile rheology is highly temperature-dependent, unlike the brittle rheology, and is such that at high enough temperatures the rocks will flow in response to a deviatoric stress.

mineral	**n**	**A (Pa^{-n} s^{-1})**	**E (kJ mol^{-1})**
dry diabase	4.7	1.2e-26	485
dry olivine	3.5	2.4e-16	530

Table 2: Compilation of dislocation creep rheological parameters used for dry diabase (Mackwell et al., 1998) and dry olivine (Hirth and Kohlstedt, 2003).

Water is incompatible and will preferentially partition into melt. Venus has experienced considerable volcanism (i.e., resurfacing) and thus without a pathway for water to return to the interior (like subduction on Earth) the interior will dry out over time (Nimmo and McKenzie, 1998). Thus, using a dry rheology for the Venusian lithosphere is an appropriate assumption.

A moho heat flux (Q_{moho}) and temperature (T_{moho}) are determined using the following equations:

$$Q_{moho} = Q_s - H_{crust} \cdot Z_{moho} \tag{7}$$

$$T_{moho} = T_{surf} + \left(\frac{Q_s}{\kappa_{tc}(z)} - \frac{H_{crust}}{2\kappa_{tc}(z)} Z_{moho}\right) Z_{moho} \tag{8}$$

The lithosphere is determined to be the depth at which a viscosity of 10^{21} Pa s is reached (Buck, 1999; Musser and Squyres, 1997). Stress and viscosity are related through equation 9, where σ is temperature-dependent for ductile rheologies,

$$\eta = {}^{\sigma}/_{2\dot{\varepsilon}} \tag{9}$$

Using the ductile rheology from equation 6, and rearranging for temperature yields:

$$T_{lith} = \frac{E}{nR}\left(\ln\left(2\dot{\varepsilon}\eta\left({}^{A}/_{\dot{\varepsilon}}{}^{1/n}\right)\right)\right)^{-1} \tag{10}$$

A steady state temperature profile for the initial conditions is calculated using equations 3 and 4.

I initially follow the practice common in the literature of using a constant thermal conductivity (3.3 W m^{-1} K^{-1}) for the entire lithosphere (Grimm, 1994; Turcotte, 1995; Brown and Grimm, 1997). However, I also develop more realistic models that assume a depth-dependent thermal conductivity, decreasing the crustal value to 2 W m^{-1} K^{-1}. This lower thermal conductivity value for a diabase crust has been used in various studies (Schubert et al., 1997; Gilmore et al., 1998; Dombard et al., 2007).

There are three applicability tests I look at to check the physicality of the initial temperature profile. First is the value of Q_{moho}. For some runs the moho heat flux is negative. For these runs the heat generated in the crust exceeds the flux out of the surface. Therefore, heat is conducted downward into the mantle through the moho; this scenario is considered unrealistic as the mantle would act as a heat sink. In this case, the entire run is terminated. I also check whether T_{moho} exceeds the solidus. The quartz solidus (used in Earth calculations) and basalt solidus are taken from Brown et al., (1992) and are given in equations 11 and 12, respectively.

$$T_{sol} = 1243 + 2.82 * z \quad (11)$$

$$T_{sol} = 1343 + 1.79 * z \quad (12)$$

If T_{moho} exceeds the solidus or the temperature at the base of the lithosphere then the crust is cut to below the solidus temperature; the steady state temperature profile is recalculated using this new depth profile. The lithosphere is also not allowed to be greater than 400 km, if it is then the run is terminated.

3.2 Constraints on parameters

3.2.1 Heat Flux

There have been no direct measurements of the surface heat flux on Venus. Some estimates are obtained scaling Earth's heat flux, whether based on whole mantle convection or on elastic thickness estimates, to Venus. If Q_S is scaled based on the planet's mass (as suggested by Solomon and Head, 1982) from an average Earth heat flux of 87 mW m^{-2} then Venus' heat flux would be 71 mW m^{-2}. This value is likely much too high as an average for Venus as it lacks plate tectonics, so I use this value only as an absolute upper limit. Mantle convection modeling (Solomatov and Moresi 1996, Reese et al., 1998, Phillips et al., 1997) predicts heat flux values significantly less than 71 mW m^{-2}. For example, Solomatov and Moresi (1996) and Reese et al., (1998) both estimate a surface heat flux around 15 mW m^{-2} under a stagnant lid regime. Phillips et al., (1997) presented an updated model from Phillips and Malin (1983) by introducing core cooling and time-dependent stagnant lid convection where the thermal boundary layer thickness is controlled by thermal diffusion and convective heat flux from beneath; this results in an average surface heat flux of 35 mW m^{-2}. Phillips et al., (1997) also provided estimates from elastic thickness (T_e) values from hotspot locations (Atla, Beta, Western Eistla Regiones) using the following equation, which was derived using elastic flexure methods.

$$\frac{\mathrm{d}T}{\mathrm{d}z} = 9.54\left(\frac{T_e}{30}\right)^{-0.817} \tag{13}$$

The temperature gradient is converted to heat flux using Fourier's Law (equation 1). Elastic thickness is estimated to be ~30 km in my study regions (McKenzie and Nimmo, 1997; Barnett et al., 1999). Elastic thickness calculations require *apriori*

assumptions, such as crustal thickness and density. In order to broaden the range of potential heat flux values I will use a low and high estimate for T_e, 10 and 40 km, respectively, based on the thinnest elastic thickness estimate determined for Venus (Johnson and Sandwell, 1994) and the thickest elastic thickness determined for Venus (Phillips, 1994). For a crustal thermal conductivity of 3.3 W m^{-1} K^{-1} this produces a heat flux range of 23-70 mW m^{-2}. If a smaller crustal thermal conductivity of 2 W m^{-1} K^{-1} the heat flux range is 15-46 mW m^{-2}. I use these two heat flux ranges to analyze my results and determine whether the model predictions comply with geologic observations.

3.2.2 Lithosphere and Crustal Thickness

The lithosphere of Venus is thought to have thickened over the past few hundred million years, currently being ~300 km thick (Solomatov and Moresi, 1996; Moore and Schubert, 1995; Moore and Schubert, 1997; Kucinskas and Turcotte, 1994). Geoid-to-topography ratios (GTR) are useful for interpreting a planet's internal structure and can determine the ADC. The ADC is an indication of the depth at which topographic features are supported. Beneath Beta and Atla Regiones the ADC are 320 km and 260 km, respectively (James et al., 2013). These values support the idea that the topographic swell observed in both regions is compensated at depth by a thermal anomaly, such as a mantle plume (Morgan and Phillips, 1983; Moore and Schubert, 1995; Hansen et al., 1997).

An ADC value this deep is not seen on Earth. Earth has a weak asthenosphere that cannot sustain significant stresses, implying that Venus does not have an asthenosphere and, thus, the lithosphere is directly coupled to mantle dynamics

(Phillips et al., 1991). This is also consistent with the idea that Venus' interior is deficient in water, as water is often assumed to the cause of the weak, low viscosity asthenosphere on Earth (Phillips et al., 1997; Kaula, 1999; Green et al., 2010).

GTRs are also used to determine the crustal thickness. James et al., (2013) used GTRs to create a global crustal thickness map. The inversions were done using an upper limit on the crustal thickness of 70 km, based on the basalt-eclogite phase transition; eclogite is negatively buoyant and would start delaminating off the crust. The study found crustal thicknesses of ~25 km for both Beta and Atla Regiones. Another study by Anderson and Smrekar (2006) used the spectral version of the GTR, known as 'admittance spectrum', in order to create a crustal thickness map of Venus; they determined the same crustal thickness for Atla Regio as James et al., (2013), but a significantly thicker crust for Beta Regio (~65 km). To incorporate error I expand a 25 km crust to a range of 20-30 km, and a 65 km crust to a 60-70 km range.

3.3 Model Evolution

3.3.1 Lower Crustal Flow

The lower crustal flow equation tracks the lateral crustal thickness variation throughout rifting. Crustal flow is driven by lateral pressure gradients caused by crustal thickness variations, as shown by the following equation:

$$\frac{\partial h}{\partial t} = \kappa_f \frac{\partial^2 h}{\partial x^2} - u\frac{\partial h}{\partial x} - h\frac{\partial u}{\partial x} \tag{14}$$

where h is the crust thickness, t is time, κ_f is the effective flow diffusivity, x is the horizontal distance from the rift center, and u is the horizontal stretching velocity. The last two terms in equation 14 "describe the advection of crustal thickness

variations and the thinning of the crust due to the prescribed velocity field" (Buck, 1991).

Flow diffusivity has units of $m^2\ s^{-1}$, analogous to a kinematic viscosity. Flow diffusivity is given by equation 15.

$$\kappa_f = \frac{g\Delta\rho^* {y_0}^3}{\eta_{moho}} \tag{15}$$

with

$$y_0 = \frac{R{T_{moho}}^2}{E\frac{\partial T_{moho}}{\partial z}} \tag{16}$$

and

$$\Delta\rho^* = \frac{\rho_c(\rho_m - \rho_c)}{\rho_m} \tag{17}$$

Buck (1991) derived equation 15 for Newtonian viscosity; therefore, the variables in flow diffusivity equation are formulated to approximate non-Newtonian rheology that is used in the model.

The boundary conditions are:

$$\frac{\partial h}{\partial x} = 0, \text{for } x = 0 \text{ and } \frac{X_L}{2} \tag{18}$$

The flow diffusivity, κ_f, is used to determine whether crustal flow is significant enough to produce a core complex; if in the time of rifting, δt (48 Myr for all Venus results), the following inequality holds,

$$(\kappa_f\ \delta t)^{1/2} > \frac{X_e}{2} \tag{19}$$

then the lower crustal flow is significant and coupled with a decrease in total force would produce a core complex rift mode. If equation 19 is satisfied, then the lower crust spreads out a distance greater than the width of the zone of extension.

3.3.2 Heat Equation

The one dimensional heat equation is used to describe the temporal evolution of heat at the center of the rift. Lateral conduction is assumed *a priori* to not have significant effect on temperature at the rift center. Equation 20 is the advection-diffusion equation with a heat source H_{crust} (crustal heat production).

$$\frac{\partial T}{\partial t} = \kappa_{td} \frac{\partial^2 T}{\partial z^2} - v \frac{\partial T}{\partial z} + H_{crust} \tag{20}$$

The first right hand side term describes thermal diffusion, which acts to diffuse heat throughout the medium, the second term is the advection term, which describes the velocity at which heat is transferred throughout the lithosphere, and the last term represents the heat production.

The boundary conditions on the heat equation are such that the surface is kept at 740°K and the base of the lithosphere is maintained at the temperature where the viscosity is 10^{21} Pa s.

3.3.3 Solution Method

Once the initial conditions are determined, the lower crustal flow and heat equations are solved with a centered finite difference approach. Equations 21 and 22 show the form for first order and second order approximations, respectively, where *f* is the function being evaluated, *i* is the location where the function is being evaluated, and Δx is the node spacing.

$$\frac{\mathrm{d}f}{\mathrm{d}x} \approx \frac{f(i+\Delta x) - f(i-\Delta x)}{2\Delta x} \tag{21}$$

$$\frac{\mathrm{d}^2 f}{\mathrm{d}x^2} \approx \frac{f(i+\Delta x) - 2f(i) + f(i-\Delta x)}{2\Delta x} \tag{22}$$

The advection of heat that accompanies rifting may force the lithosphere to thin. In order to accommodate for this effect on the depth array, the heat equation is solved in a moving reference frame associated with changes of thickness of the crust and the lithosphere. The velocity, υ, is adjusted so that the grid nodes remain equally spaced in the crust and in the mantle, with a specific node following the base of the crust and another the base of the lithosphere.

In the crust, the depth of the moho is determined at each time step by solving the lower crustal flow equation, thus the motion of all points in the crust will be known as well. The depth points in the crust are distributed by the following,

$$Z_{crust} = \left(\frac{j-1}{N_C - 1}\right) \cdot Z_{moho} \tag{23}$$

Where j indicates the array element number, N_c is the total number of nodes in the crust, and Z_{moho} is the current depth of the moho. As the depth at which the lower crustal flow is significant is not defined we consider the change of thickness is uniformly distributed inside the crust. Therefore, in the crust material velocities are equal to the grid velocity and the heat equation in the crust reduces to,

$$\frac{\partial T}{\partial t} = \kappa_{td} \frac{\partial^2 T}{\partial z^2} + H_{crust} \tag{24}$$

Things are more complicated in the mantle where the grid points move vertically in response not only to the thinning crust, but also due to advection effects. The mantle points are re-gridded based on the following equation,

$$Z_{mantle} = Z_{moho} + \left(\frac{j - N_C}{N_L - N_C}\right)(Z_L - Z_{moho}) \tag{25}$$

Where Z_{moho} is the moho depth, j is the depth element number, N_L is the total number of elements in the lithosphere, and Z_L is the depth of the lithosphere at the current time. The physical velocity in the mantle due to advection is given by,

$$\upsilon_p = -\dot{\varepsilon}(z - Z_{moho}) + \frac{\mathrm{d}Z_{moho}}{\mathrm{d}t} \tag{26}$$

Thus the total velocity in the mantle is υ_p-υ_g

$$\nu_{tot} = -\dot{\varepsilon}(z - Z_{moho}) - \left(\frac{j - N_C}{N_L - N_C}\right)\left(\frac{\mathrm{d}Z_L}{\mathrm{d}t} - \frac{\mathrm{d}Z_{moho}}{\mathrm{d}t}\right) \tag{27}$$

This equation requires us to determine the velocity of lithospheric thickness changes, $\frac{\mathrm{d}Z_L}{\mathrm{d}t}$. In order to solve for this we need to determine the heat flux balance at the base of the lithosphere. There is a basal heat underneath the lithosphere, Q_a, due to convective processes beneath the lithosphere and a heat flux into the lithosphere, Q_L, due to the advective-diffussive processes described by the heat equation. In this scenario the heat equation at the base becomes,

$$\rho C_p\left(\frac{\partial T}{\partial t} + \upsilon_{tot}\frac{\partial T}{\partial z}\right) = -\frac{\partial Q}{\partial z} \approx -\frac{(Q_a + Q_L)}{\delta z} = -\frac{\left(Q_a + \kappa_{tc}\frac{\partial T}{\partial z}\right)}{\delta z} \tag{28}$$

In a reference frame moving with the grid, the change in temperature at the base of the lithosphere is zero $\left(\frac{\partial T}{\partial t} = 0\right)$ as the lithosphere is thermally defined, and we can solve for $\frac{\mathrm{d}Z_L}{\mathrm{d}t}$ giving,

$$\frac{\mathrm{d}Z_L}{\mathrm{d}t} = \frac{\mathrm{d}Z_{moho}}{\mathrm{d}t} - \dot{\varepsilon}(Z_L - Z_{moho}) + \kappa_{td}\left(\frac{Q_a}{\kappa_{tc}\delta T} + \frac{1}{\delta z}\right) \tag{29}$$

Where δT and δz are the change in temperature and depth, respectively, at the base of the lithosphere when determining Q_L. The heat equation in the rest of the mantle becomes,

$$\frac{\partial T}{\partial t} = \kappa_{td}\frac{\partial^2 T}{\partial z^2} - \left(\kappa_{td}\left(\frac{Q_a}{\kappa_{tc}}\frac{1}{\delta T} + \frac{1}{\delta z}\right)\right)\frac{\partial T}{\partial z} \tag{30}$$

Since we explicitly determine the depth of the lithosphere with equation 29, the boundary condition at Z_L is $\frac{\partial T}{\partial t} = 0$ as the lithosphere is thermally defined.

The model was programmed as a series of MATLAB scripts and utilizes the ODE15s solver to solve the heat and lower crustal flow equations. All the codes used are included in the appendix.

3.4 Total Force

The total force necessary to continue rifting the lithosphere determines what type of rift forms. The total force is the sum of the integrated yield strength (equation 31), crustal, buoyancy (equation 32), and thermal buoyancy (equation 33).

$$F_{ys} = \int_0^{Z_L} \sigma \, \mathrm{d}z \tag{31}$$

$$F_{cb} = g\int_0^{Z_L} (\rho_m - \rho_c) z \, \mathrm{d}z \tag{32}$$

$$F_{tb} = \int_0^{Z_L} (\rho(z) \cdot \alpha \cdot \delta T(z) \cdot z)\mathrm{d}z \tag{33}$$

The stress, σ, in equation 31 is the lesser of the brittle and ductile strength of the lithosphere (equations 5 and 6, respectively).

The dry rheologies used produce a smaller strength contrast between the crust and mantle of Venus compared to the strength contrast appropriate for the Earth. The

strength contrasts favors wide rifting as the thinned crust is replaced by a stronger mantle upon rifting and, thus, increases lithospheric yield strength. The effect is less important on Venus than on Earth.

As an example, a scenario with crust thickness of 30 km and surface heat flux of 45 mW m^{-2} is outlined in figures 7-11. The evolution of forces is shown in figure 7. The integrated yield strength and the crustal buoyancy dominate the change in force; the thermal buoyancy contributes negligibly to the overall force change due to the small temperature change, $\delta T(z)$, each depth element experiences. The strength of the lithosphere increases up until ~15 Myr, then it decreases until rifting ends at 48 Myr. This is observed in the temperature and strength profiles in figures 8-11. The temperature profile in figure 9 shows an initial cooling, and subsequent strengthening, of the lithosphere. Figures 10 and 11 show modest increasing lithospheric temperature and weakening. The strength at the end of rifting of nearly the same as the initial strength, and the crustal buoyancy dominates the change in force, favoring a wide rift. Crustal buoyancy is much larger when the initial crust is relatively thick. This is because crustal buoyancy relies on the total amount of crustal thinning, not a ratio of the initial and final crust thickness, and a thicker crust will have a greater amount of thinning than a crust that starts relatively thin.

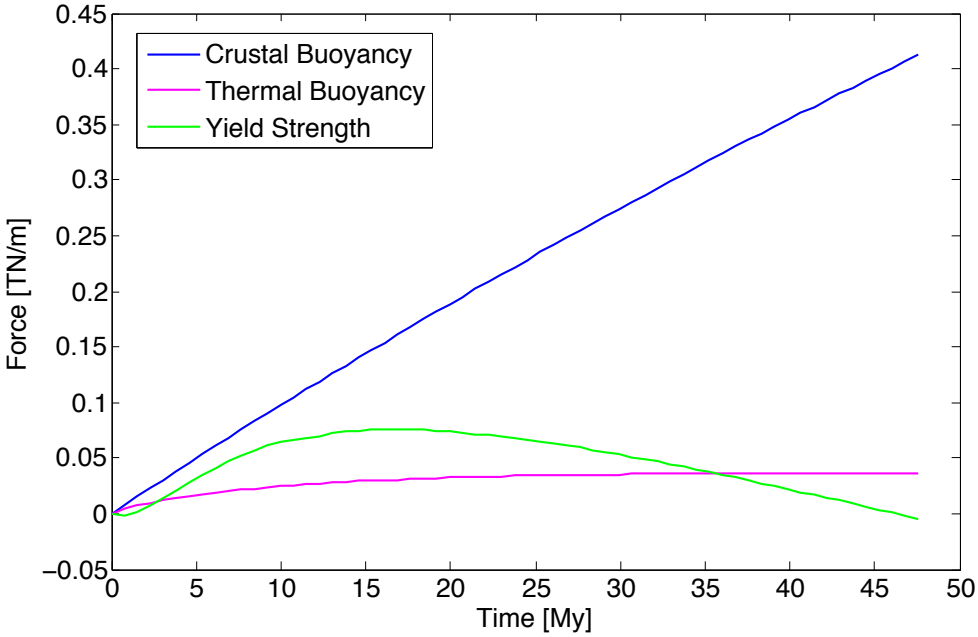

Figure 7: Example of the temporal evolution of change in forces throughout rifting for an initial crust of 30 km and a surface heat flux of 45 mW m^{-2}. The crustal buoyancy (blue) and yield strength (green) dominate force evolution, with thermal buoyancy (pink) having a smaller contribution due to the small temperature changes at the depth points. In this scenario, the yield strength initially increases, then decreases to roughly the initial strength. The crustal buoyancy increase dominates, and a wide rift is predicted.

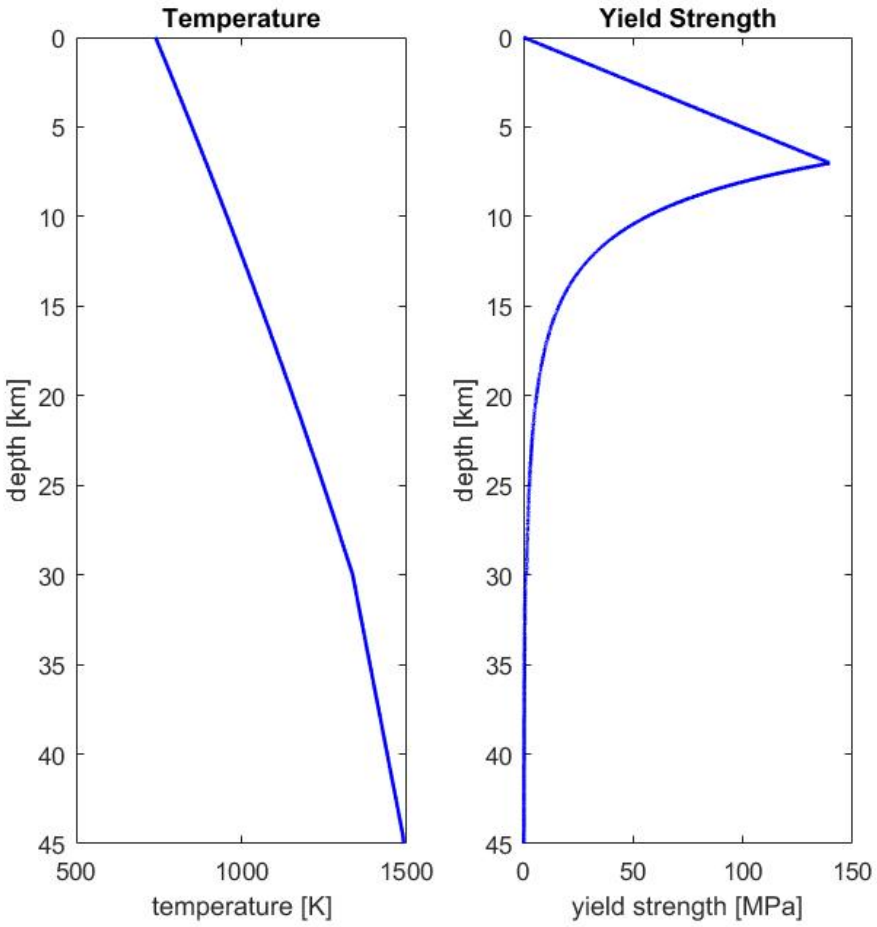

Figure 8: The initial steady state temperature profile (left) and associated yield strength envelope (right) for the model in figure 8.

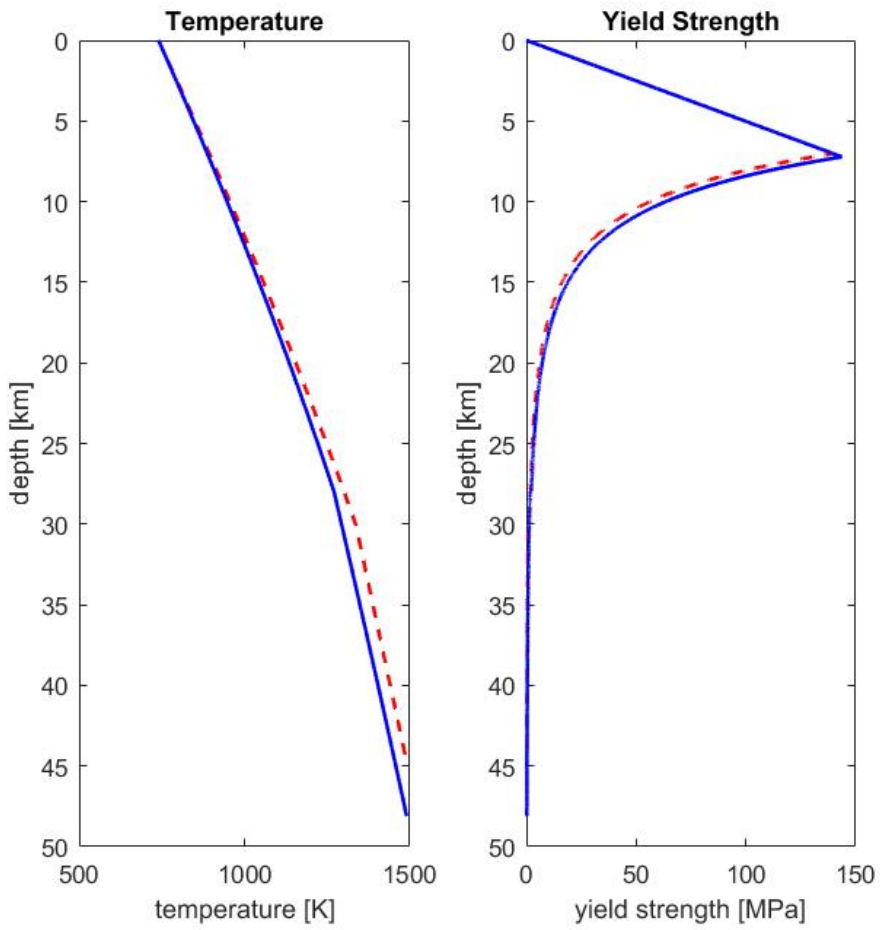

Figure 9: Comparison of the temperature (left) and yield strength (right) profiles after 22 Myr of extension (blue) and the initial values (dashed red) for the model in figure 9.

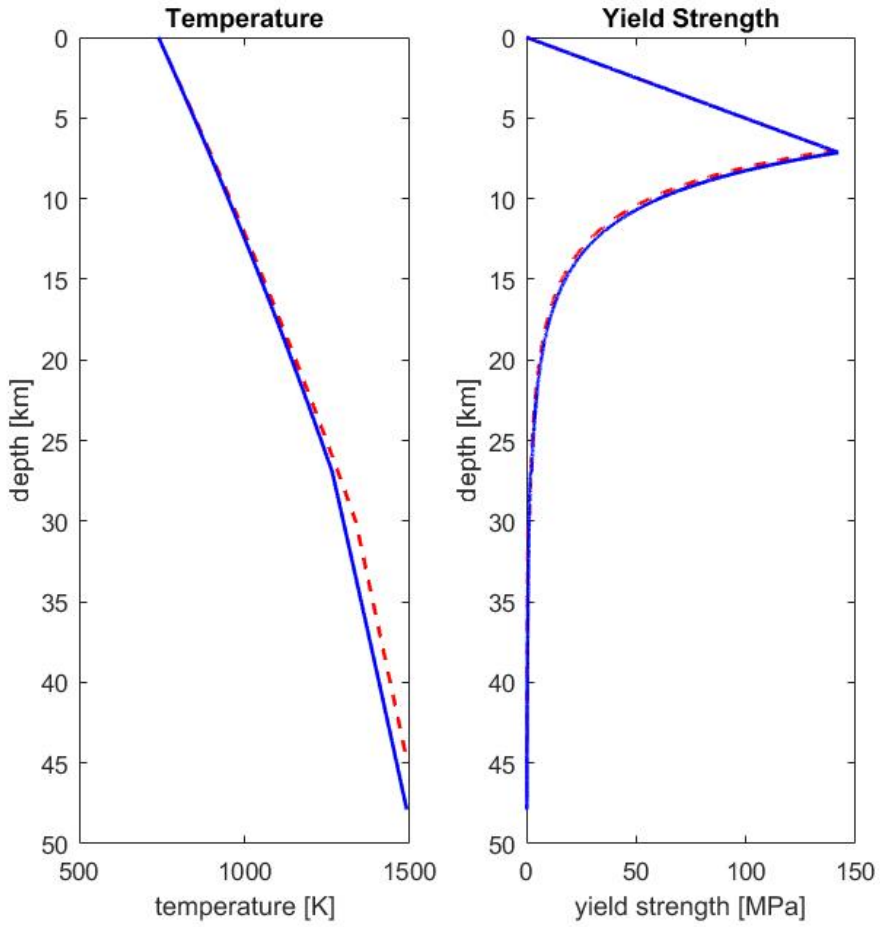

Figure 10: Comparison of the temperature (left) and yield strength (right) profiles after 34 Myr of extension (blue) and the initial values (dashed red) for the model in figure 9.

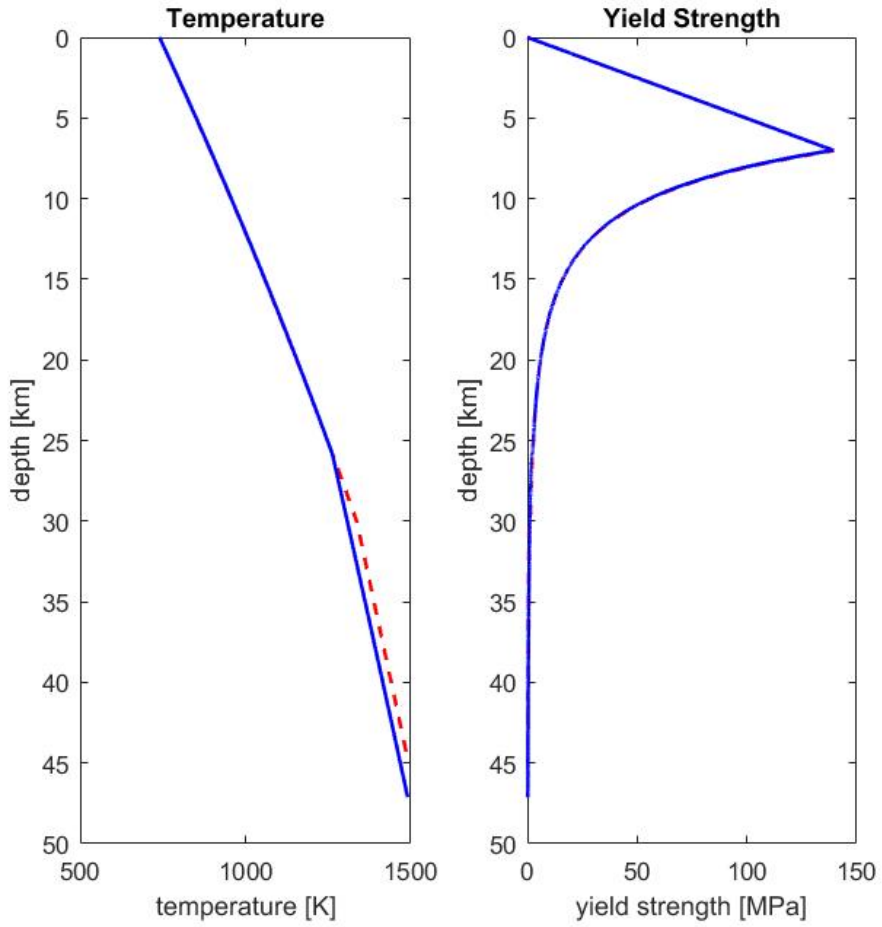

Figure 11: Comparison of the temperature (left) and yield strength (right) profiles after 48 Myr of extension (blue) and the initial values (dashed red) for the model in figure 9.

4. Results

4.1 Earth (comparison to Buck, 1991)

To test our code we compare first our results to those shown in Buck (1991). Although Buck included multiple rheologies and rift initial conditions, I only include a comparison for the rifting scenario of a dry quartz crust, wet olivine mantle, X_e = 40 km, X_L = 250 km, u_x = 1 cm yr^{-1}, and a maximum strain of 0.25.

When using results from a code that does not account for high crustal temperature and does not include a moving boundary that accounts for lithospheric necking, results (figure 13) are similar to those given in Buck (1991) (figure 12),

however, there are a few differences that need to be pointed out. First, my results predict more wide rifts than those from Buck (1991), specifically for runs with thicker crust. Second, my results predict less core complex rifts than the results from Buck (1991). I do not perfectly replicate Buck's results, as I do not know the details on how Buck solved for the initial temperature profile and the differential equations.

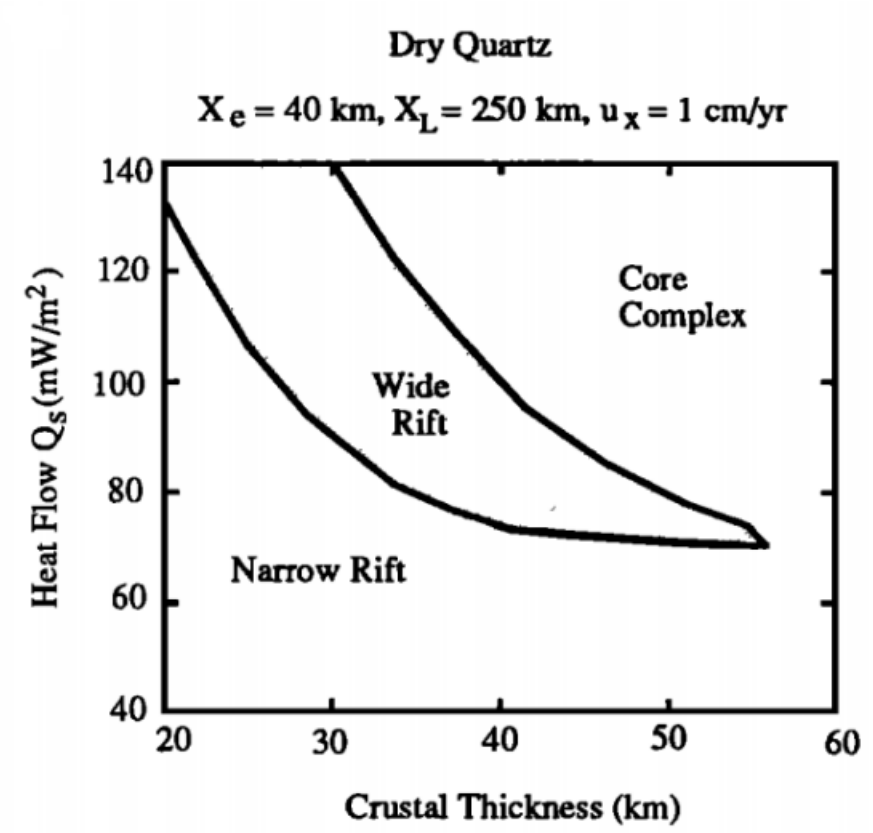

Figure 12: Rift mode boundaries in crustal thickness-surface heat flux space provided from Buck (1991). Crustal thickness and surface heat flux are the initial values used in the model setup, as opposed to using the crustal thickness modified by lower crustal flow.

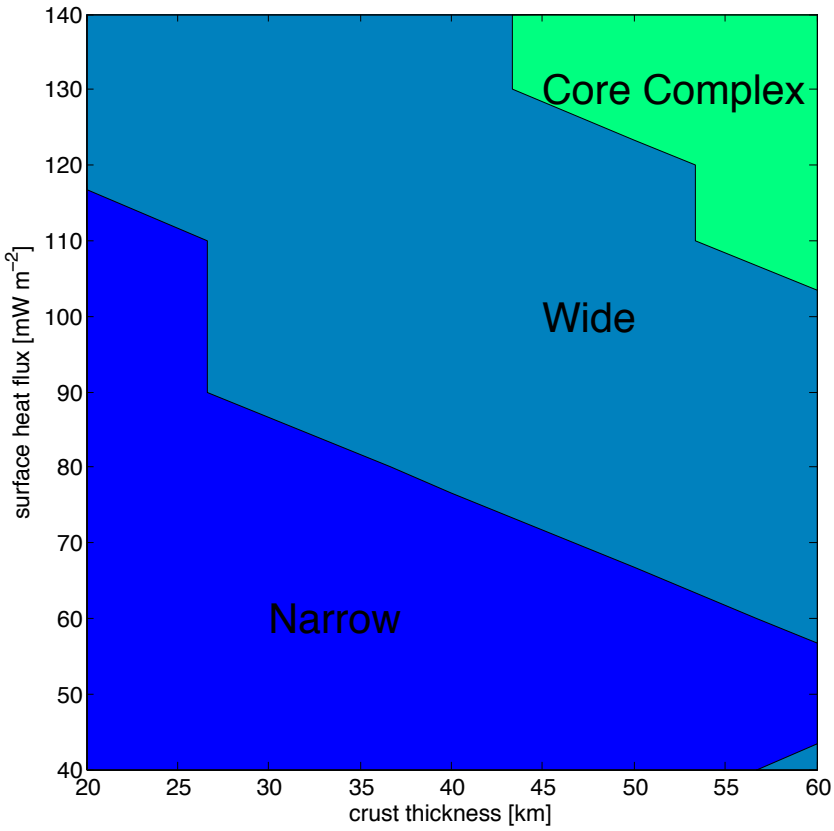

Figure 13: Rifting mode for a model similar to that of Buck (1991) with a fixed grid and including model outputs that would not be geologically realistic.

When using a more complex code that rejects the unrealistic conditions I outlined in section 4.1 and uses a moving point boundary there are some more substantial differences with combinations of thick crust and high heat flux, at which point magmatic processes become important.

The second set of results is shown in figure 14. The white space indicates runs that result in one of the non-geological conditions outlined previously (for a thick crust and high heat flux this corresponds to exessive moho temperatures, and for thick crust and low heat flux this corresponds to a negative moho heat flux or a lithosphere that exceeds 400 km). The condition that is met is labeled on the figure 14, as in all the result figures in the following sections. The transition from narrow

rift to wide rift is similar to the Buck (1991) results (figure 12); however, core complexes are predicted in a narrower region.

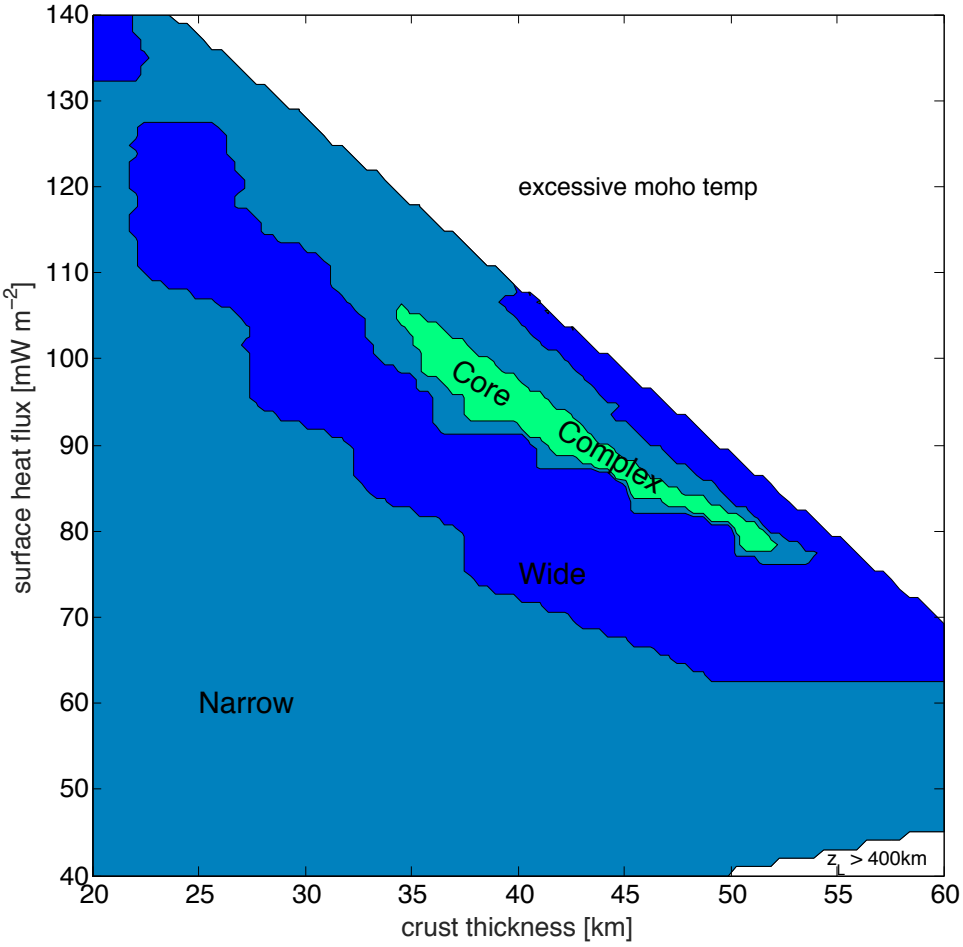

Figure 14: Rift modes predicted for a model that uses my moving grid algorithm and rejects geologically unrealistic model outcomes. Model setup is similar to Buck (1991).

Buck (1991) allows for very high moho temperatures (figure 15), which he acknowledges might not be attainable and because the lower crust would start to melt and/or convect. This differs from my code which does not allow for a crust that partially melts (section 4.1). This, along with not knowing the details of how Buck accounted for lithospheric thinning and solved the differential equations, lead to terrestrial results that differ from those presented in Buck (1991).

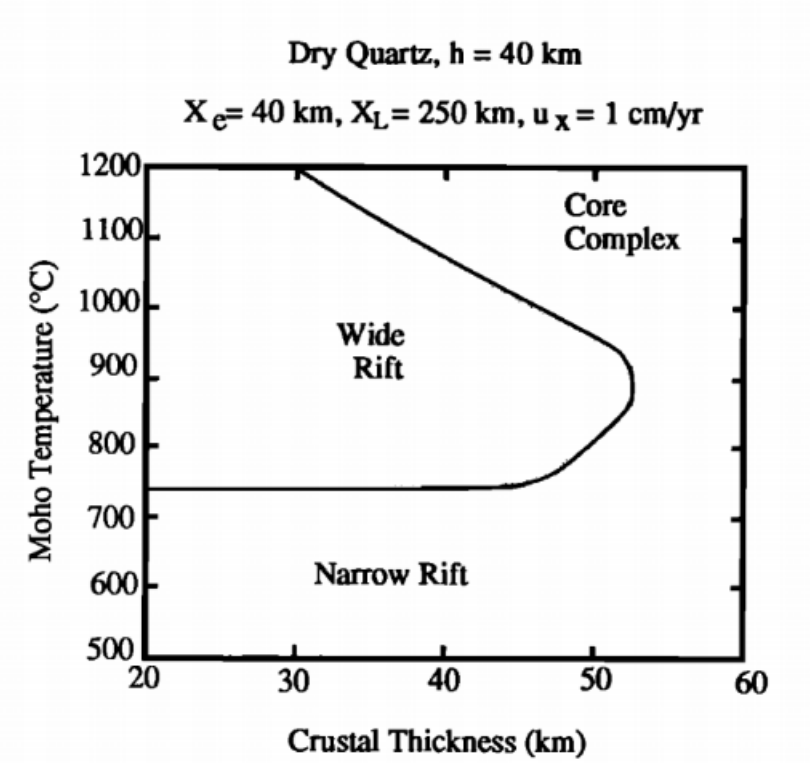

Figure 15: Plot of crust thickness vs. moho temperature from Buck (1991). This indicates that for many runs the crust attains high enough temperatures to begin melting.

4.2 Venus Results

When presenting the Venus model results, the pink rectangle indicates the crustal estimate range for Devana and Ganis Chasmata using James et al., (2013), the teal rectangle indicates the crustal estimate for the Devana Chasma area from Anderson and Smrekar (2006), and the green rectangle indicates the crustal estimate range for Parga and Hecate Chasmata from Smrekar et al., 2010. The surface heat flux is even more uncertain and I use the ranges described in section 3.3.2 for all the rifts; Parga and Hecate are likely on the higher end of the heat flux range due to the increased magmatic activity and lower elastic thickness values.

4.2.1 Constant and depth-dependent thermal conductivity

Two initial results are shown, one for a constant lithospheric thermal conductivity (figure 16) and for a depth-dependent thermal conductivity (figure 17). It

is evident that the thermal conductivity of the crust has a significant effect on the results. A constant thermal conductivity produces rifts that are compatible with observations for Devana and Ganis Chasmata (James et al., 2013) at crustal thicknesses <24 km and heat fluxes <50 mW m^{-2}, while the Devana Chasma crustal estimates from Anderson and Smrekar (2006) result in geologically unrealistic model outcomes for all model runs in this region. A depth dependent thermal conductivity models the lithosphere more accurately, however, it is clearly not compatible with observations as wide rifting is predicted for nearly the Devana and Ganis Chasmata (James et al., 2013) estimates and, again, the Anderson and Smrekar (2006) crustal estimate fails to reproduce results. The crust estimate of 65 km seems unlikely given these results, and I will only focus on the James et al., (2013) crustal estimates for Devana and Ganis Chasmata from now on. Assuming that these crustal thickness and surface heat flux estimates are not severely wrong, there must be some mechanism working in conjunction with rifting to produce the narrow rifts Devana and Ganis Chasmata in spite of the reduced thermal conductivity of the crust.

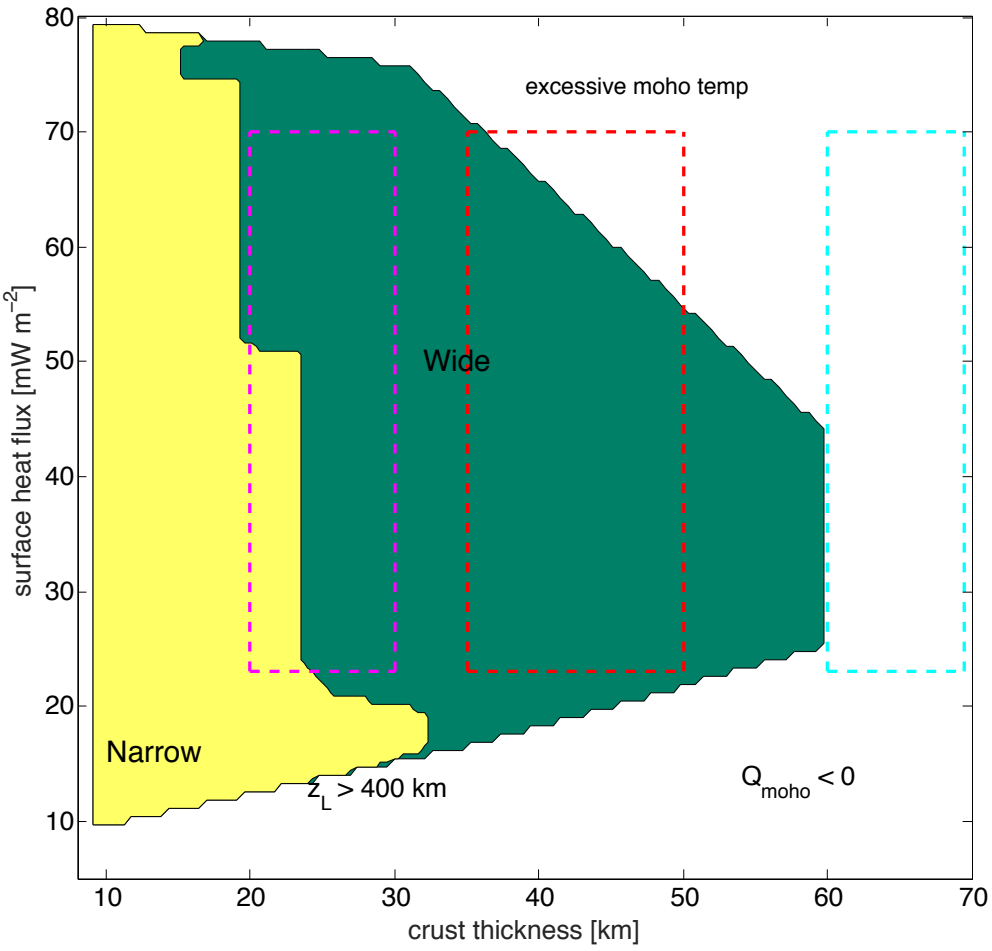

Figure 16: Rifting modes predicted for a constant lithosphere thermal conductivity of 3.3 W m^{-1} K^{-1}. The rectangles indicate crustal thickness and heat flux estimate ranges. Pink: Devana and Ganis Chasma (James et al., 2013), red: Parga and Hecate Chasmata (Martin et al., 2007; Smrekar et al., 2010), teal: Devana Chasma (Anderson and Smrekar, 2006).

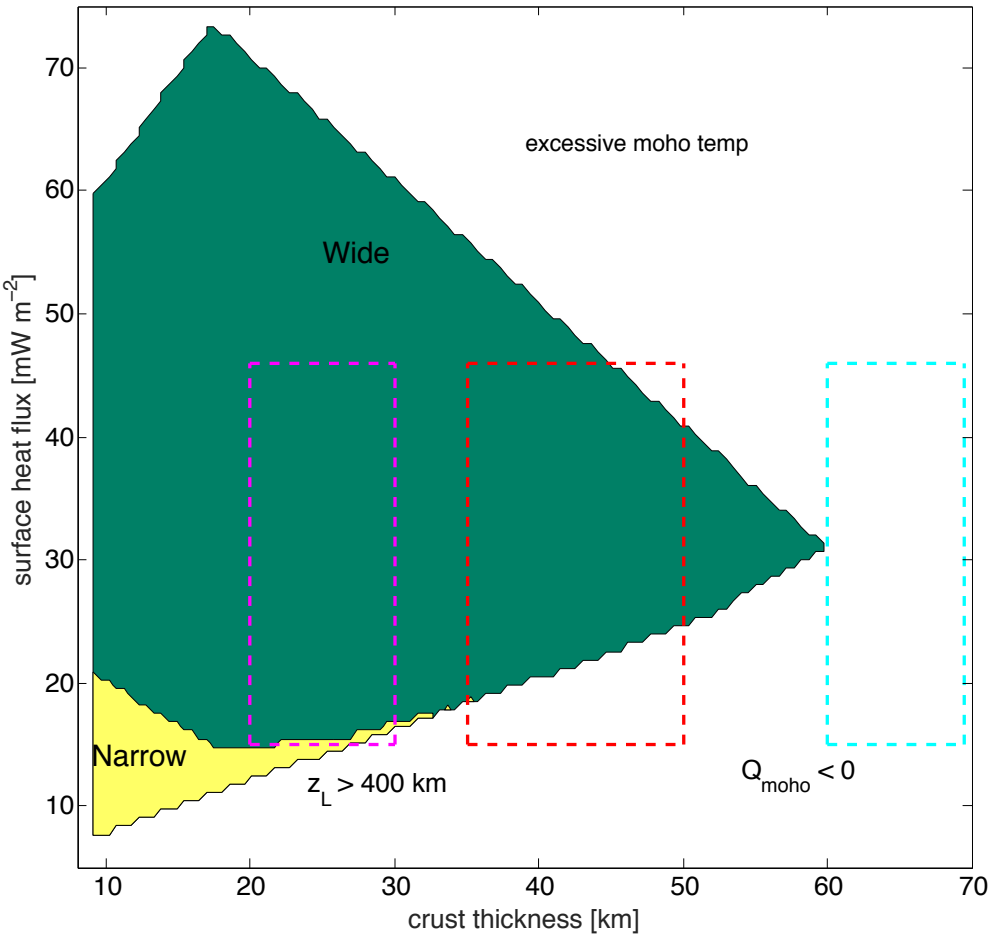

Figure 17: Rifting modes predicted for a depth dependent thermal conductivity; 2 W m^{-1} K^{-1} in the crust and 3.3 W m^{-1} K^{-1} in the mantle. The dashed rectangles indicate the same estimate ranges as described in Figure 16, and are the same for all following result figures.

As another application of my model I analyze the results in the context of the rifts Parga and Hecate Chasmata, which, as mentioned in section 1.2, are wide rifts in the BAT region but are associated with coronae. The results for constant thermal conductivity comply well with observations as wide rifts are predicted for nearly all of the runs. For roughly 25% of the runs there is an excessive moho temperature and no results are recorded. Wide rifts are predicted in the depth-dependent thermal conductivity results for the vast majority of model runs, except for the lowest surface

heat flux estimates (< 25 mW m^{-2}), which result in a lithosphere that exceeds the 400 km limit.

4.3 Possible Mechanism to Produce Narrow Rifting

It is evident that the standard model, following Buck (1991) does not accurately describe the physics of rifting: using the more realistic depth-dependent thermal conductivity, the model typically predicts wide rifts on Venus where narrow rifts are observed. Two mechanisms may be envisioned that would encourage the localization of deformation needed for narrow rifting: strain-weakening and diking.

4.3.1 Strain-Weakening

The geological record shows that ductile creep surprisingly often forms shear zones, which accommodate high levels of strain and typically feature gain size reduction (Braun et al., 1999; Yamasaki 2004; Montési, 2013; Gueydan and Precigout, 2014). Many shear zones on Earth are found in exhumed portions of the lower crust and mantle and are characterized by mylonites (figure 18). The fine-grained mylonitic texture is the product of dynamic recrystallization, and may enable grain size sensitive deformation mechanisms to be activated (Etheridge and Wilkie, 1979). Hydrated minerals and a layered fabric are also thought to play an important role in ductile localization on Earth (Gueydan et al., 2003; Holyoke and Tullis, 2006; Montési 2007, 2013). However, these mechanisms may not translate to a presumably dry Venus. A switch in rheology from grain size insensitive (dislocation creep) to grain size dependent (diffusion creep or dislocation-accommodated grain boundary sliding, also called dis-GBS) may enable ductile localization on Venus. This

rheological transition been proposed as a mechanism for strain localization on Earth (Drury, 2005; Warren and Hirth, 2006; Precigout et al., 2007; Gueydan et al., 2014).

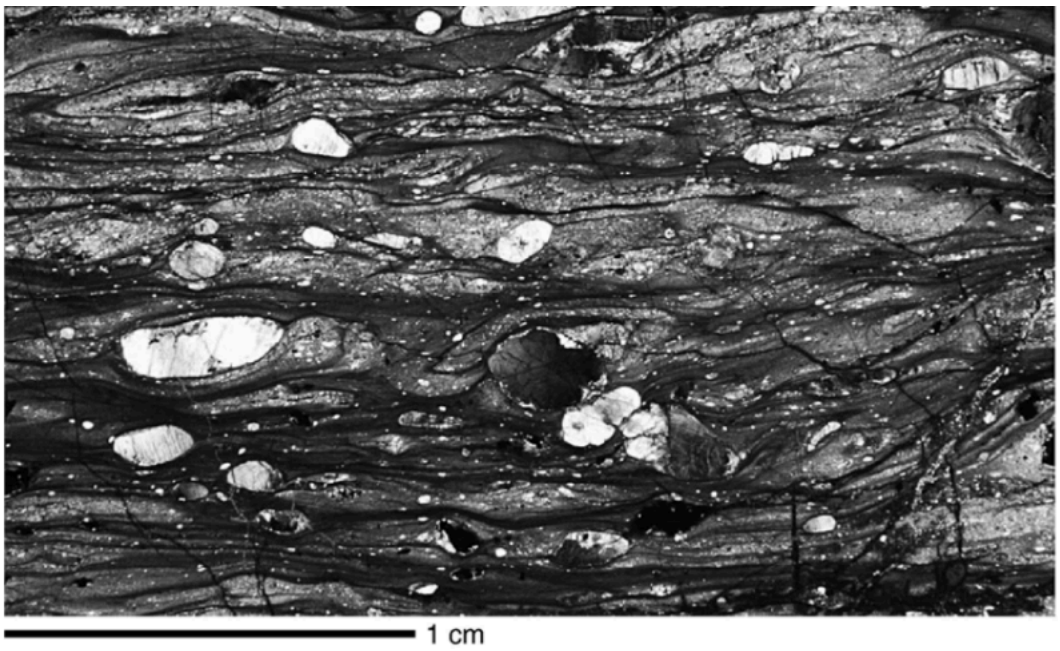

Figure 18: An example of a shear zone with mylonitic texture produced by grain size reduction (Warren and Hirth, 2006). This sample of peridotite shows bands of coarse and fine grains formed from grain size sensitive deformation.

I do not focus on specific mechanisms for imposing weakening in the lithosphere. The importance of these processes is that they reduce the strength of the lithosphere, which reduces the total force needed to continue rifting and therefore favor the development of narrow rifts. To evaluate the potential of strain-weakening to change the mode of rifting on Venus I adopt the simplified strain-weakening formulations of Gueydan et al. (2014), who approximate the effect of various weakening processes on strength as an exponential function of strain:

$$\sigma(\varepsilon) = \sigma_0 \exp\left(-\frac{\varepsilon}{\varepsilon_C}\right) \tag{34}$$

In this formulation, σ_0 is the pre-weakened strength and ε_c is the critical strain that determines the time scale of weakening. A low ε_c means faster, more efficient

weakening, and therefore more intense localization. Gueydan et al. (2014) note that the critical strain is poorly constrained; in the mantle, estimates are based on laboratory work on grain size reduction and in the crust, they rely on kinetics of metamorphic reactions. Both are very poorly constrained. Gueydan et al. (2014) vary ε_c between 0.5 and 2. I show results using values between 0.1 and 0.5; these lower values are necessary to significantly affect the results, considering the limited strain accumulated in the Venusian rifts. It may be that the weakening processes acting on Venus operate faster than on Earth, or that the estimates for Earth are in error.

Gueydan et al. (2014) assume grain size reduction as the mechanism for localization in the mantle, which could be appropriate for Venus. However, in the crust they suppose microstructural evolution, the development of phyllosilicate minerals such as mica and talc. These minerals are not expected on a dry Venus and thus are not applicable mechanisms to induce localization. It is noted in Montési (2013) that the presence of melt is often associated with shear zones and may act to localize deformation; this might be an active mechanism on Venus. Additionally, Hirth and Kohlstedt (1995) experimentally show that the dynamically recrystallized grain size in mantle rocks may decrease with the addition of melt due to melt inhibiting grain growth. This decrease in grain size may promote a transition from dislocation creep to grain size sensitive creep.

I consider two scenarios for lithospheric weakening; one which includes strain weakening in both the ductile and brittle regimes (figures 19, 20, 21) and one that only includes it for the ductile regime (figures 22, 23). These results are for a depth

dependent thermal conductivity, 2 W m^{-1} K^{-1} in the crust and 3.3 W m^{-1} K^{-1} in the mantle.

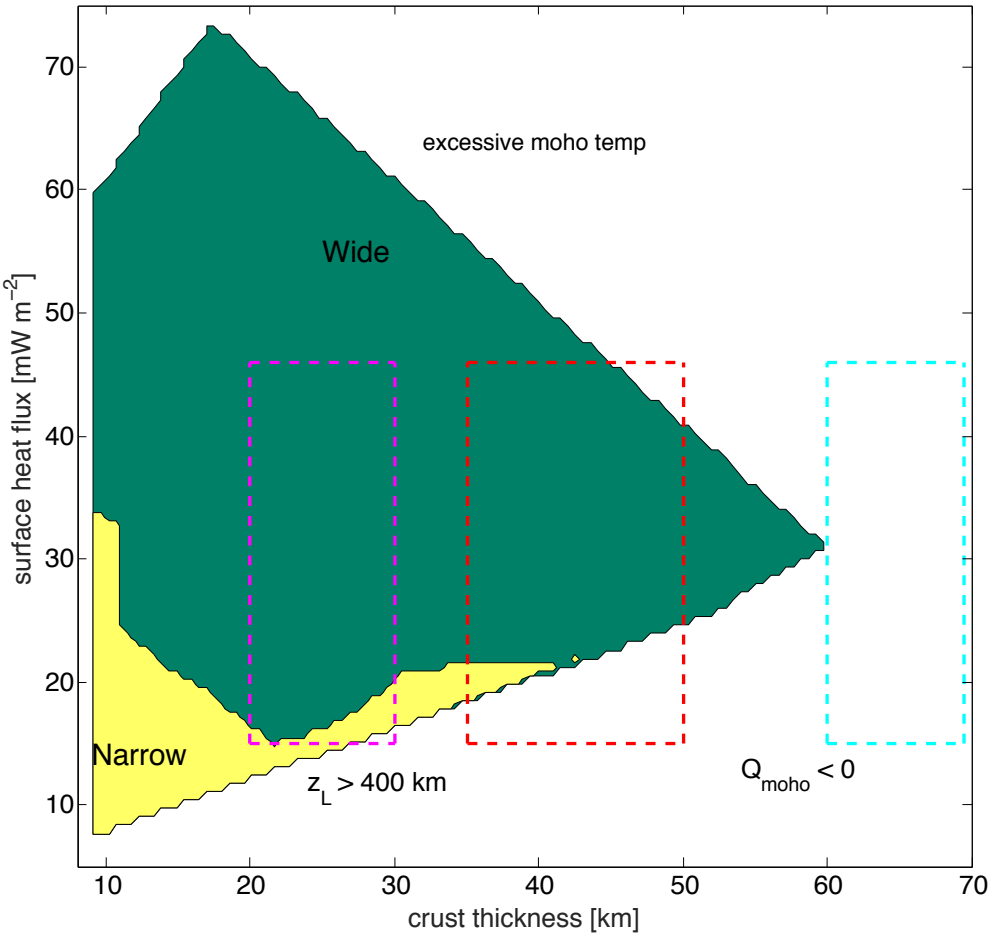

Figure 19: Rifting modes predicted for a depth dependent thermal conductivity; 2 W m^{-1} K^{-1} in the crust and 3.3 W m^{-1} K^{-1} in the mantle. There is weakening in both brittle and ductile regimes (ε_c = 0.5).

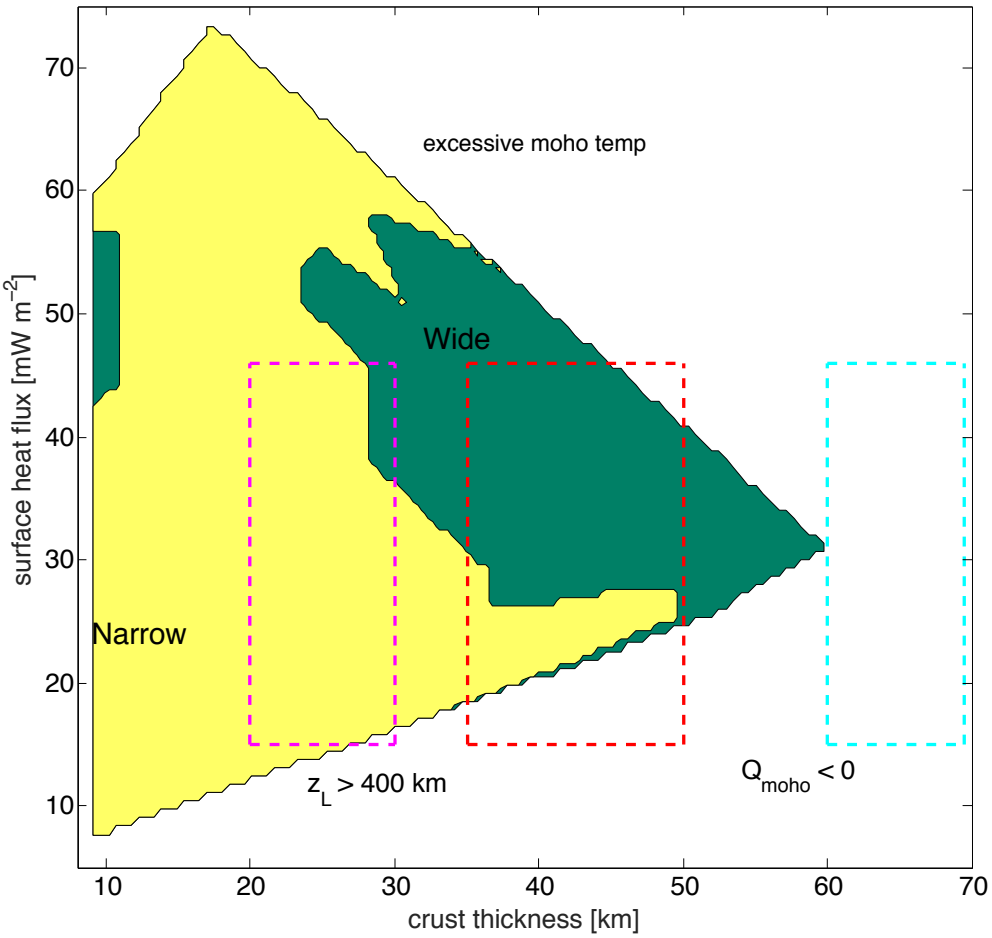

Figure 20: Rifting modes predicted for a depth dependent thermal conductivity; 2 W m^{-1} K^{-1} in the crust and 3.3 W m^{-1} K^{-1} in the mantle. There is weakening in both brittle and ductile regimes (ε_c = 0.25).

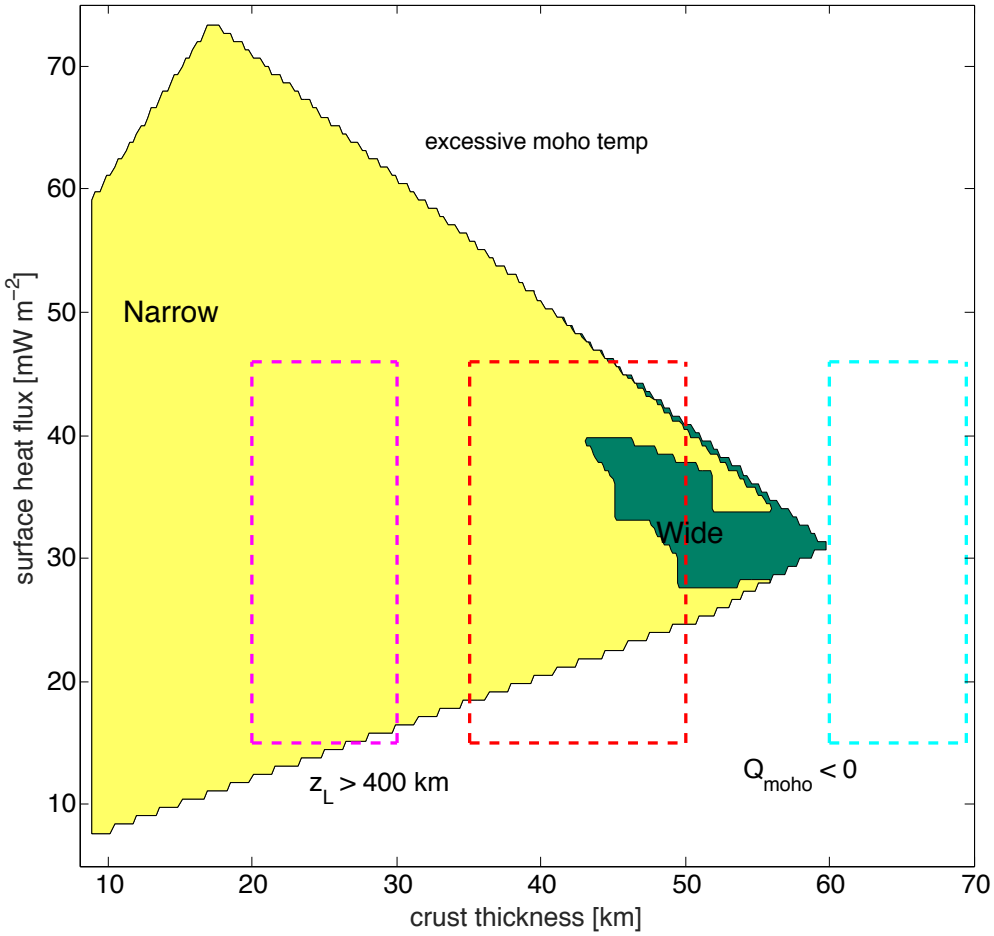

Figure 21: Rifting modes predicted for a depth dependent thermal conductivity; 2 W m^{-1} K^{-1} in the crust and 3.3 W m^{-1} K^{-1} in the mantle. There is weakening in both brittle and ductile regimes (ε_c = 0.1).

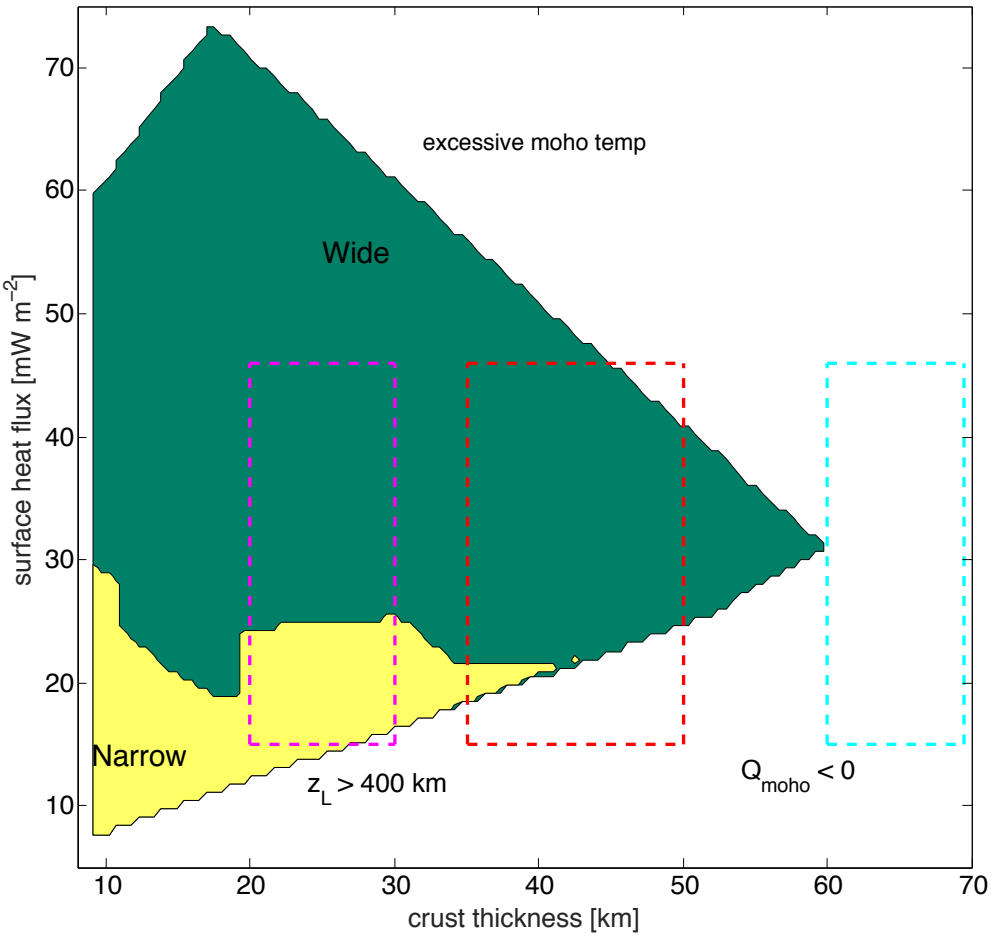

Figure 22: Rifting modes predicted for a depth dependent thermal conductivity; 2 W m^{-1} K^{-1} in the crust and 3.3 W m^{-1} K^{-1} in the mantle. There is weakening in only the ductile regimes (ε_c = 0.25).

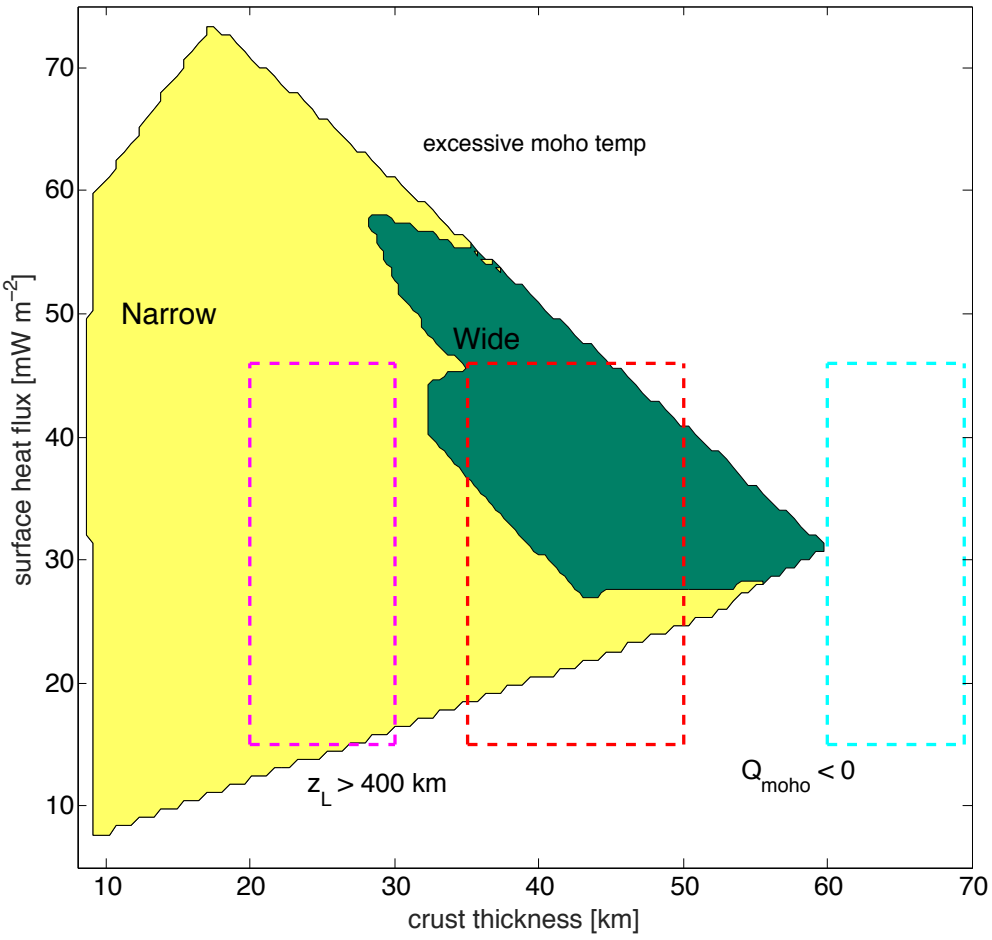

Figure 23: Rifting modes predicted for a depth dependent thermal conductivity; 2 W m^{-1} K^{-1} in the crust and 3.3 W m^{-1} K^{-1} in the mantle. There is weakening in only the ductile regimes (ε_c = 0.1).

Figure 20 shows weakening in both the brittle and ductile regimes for ε_c=0.5. A larger model space than in the case without weakening (figure 19) results in narrow rifts. Conditions describing Devana and Ganis Chasmata (pink outline) only predict narrow rifts for surface heat flux < 25 mW m^{-2}. The conditions for Parga and Hecate Chasmata (red outline) predict wide rifts for heat flux > 25 mW m^{-2}, or about half of the allowed parameter space.

The effects of weakening are enhanced by decreasing ε_c to 0.25 (figure 20) causing a substantial change in the predicted rifting mode. When ε_c = 0.25, narrow rifts are predicted for nearly all the conditions representing Devana and Ganis

Chasmata. Wide rifts are predicted for about half of the Parga and Hecate Chasmata conditions, with the remaining runs resulting in narrow rifts or a geologically unrealistic outcome. Rift modes predicted for a critical strain of ε_c =0.1 is shown in figure 21. In this scenario, weakening is so significant that narrow rifts are predicted for the entire parameter space; this amount of weakening seems excessive as Parga and Hecate Chasmata are observed to have characteristics of wide rifts. While the critical strain is a poorly constrained parameter, a value of 0.25 produces significantly faster weakening than the proposed average terrestrial value in Gueydan et al., (2014). Venus conditions, such as elevated temperature and rheology, may encourage enhanced weakening mechanisms.

Figures 22 and 23 show results when weakening is restricted to the ductile regime. An even lower critical strain that before is required to match the rifting style observed on Venus. A ε_c of 0.25 (figure 20) is no longer enough to form narrow rifts for the crustal thickness and heat flux estimates representing Devana and Ganis Chasmata; the critical strain needs to be decreased to 0.1 in order to obtain the correct rifting mode (figure 23). As before, though, only about half of the surface heat flow values result in wide rifts at Parga and Hecate Chasmata. More work needs to be done in order to properly constrain whether such a critical strain value is realistic. Instead, I use these results to argue that for both results, including brittle weakening and not including it, weakening mechanisms on Venus must be enhanced compared to the current terrestrial understanding.

4.3.2 Diking

Magmatic intrusions, such as dikes, have been invoked as a mechanism for reducing the brittle lithospheric strength (Buck, 2004; Buck, 2006; Bialas et al., 2010). In particular, diking significantly reduces the amount of force necessary to initiate rifting (figure 24).

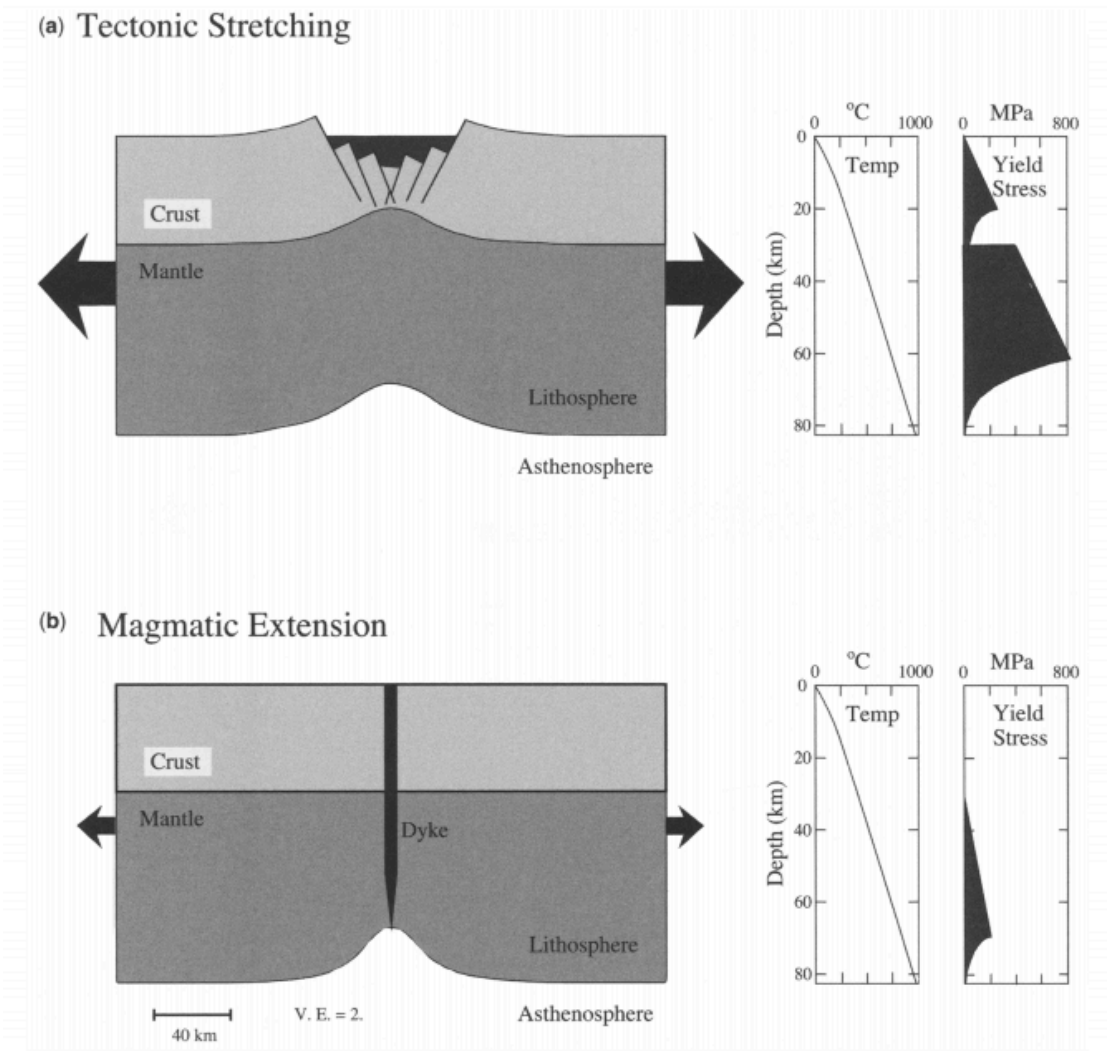

Figure 24: a) Tectonic extension of the lithosphere with associated yield strength profile. b) Extension via magmatic processes (i.e., diking) with associated yield strength profile. Note the dramatic reduction in strength for the magmatic scenario. The larger arrows in figure a indicates the larger force necessary to rift the lithosphere compared to figure b. (Buck, 2006)

Diking causes the brittle lithospheric yield strength to increase linearly with depth and depends on the density contrast between the magma and the surrounding rock (Buck, 2004; Buck, 2006), so that the brittle strength becomes,

$$\sigma_b(z) = \left(\rho_S - \rho_{magma}\right) \cdot g \cdot z \tag{35}$$

where ρ_s is the density of the surrounding rock and the magma density (ρ_s) is taken to be 2700 kg m^{-3}. Dikes can also thermally weaken the lithosphere, but this effect is not taken into account in my work and I focus solely on the strength reduction due to the density contrast.

Based on a buoyancy argument, all dikes on Venus should propagate to the surface after initiation. Since compaction effects on crustal density are not taken into account, the magma is always less dense than the surrounding crustal rocks and will not encounter a level of neutral buoyancy. As shown in Parfitt and Wilson (2008), density traps are more influential on dike propagation than stress traps related to fracturing the crustal rock. This physical argument coupled with the observations of surficial fractures associated with dikes on Beta and Atla Regiones (Grosfils and Head, 1994a; Nagasawa et al., 1998; Ernst et al., 2001) support the idea that dikes typically propagate to the surface.

The solidus from Hirshmann (2000) is used to determine if and when the mantle begins to partially melt and allow dike propagation.

$$T_{solidus} = -5.1404654 \cdot P^2 + 132.8999012 \cdot P + 1120.66061 \tag{36}$$

For each time step the solidus temperature profile is determined and compared to the lithosphere temperature profile. If the mantle crosses the solidus then a dike is emplaced at the associated depth and is propagated to the surface.

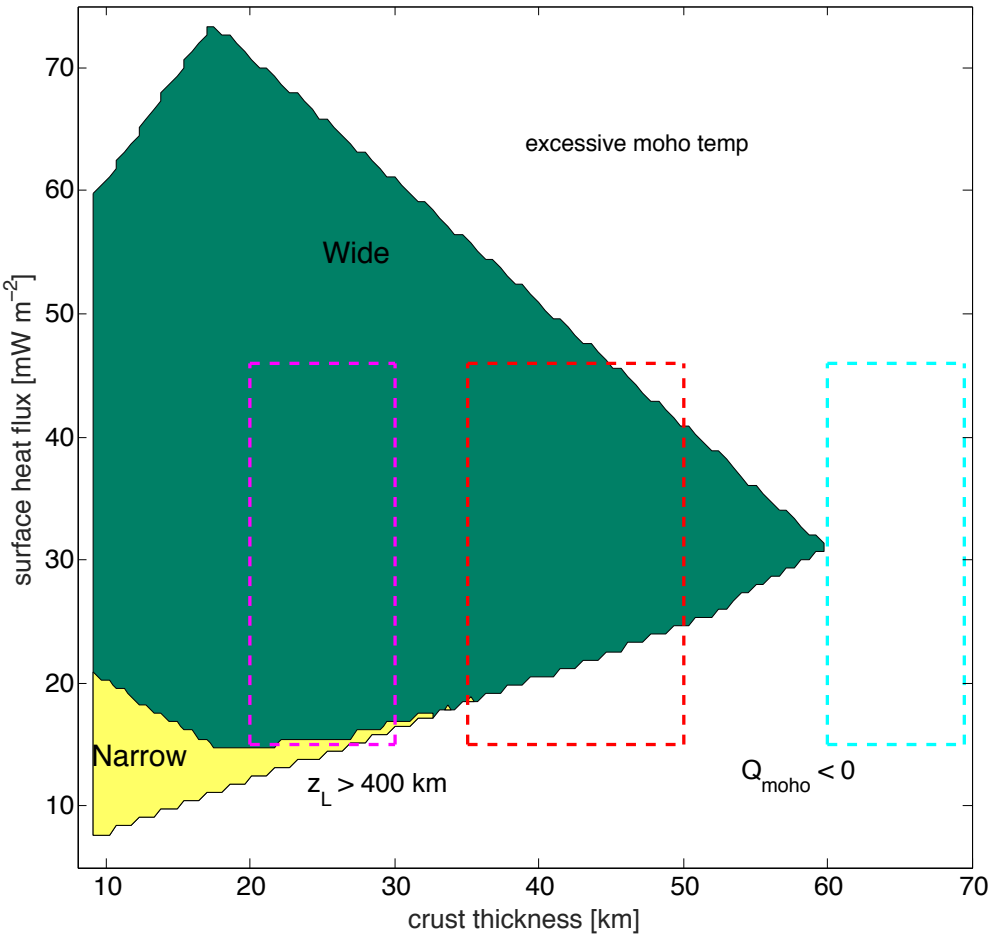

Figure 25: Rifting modes predicted for a depth dependent thermal conductivity; 2 W m^{-1} K^{-1} in the crust and 3.3 W m^{-1} K^{-1} in the mantle, with diking. Diking produces no effect on the results.

Model results show that diking has no impact of the resulting rift styles (figure 25 is identical to figure 17). Most runs do not result in partial melting in the mantle, and for all of the runs that do the solidus is crossed at the moment of rift initiation. If partial melting starts after the onset of rifting, then there is a significant strength reduction from the initial strength profile and the final strength profile. However, if partial melting occurs for the initial steady state profile (at t=0), then there is no significant strength reduction between the initial strength profile and the final strength profile (figure 26), although the force necessary for rifting is always low. The model relies on the change in *total* force. Thus, if the lithosphere starts out weakened by a

dike intrusion, the change in lithosphere strength is small and does not encourage narrow rifting.

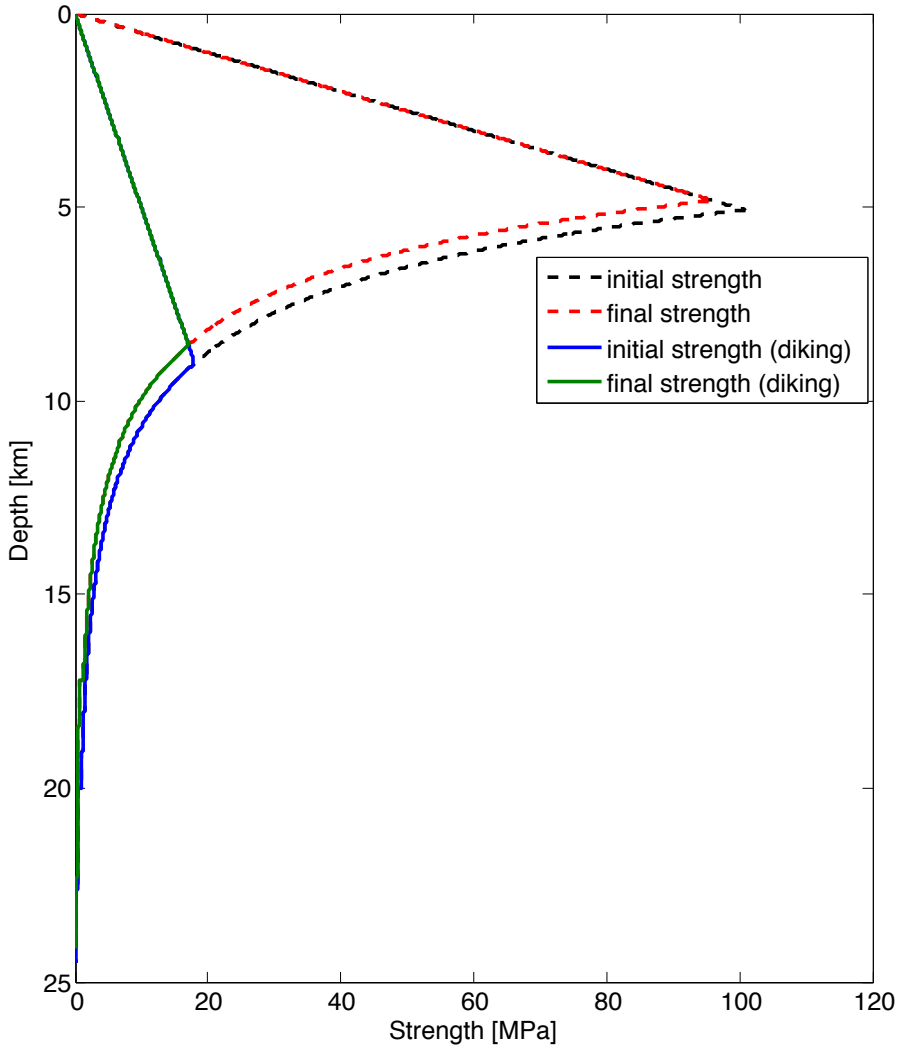

Figure 26: A comparison of lithospheric strength when there is no diking (dashed) and when diking is included (solid). In this case (20 km crust and 70 mW m^{-2} heat flux) and all other runs that have mantle partial melting, the temperature crosses the solidus at the onset of rifting, which causes the overall strength reduction to be small. A wide rift is predicted for both runs, with and without diking.

I also include results where the effects of rheological weakening and diking are combined. Diking in combination with strain weakening does not facilitate narrow rifting. There is no change in the predicted rift modes, as seen in figure 27 for a critical strain of 0.5. At this critical strain value the results are identical to those in

figure 19 where there is only strain-weakening. At a critical strain of 0.1 and no brittle weakening the addition of diking promotes *wide* rift modes (figure 28). As mentioned, mantle partial melting always occurs at the onset of rifting in these results, creating a lithospheric yield strength that starts out weakened. The effects on strength reduction from strain- weakening are hindered because if the lithosphere is already weak there is less of an effect of the strength reduction. It is clear in figure 30 that the yield strength with only weakening has a substantially larger strength reduction than the scenario that includes both weakening and diking. For weakening and diking, processes that delocalize deformation (i.e., crustal buoyancy) dominate the force evolution producing a wide rift.

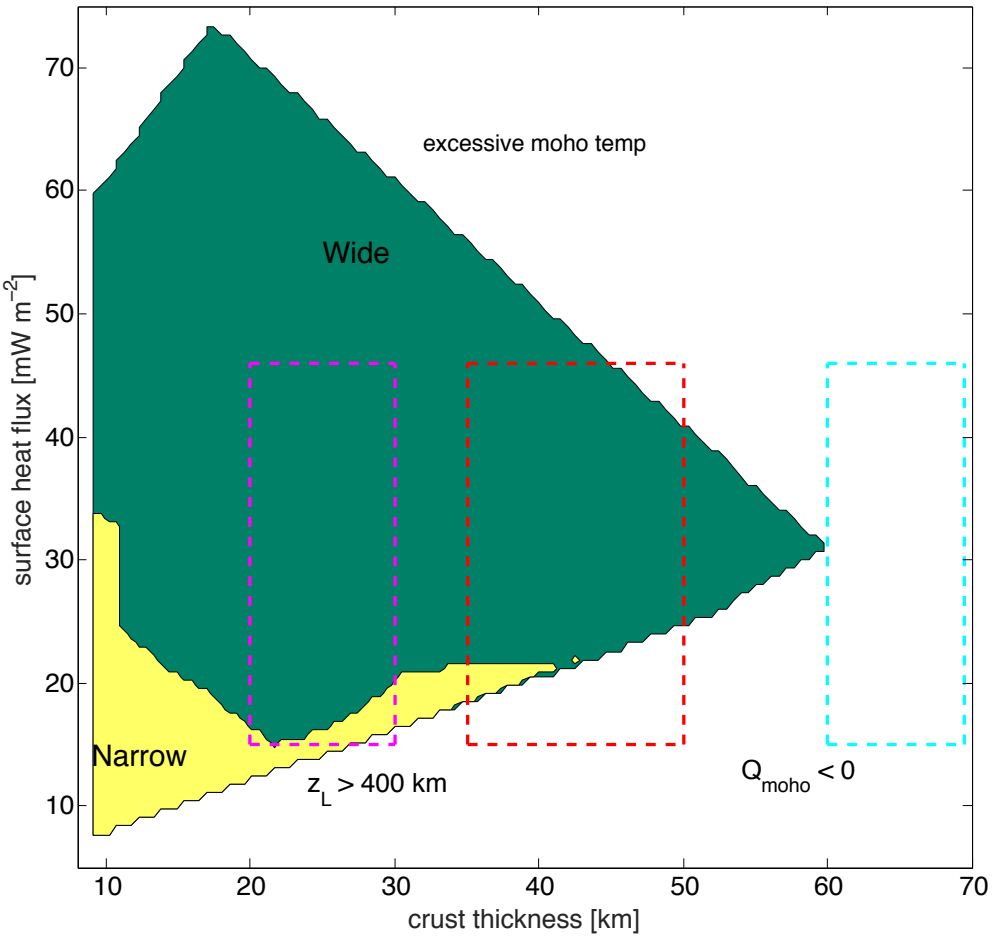

Figure 27: Rifting modes predicted for a depth dependent thermal conductivity; 2 W m^{-1} K^{-1} in the crust and 3.3 W m^{-1} K^{-1} in the mantle. There is weakening in both the brittle and ductile regimes (ε_c = 0.5) and diking is allowed. The addition of diking has no effect and the results are the same as figure 19.

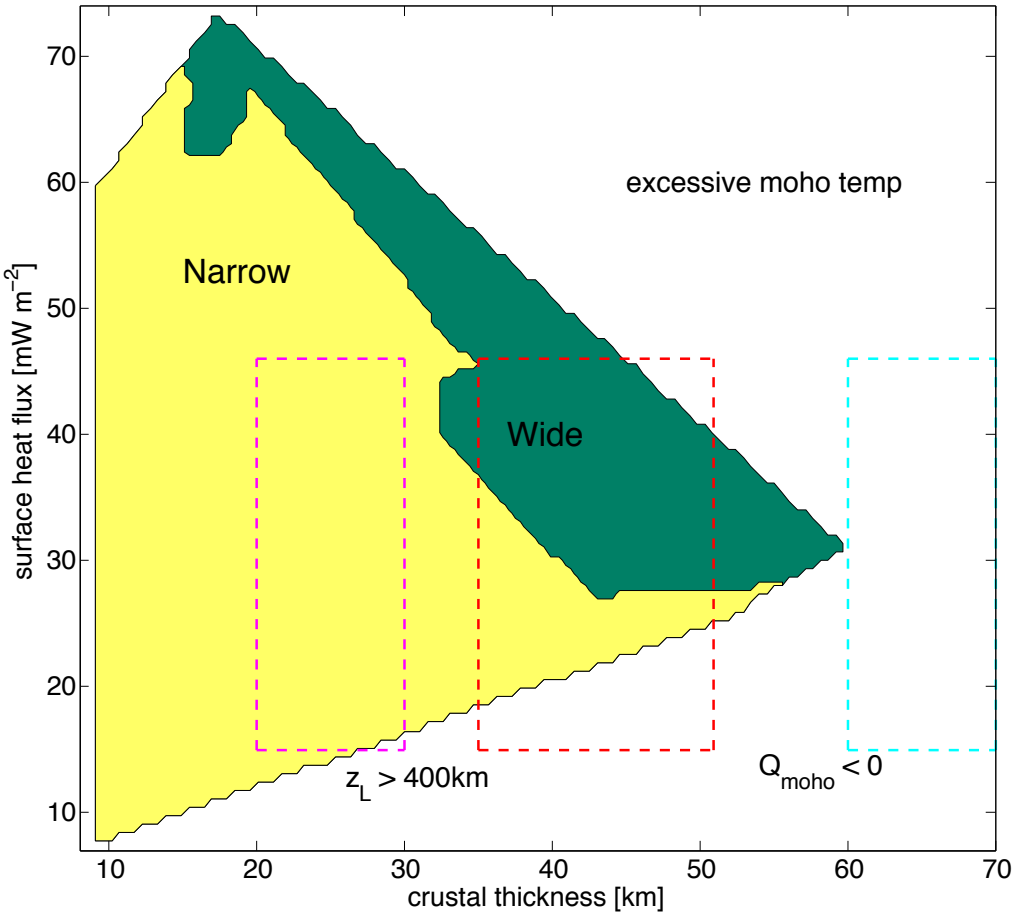

Figure 28: Rifting modes predicted for a depth dependent thermal conductivity; 2 W m^{-1} K^{-1} in the crust and 3.3 W m^{-1} K^{-1} in the mantle. There is weakening in only the ductile regimes (ε_c=0.1) and diking is allowed. Diking promotes more wide rifts than the weakening only case.

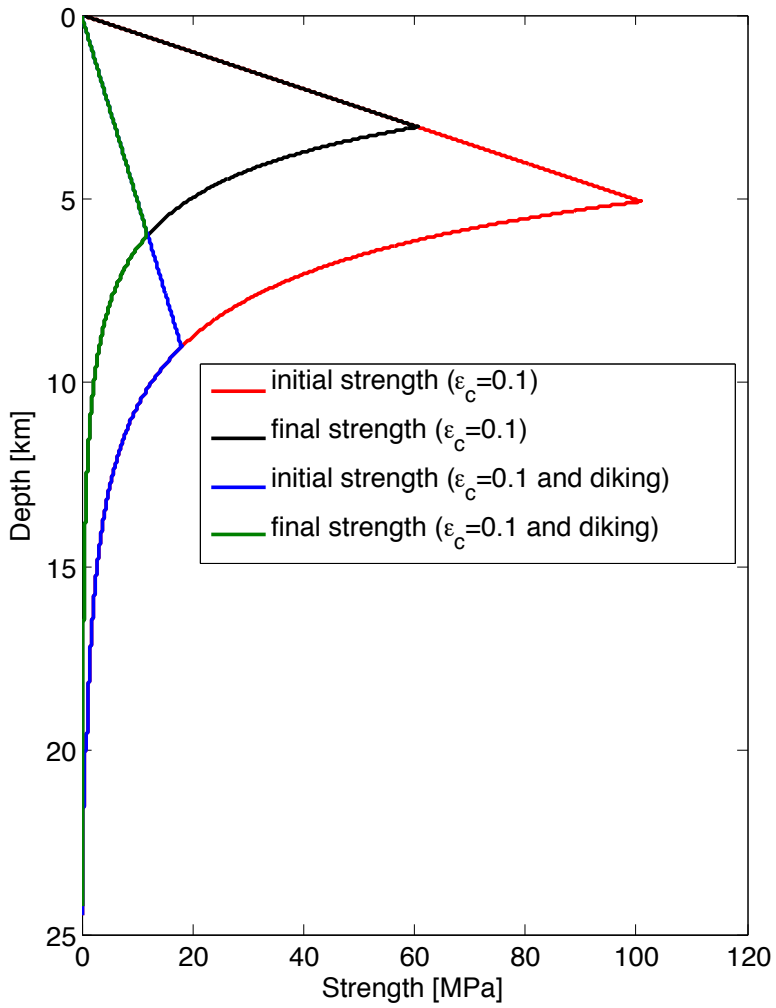

Figure 29: A comparison of the yield strengths for weakening only and weakening with diking. The yield strength is greatly reduced when diking is included, and the weakening effects have less of an impact on the overall yield strength evolution.

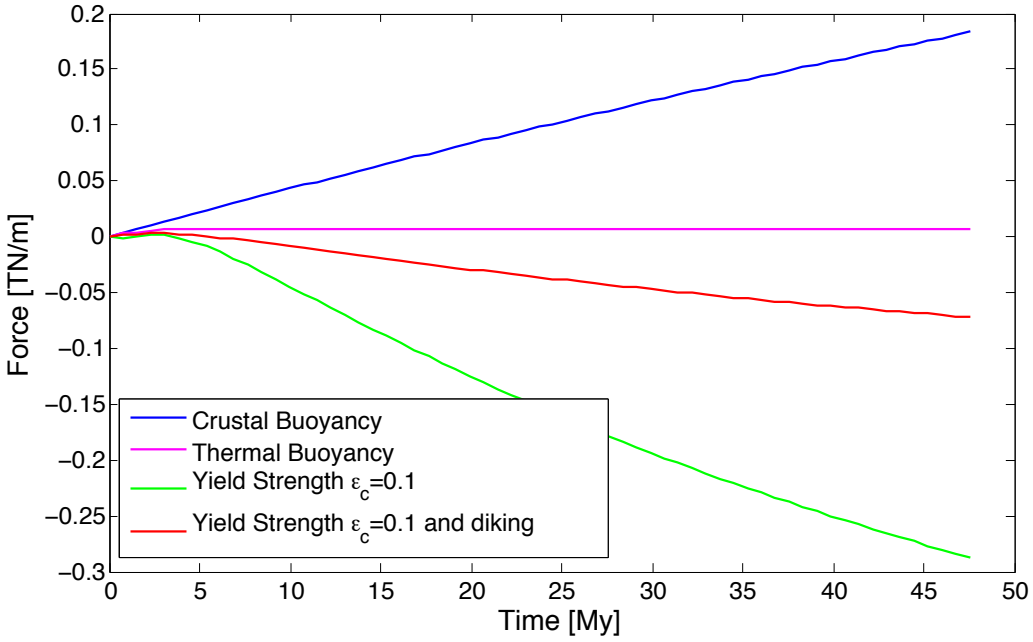

Figure 30: A comparison of the force evolution for weakening only and weakening with diking. The crustal and thermal buoyancy forces are the same for both scenarios. The lithospheric strength experiences less of a reduction when diking is included because the lithosphere is significantly weakened at the onset of rifting.

It appears from this work that diking is not a sufficient mechanism to produce the narrow rifts observed in Beta and Atla Regiones as partial melting occurs at the onset of rift initiation. It is more likely that diking encouraged rift initiation, as argued by various literature (Buck, 2006; Bialas et al., 2010; Kendall and Lithgow-Bertelloni, 2016), but, as stated previously, this is not a factor in selecting the mode of rifting.

5. Discussion

These results indicate that using a stratified, thermal conductivity exerts a strong influence on the resulting rift mode. A constant lithospheric thermal conductivity, generally representative of the mantle, is commonly used in literature but may not accurately capture the structure of the lithosphere. The initial results

shown for depth-dependent thermal conductivity do not comply with geologic observations on Venus, and force us to look toward additional mechanisms that may play an impactful role in the formation of narrow rifts.

Based on section 4.3.2, the inclusion of diking does not have a meaningful effect on the formation of narrow rifts. For the runs that do produce partial melt, diking begins at the onset of rifting, creating an initially weak lithosphere. Cross-cutting relationships indicate that the limited volcanism on Beta and Atla is likely concurrent with extension (Basilevsky, 1993; Basilevksy and Head, 2007). Therefore, while diking associated with volcanism is observed, it may not be a contributing factor to narrow rift formation. When diking is used in conjunction with strain-weakening, there is either no effect on the resulting rift modes or more wide rifts are predicted. However, the thermal effects of diking have not been accounted for, and they may further influence the rift evolution.

Rheological weakening seems most promising in helping the formation of narrow rifts. The low critical strain needed seems to imply that weakening mechanisms are more efficient and act over shorter time scales than are typically thought to happen on Earth. It seems likely that weakening is needed in both the ductile and brittle regimes, through a transition to grain size sensitive creep and melt embrittlement of fault zones, respectively, to produce narrow rift for Devana and Ganis Chasmata. The addition of melt to achieve brittle strain-weakening is limited by the magma budget. Partial melt may be a product of decompression melting of the asthenosphere as it moves upward in response to the thinned lithosphere (White and McKenzie, 1989). It is also possible that the addition of CO_2 (from the CO_2 rich

atmosphere) in the mantle could reduce the solidus (Falloon and Green, 1989), allowing for increased melt generation.

All the results presented here used a strain rate of 10^{-16} s^{-1}, which is an average estimate of the expected strain rate on Venus (Nimmo and McKenzie, 1998; Solomatov and Moresi, 1996). The narrow rifts Devana and Ganis Chasmata are on uplifted regions related to an underlying mantle plume. It is possible that this geologic setting is associated with higher strain rate, 10^{-14}-10^{-15} s^{-1}. If so, the results would favor narrow rift formation since at higher strain rates heat is advected more efficiently, leading to a weakened lithosphere. An increased strain rate would also increase the amount of partial melt available to induce brittle strain-weakening. It can be speculated that the main factor in the difference between wide and narrow rift formation is a difference in strain rate (narrow rifts requiring a faster strain rate) or the inclusion of melt to enable brittle strain-weakening (narrow rifts requiring brittle strain-weakening).

6. Conclusions

The aim of this research is to understand the processes involved in forming narrow rifts on Venus. I focused on the rifts Devana and Ganis Chasmata, which are some of the youngest features on Venus and are morphologically similar to terrestrial narrow rifts of the East African rift system. The lithospheric extension model proposed by Buck (1991) was used to relate the lithospheric structure and force evolution to determine the type of rift that forms. This model focuses on three forces that act to delocalize (crustal buoyancy) or localize (thermal buoyancy and yield strength) deformation. I used a moving point boundary formulation when solving the

heat equation in order to capture the thinning effects of the lithosphere, which have a substantial influence on the yield strength calculations. I use two types of lithospheric thermal conductivity values- a constant value (which is largely used in literature) and a more physically accurate, depth-dependent value. A constant κ_{tc} produced more favorable results, while a depth-dependent κ_{tc} produced results that did not comply with observations.

I then added two mechanisms, diking and lithospheric weakening, to help promote narrow rifting. Diking did not produce a substantial effect on the results since partial melting was not abundant and for the instances when it was, it was concurrent with the onset of rifting meaning there was no large overall strength reduction due to diking. An exponential form of lithospheric weakening was used to act a proxy for various ductile weakening mechanisms. For critical strain values of 0.25 and 0.1 (depending on whether brittle weakening was included or not) narrow rifting was predicted for Devana and Ganis Chasmata, complying with geologic observations. These values of weakening generally comply with observations for Parga and Hecate Chasmata, except for a critical strain of 0.25 with brittle and ductile strain-weakening where narrow rifts are generally predicted for Parga and Hecate Chasmata.

These results imply that Venus must have mechanisms to induce ductile localization needed for narrow rifting. In the mantle this is likely the result of the transition from grain size insensitive to grain size sensitive rheology, which is also thought to be important in forming terrestrial, shear zones. However, localization in the brittle regime on Earth is thought to be due to hydrated, foliated minerals such as

serpentines and micas, which are not prominent on a dry Venus. Therefore, brittle weakening on Venus must occur by some other mechanism, possibly the inclusion of melt in the shear zones.

These results help elucidate the formation of narrow Venusian rifts, which are similar to narrow rifts on Earth. The similarities between Venus and Earth must be studied in order to understand how they became such different planets. Future experimental work should be done to better constrain weakening mechanisms under Venusian conditions. This study would be greatly improved by better constraints on the parameters used, such as the crust thickness, surface heat flux, and crustal heat production.

Appendices

Rifting_Venus.m

```
clear;
close all;

tstart=tic;        % Program starting time:

SAVEFILES=0; %save xXyY and Dike data
SAVEFILES2=0; %save T, YS, LCF, Depth data

% Making variables global, for use in calle functions:
global z_ktd v z_H_Fn z zmohoInit edot zmoho_Fn zspc ...
   u_Fn xspan xspc ux Xe dudx_Fn nx nz delRho ...
   z_E z_n R g z_A testvar yr IntData  depth_Fn ...
   zblith Nc Nl T_blith t0  Qmoho k_td z_ktc ...
   Qa nt


%% MASTER LOOP

%surface heat flux values to loop through:
QsArray=10:5:70;
narrow=0;wide=0;corecomp=0;
runs=size(QsArray,2);

P=[];L={};
%strain rate and crustal heat production
edot=1*10^-16;%STRAIN RATE(Nimmo and McKenzie 1998)
H_buck=3.5e-7; %avg of Venera 9&10 data (172 and 74 W/kg, respectively)
%H_buck=2.14e-7; %Venera 10 data
%H_buck=4.98e-7; %Venera 9 data
%H_buck=6.4e-8; %Low Venus Heat Production
H_buck_exp=floor(log10(H_buck));edot_exp=floor(log10(edot));

ColorID=[0 0 1;1 0 0;0 1 0;1 1 0;1 0 1;0 1 1;0 0 0];
xXyY=[];
SolidusIND_zTOT=[];
SolidusIND_tTOT=[];
dFtot=[];
ec=0.1; %add weakening? if = 0, no weakening
DIKING=0; %add diking in brittle regime?

%crust thickness values to loop through
for zmohoInit=10*1000:5*1000:70*1000;
```

```
mohoStart=zmohoInit;
viscTotal=[];
YSTotal=[];
TinitTotal=[];
zTotal=[];
plV=[];

for q=1:runs % MASTER LOOP!
error=0;
sameP=0;

%Physical Constants Database (from Buck
'91):~~~~~~~~~~~~~~~~~~~~~~~~~~~~~~~~
   yr =31556926;   % One Year [s]
  % k_tc = 3.3;    %Earth thermal conductivity
  % k_tc = 2.0;     % Thermal Conductivity [W m^-1 K^-1] of crust **schubert et al
Venus II
   z_ktc    = @(z,zmoho) 2*(z<zmoho)+3.3*(z>=zmoho);
  % pc = 2800;     %Earth crust
   pc = 2900;      % Crustal Density [kg m^-3], Venus crust is dry diabase
   pm = 3300;      % Mantle Density [kg m^-3] saying the same as Earth, peridotite
   pmelt=2700;     % Partial Melt density of mantle (used for diking)
   a = 3.0E-5;     % Thermal Expansion Coefficient [K^-1]
   g = 8.87;       % Acceleration due to Gravity [m s^-2]
   R = 8.31;       % Universal Gas Constant [J mol^-1 K^-1]
   k_td = 1E-6;       % Thermal Diffusivity (kappa)
                % (eq. 4.69 in Turcotte & Schubert)
                % K = k / [rho * (specific heat)]
   delRho=pc*(pm-pc)/pm;



%Rheological Constants Database (from Buck
'91):~~~~~~~~~~~~~~~~~~~~~~~~~~~~~~~~
%Diabase from Mackwell et al. 1998
%dry olivine from Hirth and Kohlstedt 2003

   %%MINERAL:      n:    A[Pa^-n s^-1]    E[J mol^-1]       C[Pa s]      cp [J kg^-1
K^-1
   Diabase=    [   4.7;   1.2E-26;       485*1000;         5.26E3;      711     ]; %
   DOlivine=   [   3.5;   2.4E-16;       540*1000;         0.158E2;     1000  ]; %Cp from
eq. 4.69
   Olivine=    [   3.0;   1.0E-15;       500*1000;         1.0E3;       576     ]; %
   Pyroxene=   [   5.3;   2.5E-37;       380*1000;         7.3E10;      787     ];%
   Anorthosite=[   3.2;   5.6E-23;       238*1000;         1.1E9;       711     ]; %
   DQuartzite= [   2.9;   5.0E-25;       149*1000;         8.0E12;      1013    ];%
```

```
    WQuartzite= [   2.4;   1.3E-20;       134*1000;         3.1E11;      1013    ];%

    %Extensional/Brittle Failure Constant (for use with Byerlee's Law)
    %gB = 22/1000;    %Earth no pore fluid pressure [MPa/m]
    gB = 19.9/1000;   %convert to Venus where g=8.87

%% MODEL SETUP

% DEPTH PARAMETERS
~~~~~~~~~~~~~~~~~~~~~~~~~~~~~~~~~~~~~~~~~~~~~~~~~~~~~~~~~~~~~~~~~~~~~~~~~~~~
zblith=500*1000;        % [m] Initial large depth of lithosphere

  %need to find the depth of lithsophere. use criteria that at depth of
  %lithosphere the visc=10e21 Pa*s
for findZL=1:2
   zmoho=zmohoInit;
    fprintf('zblith = %d \n', zblith)
    fprintf('Crust thickness = %g \n Heat Flux = %d \n', zmohoInit, QsArray(q))

ux=0.1*(0.01/yr);     % [m/s] Rifting velocity (Buck uses cm/yr)
edot=1e-16;
Xe=ux/edot;


zspc=500;           % [m] depth step size
z=0:zspc:zblith;    % INITIAL DEPTH ARRAY
zNumStps=size(z,2);
nz=zNumStps;
Nc=find(z==zmohoInit);
Nl=size(z,2);



% TIME PARAMETERS
~~~~~~~~~~~~~~~~~~~~~~~~~~~~~~~~~~~~~~~~~~~~~~~~~~~~~~~~~~~~~~~~~~~~~~~~~~~~
tNumStps=63;                    % Number of time steps
 yr =31556926;   % One Year [s]                % [s] Integration run time
strainlim=0.15;   %48 Myr               % Strain limit at which model ends
tmax=strainlim/edot;            % [s] Integration run time, defined by
% strain (as per Buck '91)
tspan=linspace(0,tmax,tNumStps); % Time Array
tspc=tspan(2)-tspan(1);          % [s] Actual time step size
nt=numel(tspan);                % Number of elements in tspan

% HORIZONTAL PROFILE PARAMETERS
```

```
Xl=Xe+200000;          % [m] Width of initially uniform lithosphere, much greater
than Zl
%Xl=250000;
xspc=100;              % [m] x array step size
xspan=0:xspc:Xl/2;     % Horizontal Array (1/2 of space)
nx=numel(xspan);       % Number of elements in xspan

hinit=xspan*0+zmohoInit;        % Initial, uniform thickness of crust


% Horizontal Rifting Velocity Profile:
u_Fn = @(x,ux,Xe) (ux/2)*(x>=(Xe/2))+(ux/2/(Xe/2)*x).*(x<(Xe/2));
% Derivative of Rifting Velocity Profile (du/dx):
dudx_Fn = @(x,ux,Xe) (0)*(x>=(Xe/2))+(ux/2/(Xe/2))*(x<(Xe/2));


% TEMPERATURE PARAMETERS
% Following Buck, 1991, we're defining the temperature profile off of the
% surface heat flux, rather than defining it (which was my
% first approach, based off of semi-infinite half-space cooling/heating).

Qs=QsArray(q)*1e-3; %convert surface heat flux to W/m^2

Tsurf = 740;                    % [K] Venus surface temp
Qmoho = Qs - H_buck*zmohoInit;                  % [W/m^2] Heat flux at Moho
Tmoho = Tsurf + (Qs-H_buck*zmohoInit/2)*zmohoInit/z_ktc(0,zmohoInit);   % [K]
Temperature at Moho
Tmelt=1100+((1150-1070)/39000)*z+273; %solidus of basalt [K]"understanding the
earth" brown, hawkesworth, wilson
Tmelt_moho=Tmelt(Nc);

%if findZL==2
%FOR ERROR WHEN QMOHO < 0 ie: heat flows into moho
if Qmoho <= 0
   error=1;
   figure(11)
   p1=scatter(zmohoInit/1000,QsArray(q),'X','MarkerEdgeColor','m','LineWidth',2);
   l1='Qmoho<0';
 %  p1=text(zmohoInit/1000,QsArray(q),'X','Color','c','FontSize',14);
   xlabel('crustal thickness km');ylabel('surface heat flux mW/m^2');
   hold on
   xX=mohoStart/1000;yY=Qs*1000; %save parameters for this run t xXyY
   newROW=size(xXyY,1)+1;
   xXyY(newROW,1)=xX;
   xXyY(newROW,2)=yY;
   xXyY(newROW,3)=0;
```

```
xXyY(newROW,4)=0;
xXyY(newROW,5)=0;
xXyY(newROW,6)=0;
xXyY(newROW,7)=0;
xXyY(newROW,8)=0;
xXyY(newROW,9)=0;
xXyY(newROW,10)=0;
xXyY(newROW,11)=0;
xXyY(newROW,12)=0; %final mohotemp
xXyY(newROW,13)=0; %initial crustal geotherm
xXyY(newROW,14)=0; %starting moho (not necessarily = to xX)
xXyY(newROW,15)=0; %final crust thickness from LCF
dFtot(newROW,1)=0;

if isempty(P) == 1
   P(1)=p1;
else
   for i=1:length(P)
      if P(i) == p1
         sameP = 1;
         disp('sameP = 1')
         break;
      end
   end
   if sameP == 1
      break
   else
      P(length(P)+1)=p1;
   end
end
if isempty(L) == 1
   L{1}=l1;
else
   for i=1:length(L)
      if strcmp(L{i},l1)
         sameL = 1;
         break;
      end
   end
   if sameL == 1
      break
   else
      L{length(L)+1}=l1;
   end

end
```

```
   sameL=0;sameP=0;
  break
end
%end


% GENERATING FUNCTIONAL MODEL PARAMETERS
###################################

% Advection Term: **** ie: vertical velocity ****
v=-edot*z;
vEulerian=v;
zmoho_Fn = @(t,zmohoInit,edot) zmohoInit.*exp(-edot.*t);
depth_Fn = @(t,z,edot) z.*exp(-edot.*t);

% MINERALOGICAL PROPERTIES: ----------------------------------------------
% (using the heavyside function (y=1 for x>0; y=0 for x<0) to differentiate
% between crust and mantle parameters, based upon the changing Moho depth)

zmoho=zmohoInit;
z_denisty  = @(z,zmoho) pm*(z>=zmoho)+pc*(z<zmoho);
%z_ktd    = @(z,zmoho) k_td*(z>=-1e100);
z_ktd    = @(z,zmoho)
z_ktc(1,2)/(pc*Diabase(5))*(z<zmoho)+z_ktc(2,1)/(pm*DOlivine(5))*(z>=zmoho);
z_H_Fn    = @(z,zmoho)
H_buck*k_td/z_ktc(0,zmohoInit)*(z<zmoho)+0*(z>=zmoho);

z_n  = @(z,zmoho) Diabase(1)*(z<zmoho)+DOlivine(1)*(z>=zmoho);
z_A  = @(z,zmoho) Diabase(2)*(z<zmoho)+DOlivine(2)*(z>=zmoho);
z_E  = @(z,zmoho) Diabase(3)*(z<zmoho)+DOlivine(3)*(z>=zmoho);
z_C  = @(z,zmoho) Diabase(4)*(z<zmoho)+DOlivine(4)*(z>=zmoho);
z_cp = @(z,zmoho) Diabase(5)*(z<zmoho)+DOlivine(5)*(z>=zmoho);


% PREDICTED TEMP AT BASE OF LITHOSPHERE ----------------------------------
% Buck defines the base of the lithosphere (ZL in his model) based upon a
% viscosity.  Viscosity isn't directly related to depth, but it *is*
% related to temperature (viscos=sigma/2*edot - where sigma is the ductile
% stress)
if findZL==1 %****finding T at Zl in order to rerun with this known value ****
   ViscosityLimit=10^21; % [Pa s] (The viscosity at the base of the lithosphere)

T_blith=z_E(2,1)/z_n(2,1)/R*(log(ViscosityLimit*2*edot*(z_A(2,1)/edot)^(1/z_n(2,
1))))^(-1);
   %**** plug-in sigma_d into visc eq, and solve for T ****
   fprintf('T_blith = %g \n', T_blith)
```

```
end

FILENAME=[num2str(edot_exp),'_',num2str(floor(H_buck/(10^(floor(log10(H_buck
))))),'e',num2str(H_buck_exp),'_',num2str(z_ktc(zmohoInit-1000,zmohoInit)),...

'_',num2str(z_ktc(zmohoInit+1000,zmohoInit)),'_',num2str(round(tspan(end)/yr/1e6))
,'_ec',num2str(ec)...
   '_Dike',num2str(DIKING),'_VENUS_MOVINGPOINT'];


% INITIAL TEMPERATURE PROFILE:----------------------------------------

% Creating Blank Profiles:
   zblank=z*0;
   Tinit=zblank;

% We're using the Buck '91 method for determining the geotherm: we define a
% surface heat flux (Qs) and crustal heat production rate (H), and then
% back-solve for the requisite temperature profile

for i=1:zNumStps

   depth=z(i); %Recalling depth
   zmoho=zmohoInit;

   if depth<=zmohoInit; %(we're in the crust)

   Tinit(i)=Tsurf+(Qs-H_buck*depth/2)*depth/z_ktc(1,2);

   else %(we're in the mantle)

      Tinit(i)=Tsurf+(Qs*zmohoInit/z_ktc(1,2))-
(H_buck/(2*z_ktc(1,2)))*zmohoInit^2+...
         (Qs*(depth-zmohoInit)/z_ktc(2,1))-(H_buck*zmohoInit/z_ktc(2,1))*(depth-
zmohoInit);

      if Tinit(i)>T_blith
         Tinit(i)=T_blith;
      end

   end
end


%IS TMOHO > T_BLITH?
%cuts off lithosphere in the crust if it is.
```

```
%Must also redetermine initial temp profile

if Tmoho > T_blith
   disp('Tmoho > T_blith')
   ind=find(Tinit==max(Tinit),1,'first');
   z_LithNewInterp=interp1(Tinit(1:ind),z(1:ind),T_blith);
   zblith=z_LithNewInterp-mod(z_LithNewInterp,500); %round to nearest 500m

   zmohoInit_interp=interp1(Tinit(1:ind),z(1:ind),T_blith-10);
   zmohoInit=zmohoInit_interp-mod(zmohoInit_interp,500);
   Qmoho = Qs - H_buck*zmohoInit;
   Nc=find(z==zmohoInit);
   Nl=find(z==zblith);
   z=z(1:Nl);
   zNumStps=size(z,2);

   Tmoho=Tinit(Nc);
   nz=zNumStps;
   v=-edot*z;
   hinit=xspan*0+zmohoInit;

   z_Arr1=zeros(nt,numel(z));
   z_Arr1(1,:)=z(:);
   for i=2:nt
     current_time=tspan(i);
    for j=1:zNumStps
         z_Arr1(i,j)=z(j);
    end
   end
   Tinit=[];
   for i=1:zNumStps
   depth=z(i); %Recalling depth
   zmoho=zmohoInit;

   if depth<=zmohoInit; %(we're in the crust)
        Tinit(i)=Tsurf+(Qs-H_buck*depth/2)*depth/z_ktc(1,2);
         if Tinit(i)>T_blith
             Tinit(i)=T_blith;
         end
   else %(we're in the mantle)
      Tinit(i)=Tsurf+(Qs*zmohoInit/z_ktc(1,2))-
(H_buck/(2*z_ktc(1,2)))*zmohoInit^2+...
          (Qs*(depth-zmohoInit)/z_ktc(2,1))-(H_buck*zmohoInit/z_ktc(2,1))*(depth-
zmohoInit);
       if Tinit(i)>T_blith
          Tinit(i)=T_blith;
```

```
      end
   end
   end

%IS TMOHO > TMELT (SOLIDUS TEMP): must shorten crust and extend
lithosphere
%Arbitrarily say that Tmoho is 5 K less than Tmelt to assure
%that it is indeed less than Tmelt once routine is rerun (findZL==2) with new
%lithosphere depth. Must also redetermine initial temp profile

elseif  Tmoho > Tmelt_moho
   disp('TMOHO > TMELT')
   ind=find(Tinit>=Tmoho,1,'first');
   z_LithNewInterp=interp1(Tinit(1:ind),z(1:ind),Tmelt_moho-10);
  % z_EndNew=roundn(z_EndNewInterp,3); %round to 1 km
   z_LithNew=z_LithNewInterp-mod(z_LithNewInterp,500); %round to 500 m
   zmohoInit=z_LithNew;
   Qmoho = Qs - H_buck*zmohoInit;

   hinit=xspan*0+zmohoInit;

   Tmoho=interp1(z(1:ind),Tinit(1:ind),z_LithNew);
   for i=1:zNumStps

   depth=z(i); %Recalling depth
   zmoho=zmohoInit;

   if depth<=zmoho; %(we're in the crust)

   Tinit(i)=Tsurf+(Qs-H_buck*depth/2)*depth/z_ktc(1,2);

   if Tinit(i)>T_blith
      Tinit(i)=T_blith;
   end
   else %(we're in the mantle)

      Tinit(i)=Tsurf+(Qs*zmohoInit/z_ktc(1,2))-
(H_buck/(2*z_ktc(1,2)))*zmohoInit^2+...
         (Qs*(depth-zmohoInit)/z_ktc(2,1))-(H_buck*zmohoInit/z_ktc(2,1))*(depth-
zmohoInit);
      if Tinit(i)>T_blith
         Tinit(i)=T_blith;
      end
   end
   end
else
```

```
 %break

end

%IS THE LAST TEMP INDEX < T_BLITH?
%then extend depth profile in order to reach T_blith
if Tinit(end) < T_blith
   disp('MUST LENGTHEN DEPTH PROFILE: T(END) < T_BLITH')
   T_extra=[];z_extra=[];
   deltaT=T_blith-Tinit(end);
   slope=(Qmoho/z_ktc(depth,zmoho));
   extraZ=deltaT/slope;
   extraSteps=extraZ/zspc;
   for i=1:ceil(extraSteps) %round up to next integer
    %  disp('HERE!!!!')
      T_extra(i)=Tinit(end)+(i*zspc*slope);
      z_extra(i)=z(end)+(i*zspc);
      if T_extra(i) > T_blith
         T_extra(i) = T_blith;
      end
   end
   Tinit_new=horzcat(Tinit,T_extra);
   z_new=horzcat(z,z_extra);
   Tinit=Tinit_new;z=z_new;nz=nz+ceil(extraSteps); v=-edot*z;
   z_Arr1=zeros(nt,numel(z));
   z_Arr1(1,:)=z(:);
   for i=2:nt
    current_time=tspan(i);
    for j=1:zNumStps
        z_Arr1(i,j)=z(j);
    end
   end
 %  for i=1:nz
  %     H_buck(i)=H0*exp(-z(i)/zmohoInit);
 %  end
end


if findZL==2
if Tinit(end) ~= T_blith
   error=4;
   figure(11)
   p4=scatter(zmohoInit/1000,QsArray(q),'X','MarkerEdgeColor',[0 .5
0],'LineWidth',2);
   l4='Tinit(end) ~= T_blith';
   %p1=text(zmohoInit/1000,QsArray(q),'X','Color','y','FontSize',14);
```

```
    xlabel('crustal thickness km');ylabel('surface heat flux mW/m^2');
    hold on
    if isempty(P) == 1
       P(1)=p4;
    else
       for i=1:length(P)
          if P(i) == p4
             sameP = 1;
             disp('sameP = 1')
             break;
          end
       end
       if sameP == 1
          break
       else
          P(length(P)+1)=p4;
       end
    end
    if isempty(L) == 1
       L{1}=l4;
    else
       for i=1:length(L)
          if strcmp(L{i},l4)
             sameL = 1;
             break;
          end
       end
       if sameL == 1
          break
       else
          L{length(L)+1}=l4;
       end

    end
    sameL=0;sameP=0;
    break
end
end
%** INITIAL CRUSTAL GEOTHERM
TempLithINDEX=find(Tinit==T_blith,1,'first');
zInterp=interp1(Tinit(1:TempLithINDEX),z(1:TempLithINDEX),T_blith,'spline');
if findZL==2
    nz=TempLithINDEX;
    z=z(1:TempLithINDEX);
  %  z=z(1:TempLithINDEX);
    Tinit=Tinit(1:TempLithINDEX);
```

```
   v=-z*edot;
end


fprintf('lithosphere depth interp from temp profile = %g \n', zInterp)
% FINDING DEPTH OF BASE OF LITHOSPHERE (ZL) ------------------------------
if findZL==1
   %zblith=max(zmohoInit,zInterp);%**** interpolating from T profile to find depth
of lithosphere ****
   zblith=z(find(Tinit >= T_blith, 1, 'first'));
 %   zblith=interp1(Tinit,z,T_blith);
   fprintf('lithosphere base depth = %g \n', zblith)
end

if findZL==2 %**** after loop is run a second time with known zblith; comparing
calculated visc to what it should be ****

VISCblith=1/2/edot*(edot/z_A(2,1))^(1/z_n(2,1))*exp(z_E(2,1)/z_n(2,1)/R/Tinit(end
));
      %stress=2*viscosity*strainrate
   fprintf('lithosphere base viscosity = %g \n', VISCblith)

end

%IS THE LITH DEPTH ABSORNALLY LARGE? IF SO-->ERROR
if findZL==2
if zblith > 400*1000 %base of lithosphere greater than 400 km
   error=5;
   figure(11)
   p2=scatter(zmohoInit/1000,QsArray(q),'X','MarkerEdgeColor','y','LineWidth',2);
   l2='zblith > 400 km';
 %  p1=text(zmohoInit/1000,QsArray(q),'X','Color','c','FontSize',14);
   xlabel('crustal thickness km');ylabel('surface heat flux mW/m^2');
   hold on
   xX=mohoStart/1000;yY=Qs*1000;
   newROW=size(xXyY,1)+1;
   xXyY(newROW,1)=xX;
   xXyY(newROW,2)=yY;
   xXyY(newROW,3)=0;
   xXyY(newROW,4)=0;
   xXyY(newROW,5)=0;
   xXyY(newROW,6)=0;
   xXyY(newROW,7)=0;
   xXyY(newROW,8)=0;
   xXyY(newROW,9)=0;
   xXyY(newROW,10)=0;
```

```
    xXyY(newROW,11)=0;
    xXyY(newROW,12)=0; %final mohotemp
    xXyY(newROW,13)=0; %initial crustal geotherm
    xXyY(newROW,14)=0; %starting moho (not necessarily = to xX)
    xXyY(newROW,15)=0; %final crust thickness from LCF
    dFtot(newROW,1)=0;

    if isempty(P) == 1
       P(1)=p2;
    else
       for i=1:length(P)
          if P(i) == p2
             sameP = 1;
             disp('sameP = 1')
             break;
          end
       end
       if sameP == 1
          break
       else
          P(length(P)+1)=p2;
       end
    end
    if isempty(L) == 1
       L{1}=l2;
    else
       for i=1:length(L)
          if strcmp(L{i},l2)
             sameL = 1;
             break;
          end
       end
       if sameL == 1
          break
       else
          L{length(L)+1}=l2;
       end

    end
    sameL=0;sameP=0;
  % break
end
end
end

if error ~= 0
```

```
   disp('BROKE LAST LOOP')
   if error == 1
      disp('Qmoho less than zero')
   elseif error == 2
      disp('Tmoho > Tmelt')
   elseif error == 3
      disp('Tmoho > T_blith')
   elseif error == 5
      disp('zblith >> 500km')

   else
      disp('Tinit(end) ~= T_blith')
   end
  %  fprintf('Tmoho = %g\nT_blith = %g\nQmoho =
%g\n\n\n',Tmoho,T_blith,Qmoho)
   continue
end
%fprintf('Tmoho = %g\nT_blith = %g\nT(end) = %g\nTblith (from equations) =
%g\n',Tmoho,T_blith,Tinit(end),Tblith)
%%**** we leave this loop with a known zblith and an initial T profile ****

%%


%% INITIAL  FLOW
DIFFUSIVITY############################################################
dhdx=0;     %crust is constant thickness before integration
pT_MOHO=interp1(z,Tinit,zmohoInit); %interpolate between depth and T profile to
find T at moho
pT_MOHO2=interp1(z,Tinit,zmohoInit-5); %interpolate between depth and T profile
to find T at moho-5km
pdTdzMOHO = (pT_MOHO-pT_MOHO2)/5; %geotherm at moho

pKf_dPdx = g*delRho*dhdx; %horizontal pressure gradient
pKf_y0   = R*pT_MOHO^2/(z_E(1,zmohoInit)*pdTdzMOHO); %**** y0 for non
newtonian approximation ****
pKf_AvgStress = max((2*pKf_y0*pKf_dPdx),1e6);   %**** avg deviatoric stress at
base of crust ****

pKf_C    = z_A(1,zmohoInit)^(-1)*(pKf_AvgStress)^(1-z_n(1,zmohoInit));
pKf_nu0  = pKf_C*exp(z_E(1,zmohoInit)/R/pT_MOHO);  %**** approx visc for
non newtonian ****
%pKf      = g*delRho*pKf_y0^3/(3*pKf_nu0);  %**IF USING CREME BRULEE
pKf      = g*delRho*pKf_y0^3/(pKf_nu0);     %**IF USING JELLY SANDWHICH
```

```
%% INTEGRATION
#################################################################

% Integration Timing (Start):
tstartint=tic;

% Test Variable
testvar=1;

% Mid-Integration Data:
IntData=[];

% ODE Integration Parameters:
IntAcc=1E-2;
%IntAcc=0.01;
options=odeset('RelTol',IntAcc,'InitialStep',1e-10);
zLITH=zblith;
Minit=[Tinit,hinit,zLITH];
% Integration Timing (Start):

t0=tspan(1);

Nc=find(z==zmohoInit,1,'first'); Nl=nz;
Qa=-Qmoho;

[t,M]=ode15s(@RIFTING_VENUS_ODE_MovingGrid,tspan,Minit,options);

%INTEGRATE TO SOLVE LCF AND HEAT EQUATIONS
%[t,M]=ode15s(@GEOL394H_JTK_FN1,tspan,Minit,options);
MOVEPOINT=1; %if 1 using moving point, if 0 not using moving point

% Creating Seperate Arrays for T and h and zlith:
T = M(:,1:nz);  h_LCF = M(:,nz+1:nz+nx);    zlith=M(:,nz+nx+1);
if MOVEPOINT == 1 %re-determine the depth arrays through time when including
   %crust thinning and advection because ode solver can't export it
  [zTOT] = MovingGridAfterODE(h_LCF, zlith);
  zTOT(1,:)=z;

end

%% EXPANDING TEMPERATURE PROFILE
#########################################
%% ******** EXPANDING THE TEMPERATURE PROFILE THE WAY JTK
DID IT MESSES UP THE BOUNDARY
%% CONDITIONS FOR THE TEMP PROFILE. INSTEAD I AM USING
%% IV=INTERP1(LINSPACE(0,1,NUMEL(V),V,LINSPACE(0,1,NEWNUM))
```

```
%% IN ORDER TO RESIZE THE TEMP AND DEPTH ARRAYS SEPARATELY

newArraySize=10000;
T2=zeros(nt,newArraySize);
z2NEW=zeros(nt,newArraySize);
for i=1:size(T,1)
   T2(i,:)=interp1(linspace(0,1,numel(T(i,:))),T(i,:),linspace(0,1,newArraySize));
   if MOVEPOINT == 1

z2NEW(i,:)=interp1(linspace(0,1,numel(zTOT(i,:))),zTOT(i,:),linspace(0,1,newArray
Size));
   end
end
if MOVEPOINT == 0
   z2=interp1(linspace(0,1,numel(z)),z,linspace(0,1,newArraySize));
   for i=1:nt
      z2NEW(i,:)=z2;
   end
end

%%DIKING----------------------
%find the time index when the mantle crosses the solidus
%this will be the time that a dike is imposed
%time when it crosses doesnt matter, the only thing that matters is that
%it crosses the solidus at SOME time since the difference in YS only
%matters so I just need to find IF it crosses the solidus and then impose a
%dike
if DIKING==1
[Tsolidus,SolidusIND_z,
SolidusIND_t,DIKE]=SolidusAndTemp(pc,pm,g,zTOT,nt,T,Nl,Nc,nt,h_LCF);
newROW_solidus=size(SolidusIND_zTOT,1)+1;
SolidusIND_zTOT(newROW_solidus,:)=SolidusIND_z;
SolidusIND_tTOT(newROW_solidus)=SolidusIND_t;
end
%% YIELD STRESS PROFILE CALCULATION
%T2=T;newArraySize=zNumStps;z_Arr2=z_Arr1;z2ARR=z;
% Creating Blank Arrays:
YS=T2*0;
YSduct=YS; % Ductile Deformation Yield Strength
YSbrit=YS; % Brittle Deformation Yield Strength
YSbritINIT=YS; % Brittle Deformation Yield Strength

% Calculating out the Ductile/Brittle Strength at each Depth/Time ~~~~~~~~~

% -- To do this, we calculate out both the ductile and brittle yield
% stresses for a given depth and time.  The actual yield stress is the
```

```
% minimum of the two.
strain=t.*edot;
  for k=1:nt %TIME LOOP

      current_time=t(k);
      %zmohoNOW=zmoho_Fn(current_time,zmohoInit,edot);
      zmohoNOW=h_LCF(k,1);
      %disp([' > Currently in loop ',num2str(k),' of ',num2str(nt),' <']);

   for i=1:newArraySize %DEPTH LOOP

       %depthNOW=z_Arr2(k,i);
       depthNOW=z2NEW(k,i);
       if ec==0 %NO WEAKENING
       YSduct(k,i) =
(edot/z_A(depthNOW,zmohoNOW))^(1/z_n(depthNOW,zmohoNOW))*...

exp(z_E(depthNOW,zmohoNOW)/(z_n(depthNOW,zmohoNOW)*R*T2(k,i)))/10^6;
       YSbrit(k,i) = gB*depthNOW;
       %Ductile Deformation:(10^-6 term at end to convert to MPa)

       else %YES WEAKENING

          %exponential decay from Gueydan et al 2014
          YSduct(k,i) = exp(-
strain(k)/ec)*(edot/z_A(depthNOW,zmohoNOW))^(1/z_n(depthNOW,zmohoNOW))
*...

exp(z_E(depthNOW,zmohoNOW)/(z_n(depthNOW,zmohoNOW)*R*T2(k,i)))/10^6;
         %  YSbrit(k,i) = gB*depthNOW*exp(-strain(k)/ec);
          YSbrit(k,i) = gB*depthNOW;
           YSbritINIT(k,i)=YSbrit(k,i);

             %linear decay
     % YSduct(k,i) = (1-
(t(k)/tmax))*(edot/z_A(depthNOW,zmohoNOW))^(1/z_n(depthNOW,zmohoNOW))
*...
      %
exp(z_E(depthNOW,zmohoNOW)/(z_n(depthNOW,zmohoNOW)*R*T2(k,i)))/10^6;

       end
      if DIKING~=0
       if DIKE(k) == 1
         % if k > 1
        %  if (YSbrit(k,i) > 30) && (depthNOW < h_LCF(k,1))
          if (depthNOW < h_LCF(k,1))
```

```
            YSbrit(k,i) = ((pc-pmelt)/100/1000)*depthNOW;
          % elseif (YSbrit(k,i) > 30) && (depthNOW > h_LCF(k,1))
           elseif (depthNOW > h_LCF(k,1))
            YSbrit(k,i) = ((pm-pmelt)/100/1000)*depthNOW;
           end
           %end
        end
       end

    end

   end

   for k=1:nt
      for i=1:newArraySize
          %Selecting Minimum as Yield Strength for given depth:
          dvbF=[YSbrit(k,i);YSduct(k,i)];
          YS(k,i)=min(dvbF); %YS is recorded in MPa
      end
   end


saveit=0;
if saveit==1

saveas(gcf,sprintf('Crust%gQs%g_TempAndYieldStrengthProfile.fig',zmohoInit/100
0,Qs*1000));
end
saveit=0;
%% INTEGRATED YIELD STRENGTH OVER TIME
#####################################
% Force from Yield Strength
% To figure out the total yield strength of the crust, we must sum up all
% the individual yield strengths for every depth for a given time step...

YSForce=t*0;
YSForceArr=T2*0;

for k=1:nt % (TIME LOOP)
    YSFsub=0;% Subtotal is zeroed before starting with the depth loop.

       for i=1:newArraySize-1 % (DEPTH LOOP)
          %zspcV2=z_Arr2(k,i+1)-z_Arr2(k,i);
          zspcV2=z2NEW(k,i+1)-z2NEW(k,i);
          YSForceArr(k,i+1)=((YS(k,i)*1E6+YS(k,i+1)*1E6)/2)*zspcV2;
          YSFsub=YSFsub+YSForceArr(k,i+1);
```

```
      end
   YSForce(k)=YSFsub; % Subtotal is recorded.
   %disp(['                    YSFsub FINAL = ',num2str(YSFsub/1e12)]);
end %

YSForceI=YSForce(1);              %Initial integrated Force
YSForceF=YSForce(end);            %Final integratd Force
DYSForce=YSForceF-YSForceI;       %Change in integrated Force

%% THERMAL BUOYANCY FORCE
##################################################

TBForce=t*0;                  % Thermal Buoyancy Force Blank Array
TBForceArr=T2*0;              % Thermal Buoyancy Force Blank Array 2

for k=1:nt % (TIME LOOP)
   TBFsub=0;% Subtotal is zeroed before starting with the depth loop.

      zmoho_NOW=h_LCF(k,1);
      for i=1:newArraySize-1 % (DEPTH LOOP)
         depth_now=z2NEW(k,i);
         depth_next=z2NEW(k,i+1);
         if k==30
            disp('')
         end
         %zspcV2=z_Arr2(k,i+1)-z_Arr2(k,i);
         zspcV2=z2NEW(k,i+1)-z2NEW(k,i);
         %TBForceArr(k,i+1)=((YS(k,i)*1E6+YS(k,i+1)*1E6)/2)*zspcV2;
         TBForceArr(k,i+1)=g*a*zspcV2/2*...
            (z_denisty(depth_now,zmoho_NOW)*(T2(1,i)-T2(k,i))*depth_now+...
            z_denisty(depth_next,zmoho_NOW)*(T2(1,i+1)-T2(k,i+1))*depth_next);

         TBFsub=TBFsub+TBForceArr(k,i+1);

      end
   TBForce(k)=TBFsub; % Subtotal is recorded.
   %disp(['                    YSFsub FINAL = ',num2str(YSFsub/1e12)]);
end

TBForceI=TBForce(1);              %Initial Force
TBForceF=TBForce(size(TBForce,1));  %Final Force
DTBForce=TBForceF-TBForceI;       %Change in Force
```

```
%% CRUSTAL BUOYANCY FORCE
#####################################################
CBForce=t*0;                    % Crustal Buoyancy Force Blank Array
CBForceArr=T2*0;                % Crustal Buoyancy Force Blank Array 2

for k=1:nt % (TIME LOOP)
   CBFsub=0;% Subtotal is zeroed before starting with the depth loop.
      zmoho_NOW=h_LCF(k,1);
      for i=1:newArraySize-1 % (DEPTH LOOP)
         depth_now=z2NEW(k,i);
         depth_next=z2NEW(k,i+1);
         %zspcV2=z_Arr2(k,i+1)-z_Arr2(k,i);
         zspcV2=z2NEW(k,i+1)-z2NEW(k,i);
         if k==30
            disp('')
         end
         %TBForceArr(k,i+1)=((YS(k,i)*1E6+YS(k,i+1)*1E6)/2)*zspcV2;
         CBForceArr(k,i+1)=g*zspcV2/2*...
            ((z_denisty(depth_now,zmoho_NOW)-
z_denisty(depth_now,zmohoInit))*depth_now+...
            (z_denisty(depth_next,zmoho_NOW)-
z_denisty(depth_next,zmohoInit))*depth_next);
         CBFsub=CBFsub+CBForceArr(k,i+1);
      end
   CBForce(k)=CBFsub; % Subtotal is recorded.
   %disp(['                    YSFsub FINAL = ',num2str(YSFsub/1e12)]);
end

CBForceI=CBForce(1);            %Initial Force
CBForceF=CBForce(size(CBForce,1));  %Final Force
DCBForce=CBForceF-CBForceI;       %Change in Force


%Buck Approximation of Crustal Buoyancy - delta F
DCBForceBA=((g*(pc*(pm-pc)/pm)*zmohoInit*(zmohoInit-h_LCF(end,1)))-...
   (g*(pc*(pm-pc)/pm)*zmohoInit*(zmohoInit-h_LCF(1,1))));
DForceTot=DTBForce/1e12+DYSForce/1e12+DCBForce/1e12;
disp(' ')
disp(['--> Total Change in Force          = ',num2str(DForceTot),' TN/m']);
disp(' ')

if abs(DYSForce)>abs(DTBForce) && abs(DYSForce)>abs(DCBForce)
   ForceDom=2;
   disp('YIELD STRENGTH IS THE DOMINATING CHANGE IN FORCE')
elseif abs(DTBForce)>abs(DYSForce) && abs(DTBForce)>abs(DCBForce)
   ForceDom=3;
```

```
   disp('THERMAL BUOYANCY IS THE DOMINATING CHANGE IN FORCE')
else
   ForceDom=1;
   disp('CRUSTAL BUOYANCY IS THE DOMINATING CHANGE IN FORCE')
end

%*****display what type of rift forms, also adding in core complex criteria
%that shouldn't be influential on Venus due to low strength contrast
%calculating final flow diffusivity terms to determine if lcf is sufficient
dF=DTBForce/1e12+DYSForce/1e12+DCBForce/1e12;
fT_MOHO=interp1(zTOT(end,:),T(end,:),h_LCF(end,1));
fT_MOHO2=interp1(zTOT(end,:),T(end,:),h_LCF(end,1)-5);
fdTdzMOHO = (fT_MOHO-fT_MOHO2)/5;
fdhdx=(h_LCF(end,end)-h_LCF(end,1))/(xspan(end)-xspan(1));
fKf_dPdx = g*delRho*fdhdx;
fKf_y0   = R*fT_MOHO^2/(z_E(1,h_LCF(end,1))*fdTdzMOHO);
fKf_AvgStress = max((2*fKf_y0*fKf_dPdx),1e6);
fKf_C    = z_A(1,h_LCF(end,1))^(-1)*(fKf_AvgStress)^(1-z_n(1,h_LCF(end,1)));
fKf_nu0  = fKf_C*exp(z_E(1,h_LCF(end,1))/R/fT_MOHO);
fKf      = g*delRho*fKf_y0^3/fKf_nu0;

if dF>0
  RIFT=1;
  disp('WIDE RIFT')
  figure(10)
  scatter(zmohoInit/1000,QsArray(q),100,'b','fill''MarkerEdgeColor','b');
  xlabel('crustal thickness km');ylabel('surface heat flux mW/m^2');
  hold on
  wide=wide+1;
else if dF<0
      CC=(fKf*tmax)^.5;
      if CC > Xe/2 %Kf*delta_t > Xe/2 from Buck 91
         RIFT=3;
        disp ('CORE COMPLEX')
        figure(10)
        scatter(zmohoInit/1000,QsArray(q),100,k,'fill');
        xlabel('crustal thickness km');ylabel('surface heat flux mW/m^2');
        hold on
        corecomp=corecomp+1;
      else disp('NARROW RIFT')
         RIFT=2;
        figure(10)
        scatter(zmohoInit/1000,QsArray(q),100,'g','fill');
        xlabel('crustal thickness km');ylabel('surface heat flux mW/m^2');
        hold on
        narrow=narrow+1;
```

```
        end
    end
end

xX=zmohoInit/1000;yY=Qs*1000;
BDTindF=find(YSduct(end,:) <= YSbrit(end,:),1);
BDTF=z2NEW(end,BDTindF);
BDTindI=find(YSduct(1,:) <= YSbrit(1,:),1);
BDTI=z2NEW(1,BDTindI);
Tmoho_end=interp1(z2NEW(end,:),T2(end,:),h_LCF(end,1));
%dTdt_crust=(Tinit(Nc)-Tsurf)/(zmohoInit/1000);
dTdt_crust=(T(end,10)-T(end,1))/(zTOT(end,10)-zTOT(end,1));
Qs_f=round(z_ktc(1,2)*dTdt_crust*1e3);

    newROW=size(xXyY,1)+1;
    xXyY(newROW,1)=xX;
    xXyY(newROW,2)=yY;
    xXyY(newROW,3)=RIFT;
    xXyY(newROW,4)=ForceDom;
    xXyY(newROW,5)=BDTI;
    xXyY(newROW,6)=BDTF;
    xXyY(newROW,7)=zmoho;
    xXyY(newROW,8)=Qmoho;
    xXyY(newROW,9)=Tmoho;
    xXyY(newROW,10)=zblith;
    xXyY(newROW,11)=ux;
    xXyY(newROW,12)=Tmoho_end;
    xXyY(newROW,13)=Qs_f;
    xXyY(newROW,14)=mohoStart;
    xXyY(newROW,15)=h_LCF(end,1);
    xXyY(newROW,16)=tmax/(yr*1e6);
    xXyY(newROW,17)=strainlim;

    dFtot(newROW,1)=dF;

if SAVEFILES2==1

disp('SAVING DATA TO FILE
##################################################')
disp(' ')
fileIDT=['TEMP',FILENAME];
save(['~/Documents/MATLAB/RIFTING/THESIS/TEMPERATURE/' fileIDT
'.mat'],'T');

fileIDYS=['YS',FILENAME];
```

```
save(['~/Documents/MATLAB/RIFTING/THESIS/YS/' fileIDYS
'.mat'],'YS','z2NEW');
fileIDlcf=['LCF',FILENAME];
save(['~/Documents/MATLAB/RIFTING/THESIS/LCF/' fileIDlcf
'.mat'],'h_LCF','xspan');
fileIDz=['DEPTH',FILENAME];
save(['~/Documents/MATLAB/RIFTING/THESIS/DEPTH/' fileIDz '.mat'],'zTOT');


disp('File Write Complete');
disp(' ');

end

if Tmoho_end > Tmelt(Nc)
   disp('Tmoho_end > Tmelt');
   figure(11)
   p1=scatter(zmohoInit/1000,QsArray(q),'o','MarkerEdgeColor','g','LineWidth',2);
   l1='Tmoho_end > Tmelt';
 %  p1=text(zmohoInit/1000,QsArray(q),'X','Color','c','FontSize',14);
   xlabel('crustal thickness km');ylabel('surface heat flux mW/m^2');
   hold on
end

end %<-- END OF MASTER LOOP
end
if SAVEFILES == 1
   fileIDxy=['xXyY',FILENAME];

save(['~/Documents/MATLAB/RIFTING/THESIS/RiftingParametersEachRun/FINA
L/FINAL' fileIDxy '.mat'],'xXyY');

   fileIDzDike=['DIKE_z',FILENAME];
   save(['~/Documents/MATLAB/RIFTING/THESIS/DIKE/' fileIDzDike
'.mat'],'SolidusIND_zTOT');
   fileIDtDike=['DIKE_t',FILENAME];
   save(['~/Documents/MATLAB/RIFTING/THESIS/DIKE/' fileIDtDike
'.mat'],'SolidusIND_tTOT');

end

dlmwrite('--xXyY_BACKUP.txt',xXyY) %in case I forgot to set SAVEFILE to 1
disp(['--> Final Program Runtime             = ',num2str(toc(tstart)/60),' minutes']);
```

Rifting_Venus_ODE_MovingGrid.m

```
function Mdot = RIFTING_VENUS_ODE_MovingGrid(t,M)

% Making variables global, for use in sub-programs:
global z_ktd z_H_Fn edot u_Fn xspan xspc ux Xe dudx_Fn...
   Kf nx nz delRho z_E z_n R g z_A Nc Nl z_ktc  Qa

% TEMPERATURE => FIRST M(1:nz)
% CRUSTAL FLOW => SECOND M((nz+1):(nz+nx))
% DEPTH OF Zl => LAST ELEMENT M(nz+nx+1)

% Generating a 'Mdot' array, to store results in
Mdot=zeros(nz+nx,1);%
% Current Depth of Moho:
zmoho=(M(nz+1)); % h at the center of the rift

%find NEW Depth Profile
[zTOT, dhdt ,vTOT] = MovingGrid(zmoho,t,edot,M);

% Current Temperature at Moho:
T_MOHO=interp1(zTOT,M(1:nz),zmoho);
% Current Temperature 5 steps above Moho:
T_MOHO2=interp1(zTOT,M(1:nz),zmoho-5);
% Current Temperature Gradient at Moho:
dTdzMOHO = (T_MOHO-T_MOHO2)/5;
% dh/dx over the whole rift
dhdx=(M(nz+nx)-M(nz+1))/(xspan(end)-xspan(1));

% Kf Components for LCF
Kf_dPdx = g*delRho*dhdx;
Kf_y0   = R*T_MOHO^2/(z_E(1,zmoho)*dTdzMOHO);
Kf_AvgStress = (2*Kf_y0*Kf_dPdx);
Kf_C    = z_A(1,zmoho)^(-1)*(Kf_AvgStress)^(1-z_n(1,zmoho));
Kf_nu0  = Kf_C*exp(z_E(1,zmoho)/R/T_MOHO);
Kf      = g*delRho*Kf_y0^3/Kf_nu0;

%% LOWER CRUSTAL FLOW EQUATION
%(FOR nz+1:nz+nx)

% Boundary Condition #1: (center of rift)
   i=nz+1;
   pos=xspan(i-nz);
   Mdot(i)=Kf*((M(i+1)-2*M(i)+M(i+1))/xspc^2)....
      - u_Fn(pos,ux,Xe)*((M(i+1)-M(i+1))/(2*xspc))...
      - M(i)*dudx_Fn(pos,ux,Xe);
   % all terms of h(i-1) were replaced with h(i+1); since this problem has
```

```
   % symmetry about x=0
%          --
%        --  --
%   -----      -----
   % Don't allow +dh/dt (thickening of crust)
   Mdot(i)=min(Mdot(i),0);
% Boundary Condition #2: (furthest extent of rift)
   Mdot(nz+nx) = 0;
% Internal Points of the Finite Difference Matrix (Horizontal Distance)
for i=nz+2 : nz+nx-1
   pos=xspan(i-nz);
   Mdot(i)=Kf*((M(i+1)-2*M(i)+M(i-1))/xspc^2) - ...
      u_Fn(pos,ux,Xe)*((M(i+1)-M(i-1))/(2*xspc)) - ...
      M(i)*dudx_Fn(pos,ux,Xe);
%   Mdot(i)=min(Mdot(i),0))
end

%% HEAT TRANSPORT EQUATION

% Boundary Condition #1: (surface of lithosphere)
Mdot(1)= 0;
% Boundary Condition #2: (base of lithosphere)
Mdot(Nl)=0;

%Internal Points of the Finite Difference Matrix
%CRUST vg=vz so v=0
for i=2:Nc
   depth=zTOT(i);
   Mdot(i)=z_ktd(depth,zmoho)*(M(i+1)-2*M(i)+M(i-1))/((zTOT(i+1)-zTOT(i-
1))/2)^2 + z_H_Fn(depth,zmoho);
end
%MANTLE vg != vz vTOT=vp-vg
for i=Nc+1:Nl-1
   depth=zTOT(i);
  % vz=-edot*(zTOT(i)-zmoho)+dhdt; %Physical velocity in mantle due to stretching
modulated by LCF
  % vg=dhdt + ((zTOT(i)-zmoho)/(zTOT(end)-zmoho))*(dZldt-dhdt); %Grid
velocity
 %  vTOT=vz-vg; %physical velocity - grid velocity is total velocity of mantle point
   vTOTnow=vTOT(i);
   Mdot(i)=z_ktd(depth,zmoho)*(M(i+1)-2*M(i)+M(i-1))/((zTOT(i+1)-zTOT(i-
1))/2)^2-vTOTnow*...
     ((M(i+1))-M(i-1))/(2*(zTOT(i)-zTOT(i-1)))+z_H_Fn(depth,zmoho);
end

%% CHANGE IN LITHOSPHERIC THICKNESS
```

```
%dZl/dt...to find new Zl
Mdot(nz+nx+1)= dhdt-edot*(zTOT(Nl)-
zmoho)+z_ktd(2,1)*((Qa/z_ktc(2,1))*(1/(M(Nl)-M(Nl-1)))+(1/(zTOT(Nl)-zTOT(Nl-
1))));

end
```

MovingGrid.m

```
function [zTOT, dhdt ,vTOT] = MovingGrid(zmoho,t,edot,M)
global zmohoInit Nc Nl Qa z_ktc z_ktd

ZlNOW=M(end); %current depth of lithosphere

if t ==0
   dhdt=0;
 %  dZldt=0;
else
   dhdt=(zmoho-zmohoInit)/t; %change in crust/time
  % dZldt=(M(end)-zblith)/t;  %change in Zl/time
end
zLCF=linspace(0,zmoho,Nc); %Crust depth points
zM=linspace(zmoho,ZlNOW,Nl-Nc+1); %Mantle depth points
zTOT=[zLCF zM(2:end)]';

dT=(M(Nl)-M(Nl-1));
dz=zTOT(end)-zTOT(end-1);
dZldt=dhdt-edot*(zTOT(end)-zTOT(Nc))+z_ktd(2,1)*(Qa/(z_ktc(2,1)*dT)+(dz)^(-
1));
disp('')
%declaring size of velocities for loop
vg=zeros(1,Nl);
vp=vg;
vTOT=vg;

if t ~=0
   for k=(Nc+1):Nl
   vg(k)=dhdt+((k-Nc)/(Nl-Nc))*(dZldt-dhdt); %mantle GRID velocity
   vp(k)=-edot*(zM(k-Nc)-zmoho)+dhdt;       %mantle PHYSICAL velocity
   vTOT(k)=vp(k)-vg(k);                    %mantle TOTAL velocity, vp-vg
   end
end

end
```

MovingGridAfterODE.m

```
function [zTOT] = MovingGridAfterODE(h_LCF, zlith)
global nt Nc Nl

zTOT=zeros(nt,Nl);

for i=2:nt
   zmohoNOW=h_LCF(i,1);
   ZlNOW=zlith(i);
   zLCF=linspace(0,zmohoNOW,Nc);
   zM=linspace(zmohoNOW,ZlNOW,Nl-Nc+1);
   zTOT(i,:)=[zLCF zM(2:end)]';
end

end
```

SolidusAndTemp.m

```
function [Tsolidus,SolidusIND_z, SolidusIND_t,
DIKE]=SolidusAndTemp(pc,pm,g,zTOT,nt,T,Nl,Nc,plotIND,h_LCF)

%NOTES:-----------------------
% Diking is begins when the temp profile crosses the solidus (Hirshmann 2000), and
%it propagated to surface. Diking makes the brittle strength a linear function of depth
%and depends on the density constrast between the melt and surrounding rock

for i=1:nt
   for j=1:Nl
      if j <= Nc
         P(i,j) = pc*g*zTOT(i,j);
      else
         P(i,j) = pc*g*zTOT(i,Nc) + pm*g*(zTOT(i,j)-zTOT(i,Nc));
      end
   end
end

a=-5.1404654;b=132.899012;c=1120.66061;
%constants: [a]=deg/GPa^2, [b]=deg/GPa, [c]=deg

%Determine Peridotite Solidus from Hirschmann 2000
%add 273 to convert to Kelvins
for i=1:nt
   Tsolidus(i,:) = a*(P(i,:)/1e9).^2 + b*(P(i,:)/1e9) + c + 273;
end


%find at what time step Solidus < Temp
```

```
%Check at what depth index for each time step the mantle is above solidus
for i=1:nt
   SolIND=find(Tsolidus(i,:) < T(i,:),1,'first');
   if isempty(SolIND)
      SolIND=0;
   end
   SolidusIND_z(i)=SolIND; %produce 1x63 array
end

%Time index for this run when mantle starts partial melting
for i=1:nt
   %returns 1 value for whole run, end of code get a 1x(run #) array
   SolidusIND_t=find(SolidusIND_z > 0,1,'first');
   if isempty(SolidusIND_t)
      SolidusIND_t=0;
   end
end

%plot Final Temp Profile and Solidus
figure(4)
plot(T(plotIND,:),zTOT(plotIND,:)/1000,Tsolidus(plotIND,:),zTOT(plotIND,:)/1000,
...
   T(1,:),zTOT(1,:)/1000,'c');
line([700 1500], [h_LCF(end,1)/1000 h_LCF(end,1)/1000],'Color','r');
set(gca,'YDir','reverse');
legend('Lithosphere Temperature','Peridotite Solidus','Initial Lithosphere
Temperature');

%When (if at all) do we impose diking?
DIKE=zeros(1,nt);
%create 1x63 array that says (for each time step) whether the temp is above
%the solidus. If this happens at t=0, diking starts then and will likely
%lead to a wide rift since we start with a weakened lithosphere
for i=1:nt
   if any(SolidusIND_z(i) ~= 0)
      DIKE(i)=1;
   else
      DIKE(i)=0;
   end
end

end
```

Bibliography

Anderson, F.S. and S.E. Smrekar (2006), Global mapping of crustal and lithospheric thickness on Venus, *Journal of Geophysical Research, 111*, E08006, doi:10.1029/2004JE002395.

Arkani-Hamed, J. (1994), On the thermal evolution of Venus. *Journal of Geophysical Research*, *99*, E1, 2019-2033, doi:10.1029/93JE03172

Barnett, D.N., F. Nimmo, and D. McKenzie (2000), elastic thickness estimates for Venus using line of sight acelerations from Magellan cycle 5, *Icarus, 146*, 404-419, doi:10.1006/icar.2000.6352

Basilevsky, A.T. (1993), Age of rifting and associated volcanism in Atla Regio, Venus. *Geophysical Research Letters*, *120*, 10, 883-886, doi:10.1029/93GL00736

Basilevsky, A.T. and J.W. Head (2000), Geologic units on Venus: evidence for their global correlation. *Planetary and Space Science*, *48*, 75-111, doi:10.1016/S0032-0633(99)00083-5

Basilevsky, A.T. and J.W. Head (2007), Beta Regio, Venus: evidence for uplift, rifting and volcanism due to a mantle plume. *Icarus*, *192*, 167-186, doi:10.1016/j.icarus.2007.07.007

Basilevsky, A.T., J.W. Head, G.G., Schaber, and R.G. Strom (1997), The resurfacing history of Venus. In: *Venus II*, Eds. S.W. Bougher, D.M. Hunten, and R.J. Phillips, 1047-1086, University of Arizona Press, Tuscon

Bassi, G., C.E. Keen, and P. Potter (1993), Constraining styles of rifting: models and examples from the eastern Canadian margin. *Tectonics*, *3*, 639-655, doi:10.1029/93TC00197

Beswick, A.E. (1982), Some geochemical aspects of alteration and genetic relations in komatiitic suites. In: *Komatiites*, Eds. N. T. Arndt and N.G. Nisbet, 211-214, London: Allen and Unwin

Bethell, E., R.E. Ernst, C. Samson, and K.L. Buchan (2016), Circumferential graben-fissure systems of Venusian coronae as possible analogues of giant circumferential dyke swarms on Earth. *47th Lunar and Planetary Science Conference*, abstract 1471

Bialas, R.W., W.R. Buck, and R. Qin (2010), How much magma is required to rift a continent? *Earth and Planetary Science Letters*, *292*, 68-78, doi:10.1016/j.epsl.2010.01.021

Bottke, W.F., D. Vokrouhlicky, B. Ghent, S. Mazrouei, S. Robbins, and S. Marchi (2016), On asteroid impacts, crater scaling laws, and a proposed younger surface age for Venus. *47th Lunar and Planetary Science Conference*, abstract 2036

Brace, W.F. and D.L. Kohlstedt (1980), Limits on lithospheric stress imposed by laboratory experiments. *Journal of Geophysical Research, 85*, B11, 6248-6252, doi:10.1029/JB085iB11p06248

Braun J., J. Chery, A. Poliakov, D. Mainprice, A. Vauchez, A. Tommasi, and M. Daignieres (1999), A simple parameterization of strain localization in the ductile regime due to grain size reduction: a case study for olivine. *Journal of Geophysical Research*, *104*, B11, 25,167-25,181, doi:10.1029/1999JB900214

Brown, C.D. and R.E. Grimm (1997), Tessera deformation and the contemporaneous thermal state of the plateau highlands, Venus. *Earth and Planetary Science Letters, 147,* 1-10, doi:10.1016/S0012-821X(97)00007-1

Brown, G.C., C.J. Hawkesworth, and R.C.L. Wilson, Eds. (1992), Understanding the Earth: a new synthesis. Cambridge University Press. ISBN: 0-521-37020-5

Brun, J.P. (1999), Narrow rifts versus wide rifts: influences for the mechanics of rifting from laboratory experiments. *Philosophical Transactions of the Royal Society, mathematical physical and engineering sciences*, *357*, 1753, 695-710, doi:10.1098/rsta.1999.0349

Buchan, K.L. and R.E. Ernst (2016), Giant circumferential dyke swarms on earth as possible analogues of coronae on Venus. *47th Lunar and Planetary Science Conference*, abstract 1183

Buck, W.R. (1991), Modes of continental lithospheric extension. *Journal of Geophysical Research*, *96*, B12 20,161-20,178

Buck, W.R. (2004), Consequences of asthenospheric variability on continental rifting. In: *Rheology and Deformation of the lithosphere at continental margins*, Eds. G.D., Taylor, B., Driscoll, N.W., Kohlsteft, D.L. Karner, 1-31. Columbia University Press, New York

Buck, W.R. (2006), The role of magma in the development of the afro-arabian rift systems. In: *The afar province within the east African rift system*. Eds. G. Yirgu, C.J. Ebinger, and P.K.H. Maguire, Geological Society, London, Special Publications, 259, 43-54, doi:10.1144/GSL.SP.2006.259.01.05

Buck, W.R., L.L. Lavier, and A.N.B. Poliakov (1999), How to make a rift wide. *Philosophical Transactions of the Royal Society, mathematical, physical and engineering sciences*, *357*, 753, 671-690

Crumpler, L.S., J.W. Head, and J.C. Aubele (1993), Relation of major volcanic center concentration on Venus to global tectonic patterns. *Science*, *261*, 5121, 591-595, doi:10.1126/science.261.5121.591

Dombard, A.J., C.L. Johnson, M.A. Richards, S.C. Solomon (2007), A magmatic loading model for coronae on Venus. *Journal of Geophysical Research, 112*, E04006, doi:10.1029/2006JE002731

Dury, M.R. (2005), Dynamic recrystallization and strain softening of olivine aggregates in the laboratory and the lithosphere. In: *Deformation Mechanisms, Rheology, and Tectonics: from minerals to the lithosphere*. Eds. D. Gapais, J.P. Brun, and P.R. Cobbold, Geological Society, London. Special Publications, 243, 143-158, doi:10.1144/GSL.SP.2005.243.01.11

Ernst R.E., D.W. Desnoyers, J.W. Head, E.B. Grosfils (2003), Graben-fissure systems in Guinevere Planitia and Beta Regio, Venus, and implications for regional stratigraphy and mantle plumes. *Icarus*, *164*, 282-316, doi:10.1016/S0019-1035(03)00126-X

Ernst R.E., E.B. Grosfils, D. Mege (2001), Giant dike swarms: Earth, Venus and Mars. *Annual Review Earth and Planetary Science*, *29*, 489-534, doi:10.1146/annurev.earth.29.1.489

Etheridge M.A. and J.C. Wilkie (1979), Grainsize reduction, grain boundary sliding and the flow strength of mylonites. *Tectonophysics*, *58*, 1, 159-178, doi:10.1016/0040-1951(79)90327-5

Falloon, T.J. and D.H. Green (1989), The solidus of carbonated, fertile peridotite. *Earth and Planetary Science Letters*, *94*, 3-4, 364-370, doi:10.1016/0012-821X(89)90153-2

Ford, P.G. and G.H. Pettengill (1992), Venus topography and kilometer-scale slopes. *Journal of Geophysical Research, 97,* E8, 13103-13114, doi:10.1029/92JE01085

Foster A. and F. Nimmo (1996), Comparisons between the rift systems of East Africa, Earth and Beta Regio, Venus. *Earth and Planetary Science Letters*, *143*, 1-4, 183-195, doi:10.1016/0012-821X(96)00146-X

Galgana G.A., E.B. Grosfils, P.J. McGovern (2013), Radial dike formation on Venus: insights from models of uplift, flexure and magmatism. *Icarus*, *225*, 538-547, doi:10.1016/S0019-1035(03)00126-X

Gilmore, M.S., G.C. Collins, M.A. Ivanov, L. Marinangeli, and J.W. Head (1998), Style and sequence of extensional structures in tessera terrain, Venus. *Journal of Geophysical Research*, *103*, E7, 16,813-16,840, doi:10.1029/98JE01322

Green D.H., W.O. Hibberson, I. Kovacs, and A. Rosenthal (2010), Water and its influence on the lithosphere-asthenosphere boundary. *Nature*, *467*, 448-451, doi:10.1038/nature09369

Grimm R.E. and P.C. Hess (1997), The crust of Venus. In: *Venus II*, Eds. Eds. S.W. Bougher, D.M. Hunten, and R.J. Phillips, 1205-1244, University of Arizona press, Tuscon

Grimm, R.E. (1994), Recent deformation rates on Venus. *Journal of Geophysical Research, 99,* E11, 23163-23171, doi:10.1029/94JE02196

Grosfils E.B. and J.W. Head (1994a), The global distribution of giant radiating dike swarms on Venus: implications for the global stress state. *Journal of Geophysical Research*, *21*, 8, 701-704, doi:10.1029/94GL00592

Gueydan F., Y.M. Leroy, L. Jolivet, and P. Agard (2003), Analysis of continental midcrustal strain localization induced by microfracturing and reaction-softening. *Journal of Geophysical Research*, *108*, B2, 2064, doi:10.1029/2001JB000611

Gueydan F., C. Morency, and, J.P. Brun (2008), Continental rifting as a function of lithosphere mantle strength. *Tectonophysics*, *460*,1-4, 83-93, doi:10.1016/j.tecto.2008.08.012

Gueydan F. and J. Precigout (2014), Modes of continental rifting as a function of ductile strain localization in the lithospheric mantle. *Tectonophysics*, *612-613*, 18-25, doi:10.1016/j.tecto.2013.11.029

Gueydan F., J. Precigout, and L.G.J. Montési (2014), Strain weakening enables continental plate tectonics. *Tectonophysics*, *631*, 189-196, doi:10.1016/j.tecto.2014.02.005

Hamilton, V.E. and E. R. Stofan (1996), The geomorphology and evolution of Hecate Chasma, Venus. *Icarus*, *121*, 171-194, doi:10.1006/icar.1996.0077

Hansen V.L, J.J. Willis, and W.B. Banerdt (1997), Tectonic overview and synthesis. In: *Venus II*, Eds. S.W. Bougher, D.M. Hunten, and R.J. Phillips, 797-844, University of Arizona press, Tuscon

Herrick, R.R. (1994), Resurfacing history of Venus. *Geology*, *22*, 703-706, doi:10.1130/0091-7613(1994)022<0703:RHOV>2.3.CO;2

Hirshmann M.M. (2000), Mantle solidus: experimental constraints and the effects of peridotite composition. *Geochemistry, Geophysics, Geosystems*, *1*, 10, doi:10.1029/2000GC000070

Hirth G. and D.L. Kohlstedt (1995), Experimental constraints on the dynamics of the partially molten upper mantle: deformation in the dislocation creep regime. *Journal of Geophysical Research*, *100*, B8, 15441-15449, doi: 10.1029/95JB01292

Hirth G. and D. Kohlstedt (2003), Rheology of the upper mantle and the mantle wedge: a view from the experimentalists. Ed. Eiler, J., *Inside the subduction factory: American Geophysical Union Geophysical Monograph*, *138*, 83-105, doi:10.1029/138GM06

Holyoke C.W. and J. Tullis (2006), Formation and maintenance of shear zones. *Geology*, *34*, 105-108, doi:10.1130/G22116.1

Hoogenboom T. and G.A. Houseman (2006), Rayleigh-taylor instability as a mechanism for corona formation on Venus. *Icarus*, *180*, 2, 292-307, doi:10.1016/j.icarus.2005.11.001

Ivanov, M.A. and J.W. Head (2015), The history of tectonism on Venus: a stratigraphic analysis. *Planetary and Space Science*, *113*, 10-32, doi:10.1016/j.pss.2015.03.016

James, P.B., M.T. Zuber, and R.J. Phillips (2013), Crustal thickness and support of topography on Venus. *Journal of Geophysical*, *118*, 4, 859-875, doi:10.1029/2012JE004237

Kaula, W.M. (1999), Constraints on Venus evolution from radiogenic argon. *Icarus*, *139*, 1, 32-39, doi:10.1006/icar.1999.6082

Kendall, J.M. and C. Lithgow-Bertelloni (2016), Why is Africa rifting? In: *Magmatic rifting and active volcanism,* Eds. T.J. Wright, A. Ayele, D.J. Ferguson, T. Kidane, and C. Vye-Brown, Geological Society, London, special publications, 420, doi:10.1144/SP420.17

Kucinskas, A.B. and, D.L.Turcotte (1994). Isostatic compensation of equatorial highlands on Venus. *Icarus*, *12*, 1, 104-116, doi:10.1006/icar.1994.1172

Kiefer, W.S. and B.H. Hager (1991), A mantle plume model for equatorial highlands on Venus. *Journal of Geophysical Research*, *96,* 20947-20966, doi:10.1029/91JE02221

Kiefer, W.S. and L.C. Swafford (2006), Topographic analysis of Devana Chasma, Venus: implications for rift system segmentation and propagation. *Journal of Structural Geology*, *28*, 12, 2144-2155, doi:10.1016/j.jsg.2005.12.002

Koenig, E. and D.D. Pollard (1998), Mapping and modeling of radial fracture patterns on Venus. *Journal of Geophysical Research*, *103*, B7, 15183-15202, doi:10.1029/98JB00577

Lopez, I., A. Marquez, and R. Oyarzun (1999), Are coronae restricted to Venus?: corona-like tectonovolcanic structures on Earth. *Earth, Moon and Planets*, *77*, 77-125, doi:10.1023/A:1006227431552

Mackwell, S.J., M.E. Zimmerman, and D.L. Kohlstedt (1998), High-temperature deformation of dry diabase with application to tectonics on Venus. *Journal of Geophysical Research*, *103*, B1, 975-984, doi:10.1029/97JB02671

Martin, P., E.R. Stofan, L.S. Glaze, and S. Smrekar (2007), Coronae of Parga Chasma, Venus. *Journal of Geophysical Research*, *112*, E4, doi:10.1029/2006JE002758

McKenzie, D., P.G. Ford, C. Johnson, B. Parsons, D. Sandwell, S. Saunders, and S.C. Solomon (1992), Features on Venus generated by plate boundary processes. *Journal of Geophysical Research*, *97*, E8, 13533-13544, doi:10.1029/92JE01350

McKenzie, D. and F. Nimmo (1997), Elastic thickness estimates for Venus from line of sight accelerations. *Icarus, 130*, 198-216, doi:10.1006/icar.1997.5770

McKinnon, W.B., K.J. Zahnle, B.A. Ivanov, and H.J. Melosh (1997), Cratering on Venus: models and observations, In: *Venus II*, Eds. S.W. Bougher, D.M. Hunten, and R.J. Phillips, 969-1014, University of Arizona press, Tucson

Montési, L.G.J. (2007), A constitutive model for layer development in shear zones near the brittle-ductile transition. *Geophysical Research Letters, 34*, L08307, doi:10.1029/2007GL029250

Montési, L.G.J. (2013), Fabric development as the key for forming ductile shear zones and enabling plate tectonics. *Journal of Structural Geology*, *50*, 254-266, doi:10.1016/j.jsg.2012.12.011

Moore, W.B. and G. Schubert (1995), Lithospheric thickness and mantle lithosphere density contrast beneath Beta Regio, Venus. *Geophysical Research Letters*, *22*, 4, 429-432, doi:10.1029/94GL02055

Moore, W.B. and G. Schubert (1997), Venusian crustal and lithospheric properties from nonlinear regressions of highland geoid and topography. *Icarus, 128*, 2, 415-428, doi:10.1006/icar.1997.5750

Morgan, P. and R.J. Phillips (1983), Hot spot heat transfer- its application to Venus and implications to Venus and Earth. *Journal of Geophysical Research*, *88*, NB10, 8305-8317, doi:10.1029/JB088iB10p08305

Musser, G.S. and S.W. Squyres (1997), A coupled thermal-mechanical model for corona formation on Venus. *Journal of Geophysical Research*, *102*, E3, 6581-6595, doi:10.1029/96JE03044

Nagasawa, C., S. Sasaki, and M. Koyama (1998), Change of stress field in Beta-Atla-Themis region on Venus, estimated from surface geometry of dike swarms, lava stratigraphy and crater density. *Geophysical Research Letters*, *25*, NO.24, 4429-4432, doi:10.1029/1998GL900097

Nimmo, F. and D. McKenzie (1998), Volcanism and tectonics on Venus. *Annual Review of Earth and Planetary Sciences, 26*, 23-51, doi:10.1146/annurev.earth.26.1.23

Parfitt, E.A. and L. Wilson (2008), Fundamentals of physical volcanology. Blackwell Publishing, ISBN: 978-0-63205443-5

Phillips, R.J. and M.C. Malin (1983), The interior of Venus and tectonic implications. In: *Venus*, Eds. D.M. Hunten, L. Colin, T.M. Donahue, V.I. Moroz, 159-214, University of Arizona press, Tuscon

Phillips R.J., R.E. Grimm, and M.C. Malin (1991), Hotspot evolution and the global tectonics of Venus. *Science*, *252*, 5006, 651-658, doi:10.1126/science.252.5006.651

Phillips, R.J. (1994), Estimating lithospheric properties at Atla Regio, Venus. *Icarus, 112*, 147-170, doi:10.1006/icar.1994.1175

Phillips, R.J., R.F. Raubertas, R.E. Arvidson, I.C. Sarkar, R.R. Herrick, N. Izenberg, and R.E. Grimm (1992), Impact craters and Venus resurfacing history. *Journal of Geophysical Research*, *97*, E10, 15923-15948, doi:10.1029/92JE01696

Phillips, R.J, C.L. Johnson, S.L. Mackwell, P. Morgan, D.T. Sandwell, and M.T. Zuber (1997), Lithospheric mechanics and dynamics of Venus. In: *Venus II*, Eds. S.W. Bougher, D.M. Hunten, and R.J. Phillips, 1163-1204, University of Arizona press, Tucson.

Phillips, R.J. and V.L. Hansen (1998), Geological evolution of Venus: rises, plains, plumes and plateaus. *Science*, *6*, 5356, 1492-1497, doi:10.1126/science.279.5356.1492

Piskorz, D., L.T. Elkins-Tanton, and S.E. Smrekar (2014), Coronae formation on Venus via extension and lithospheric instability. *Journal of Geophysical Research*, *119*, 12, 2568-2582, doi:10.1002/2014JE004636

Precigout, J., F. Gueydan, D. Hapais, C.J. Garrido, and A. Essaifi (2007), Strain localization in the subcontinental mantle- a ductile alternative to the brittle mantle. *Tectonophysics*, *445*, 318-336, doi:10.1016/j.tecto.2007.09.002

Prinn, R.G. and B. Fegley (1987), The atmosphere of Venus, Earth and Mars- a critical comparison. *Annual Review of Earth and Planetary Sciences*, *15*, 171-212, doi:10.1146/annurev.ea.15.050187.001131

Rathburn, J.A., D.M. Janes, and S.W. Squyres (1999), Formation of Beta Regio, Venus: results from measuring strain. *Journal of Geophysical Research, 104*, E1, 1917-1927, doi:10.1029/1998JE900026

Reese, C.C.,V.S. Solomatov, and L.N. Moresi (1998), Heat transport efficiency for stagnant lid convection with dislocation viscosity: application to Mars and Venus. *Journal of Geophysical Research*, *103*, E6, 13643-13657, doi:10.1029/98JE01047

Romeo, I. and D.L. Turcotte (2010), Resurfacing on Venus. *Planetary and Space Science*, *58*, 10, 1374-1380, doi:10.1016/j.pss.2010.05.022

Schubert, G., W.B. Moore, and D.T. Sandwell (1994), Gravity over coronae and chasmata on Venus. *Icarus*, *112*, 1, 130-146, doi:10.1006/icar.1994.1174

Schubert, G. and D.T. Sandwell (1995), A global survey of possible subduction sites on Venus. *Icarus*, *117*, 173-196, doi:10.1006/icar.1995.1150

Schubert, G., V.S. Solomatov, P.J. Tackley, and D.L. Turcotte (1997), Mantle convection and the thermal evolution of Venus. In: *Venus II*, Eds. S.W. Bougher, D.M. Hunten, and R.J. Phillips, 1245-1288, University of Arizona press, Tucson

Sclater, J.G., C. Jaupart, and D. Galson (1980), The heat flow through oceanic and continental crust and the heat loss of the Earth. *Reviews of Geophysics and Space Physics*, *18*, 1, 269-311, doi:10.1029/RG018i001p00269

Sengor, A.M.C. and K. Burke (1978), Relative timing of rifting and volcanism on Earth and its tectonic implications. *Geophysical Research Letters*, *5*, 6, 419-421, doi:10.1029/GL005i006p00419

Smrekar, S.E., W.S. Kiefer, and E.R. Stofan (1997), Large volcanic rises on Venus. In: *Venus II*, Eds. S.W. Bougher, D.M. Hunten, and R.J. Phillips, 845-878, University of Arizona press, Tucson

Smrekar, S.E., T. Hoogenboom, E.R. Stofan, and P. Martin (2010), Gravity analysis of Parga and Hecate Chasmata: implications for rift and corona formation. *Journal of Geophysical Research*, *115*, E07010, doi:10.1029/2009JE003435

Smrekar, S.E., E.R. Stofan, P. Martin, and T. Hoogenboom (2010), Models of Hecate Chasma, Venus and implications for active(?) extension. *41st Lunar and Planetary Science Conference*, abstract 1422

Solomatov, V.S. and L.N. Moresi (1996), Stagnant lid convection on Venus. *Journal of Geophysical Research*, *101*, E2, 4737-4753, doi:10.1029/95JE03361

Solomon, S.C. and J.W. Head (1982), Mechanisms for lithospheric heat-transport on Venus: implications for tectonic style and volcanism. *Journal of Geophysical Research*, *87*, NB11, 9236-9246, doi:10.1029/JB087iB11p09236

Stamps, D.S., L.M. Flesch, and E. Calais (2010), Lithospheric buoyancy forces in African from a thin sheet approach. *International Journal of Earth Sciences*, *99*, 7, 1525-1533, doi:10.1007/s00531-010-0533-2

Stofan, E.R., V.E. Hamilton, D.M. Janes, and S.E. Smrekar (1997), Coronae on Venus: morphology and origin. In: *Venus II*, Eds. S.W. Bougher, D.M. Hunten, and R.J. Phillips, 931-968, University of Arizona press, Tucson

Stofan, E.R., J.W. Head, D.B. Campbell, S.H. Sisk, A.F. Bogomolov, O.N. Rzhiga, A.T. Basilevsky, and N. Armand (1989), Geology of a rift zone on Venus-Beta Regio and Devana Chasma. *Geological Society of America Bulletin*, *101*, 143-156, doi:10.1130/0016-7606(1989)101<0143:GOARZO>2.3.CO;2

Stofan, E.R. and S.E. Smrekar (2005), Large topographic rises, coronae, large flow fields, and large volcanoes on Venus: evidence for mantle plumes? In: *Plates Plumes and Paradigms*. Eds. G.R. Foulger, J.H. Natland, D.C. Presnall, 388, doi:10.1130/2005.2388(47)

Surkov, Y.A., F.F. Kirnozov, V.N. Glazov, A.G. Duchenko, L.P. Tatsy, and O.P. Sobornov (1987), Urnaium, Thorium, and Potassium in the Venusian rocks at the landing site of Vega 1 and 2. *Journal of Geophysical Research*, *92*, NO. B4, 537-540

Svedhem, H., D.V. Titov, F.W. Taylor, and O. Witasse (2007). Venus as a more Earth-like planet. *Nature, 450*, 629-632, doi:10.1038/nature06432

Turcotte, D.L. (1995), How does Venus lose heat? *Journal of Geophysical Research*, *100*, E8, 16931-16940, doi:10.1029/95JE01621

Turcotte, D.L., G. Morein, D. Roberts, and B.D. Malamud (1999), Catastrophic resurfacing and episodic subduction on Venus. *Icarus*, *139*, 49-54, doi:10.1006/icar.1999.6084

Warren, J.M. and G. Hirth (2006), Grain size sensitive deformation mechanisms in naturally deformed peridotites. *Earth and Planetary Science Letters*, *248*, 438-450, doi:10.1016/j.epsl.2006.06.006

White, R. and D. McKenzie (1989), Magmatism at rift zones: the generation of volcanic continental margins and flood basalts. *Journal of Geophysical Research, 94*, B6, 7685-7729, doi:10.1029/JB094iB06p07685

Yamasaki, T. (2004), Localized rheological weakening by grain-size reduction during lithospheric extension. *Tectonophysics*, *386*, 3-4, 117-145, doi:10.1016/j.tecto.2004.05.006

Zharkov, V.N. and V.S. Solomatov (1992), Models of the thermal evolution of Venus. In: *Venus Geology Geochemistry and Geophysics: research results from the USSR*. Eds. V.L. Barsukov, A.T. Basilevsky, V.P. Volkov, V.N. Zharkov, University of Arizona press, Tucson and London.